DOT/FAA/AR-99/11

Office of Aviation Research
Washington, D.C. 20591

Large Engine Uncontained Debris Analysis

May 1999

Final Report

U.S. Department of Transportation
Federal Aviation Administration

NOTICE

This document is disseminated under the sponsorship of the U.S. Department of Transportation in the interest of information exchange. The United States Government assumes no liability for the contents or use thereof. The United States Government does not endorse products or manufacturers. Trade or manufacturer's names appear herein solely because they are considered essential to the objective of this report. This document does not constitute FAA certification policy. Consult your local FAA aircraft certification office as to its use.

This report is available at the Federal Aviation Administration William J. Hughes Technical Center's Full-Text Technical Reports page: www.tc.faa.gov/its/act141/reportpage.html in Adobe Acrobat portable document format (PDF).

Technical Report Documentation Page

1. Report No.	2. Government Accession No.	3. Recipient's Catalog No.
DOT/FAA/AR-99/11		

4. Title and Subtitle	5. Report Date
LARGE ENGINE UNCONTAINED DEBRIS ANALYSIS	May 1999
	6. Performing Organization Code: 418300D

7. Author(s)	8. Performing Organization Report No.
C.E. Franeknberger, III	

9. Performing Organization Name and Address	10. Work Unit No. (TRAIS)
Naval Air Warfare Center, Weapon Division Survivability Division System Vulnerability Branch China Lake, CA 93555-6001	11. Contract or Grant No.: DTFA03-95-X-90019

12. Sponsoring Agency Name and Address	13. Type of Report and Period Covered
U.S. Department of Transportation Federal Aviation Administration Office of Aviation Research Washington, DC 20591	Final Report
	14. Sponsoring Agency Code: ANM-110

15. Supplementary Notes

The Federal Aviation Administration William J. Hughes Technical Center COTR was Robert H. Pursel, AAR-432.

16. Abstract

Under contract to the FAA William J. Hughes Technical Center, the Naval Air Warfare Center has conducted an analysis to define the characteristics of large commercial transport turbine engine uncontained debris. The objective of the analysis was to define the debris size, weight, exit velocity, and trajectory that can be used to update Advisory Circular (AC) 20-128A. The effort was conducted by gathering historical data from uncontained engine failures. This data included, when available, phase of flight, engine operating condition, the failed engine component, aircraft damage location, and damage size. With this basic information, debris size was correlated to damage size. A methodology was developed to estimate debris exit velocity. Representative engine cases and cowls were defined and existing ballistic penetration equations used to calculate debris exit velocity. This analysis was conducted for disk and blade failures on fan, compressor, and turbine components.

Results of the analysis provided some interesting insight to these events. Looking at the debris trajectories, the analysis shows that the trajectories defined in AC 20-128A are too narrow and should be expanded significantly. Also, the analysis highlights the fact that during an uncontained event the aircraft is subjected to multiple "small" fragment impacts, not just a single impact. It is the combined effects from the small fragments that pose the highest hazard potential to the aircraft.

17. Key Words	18. Distribution Statement
Uncontained failure, Debris characterization, Debris database, Blade debris, Disk debris, Uncontained blade failure, Uncontained debris trajectory, Residual debris energy, Trajectory angles, Disk failure, Blade failure, Fan failure, Rim failure, BARRIER, Engine case penetration, Residual velocity, Damage ratio, Multiple debris	This document is available to the public through the National Technical Information Service (NTIS) Springfield, Virginia 22161.

19. Security Classif. (of this report)	20. Security Classif. (of this page)	21. No. of Pages	22. Price
Unclassified	Unclassified	88	

TABLE OF CONTENTS

		Page
EXECUTIVE SUMMARY		ix
1.	INTRODUCTION	1-1
1.1	Uncontained Event History	1-2
2.	MODEL DEVELOPMENT	2-1
2.1	Assumptions	2-1
2.1.1	Debris Database Assumptions	2-1
2.1.2	Debris Energy Assumptions	2-1
2.1.2.1	Blade Debris From Disk Failures	2-1
2.1.2.2	Engine Casings and Cowlings	2-2
2.1.2.3	Blade Debris From Uncontained Blade Failures	2-2
2.1.2.4	Aerodynamic Effects on Blade Debris	2-5
2.1.2.5	Aerodynamic Effects on Disk Debris	2-5
2.2	Procedure	2-6
2.2.1	Analytical Procedure	2-6
2.2.1.1	Blade Debris From a Disk Failure	2-6
2.2.1.2	Disk Debris Aerodynamic Effects	2-8
2.2.1.3	Blade Debris From a Blade Failure	2-8
3.	DEBRIS DATABASE OVERVIEW	3-1
4.	DEBRIS CHARACTERIZATION	4-1
4.1	Fan Analysis	4-1
4.1.1	Fan Disk Failure	4-1
4.1.1.1	Fan Blade Damage From a Disk Failure	4-1
4.1.1.2	Fan Disk Aerodynamic Effects	4-6
4.1.1.3	Fan Disk Damage	4-9
4.1.2	Fan Blade Failure	4-10
4.1.2.1	Aft Trajectory Angles—Engine Case Penetration	4-12

4.1.2.2 Forward Trajectory Angles—Helical Model 4-13
4.1.2.3 Forward Trajectory Angles—Reingestion Model 4-16

4.1.3 Fan Issues 4-16

4.2 Compressor Analysis 4-17

4.2.1 Compressor Disk Failure 4-17

4.2.1.1 Compressor Blade Damage From a Disk Failure 4-17
4.2.1.2 Compressor Disk Aerodynamic Effects 4-20
4.2.1.3 Compressor Disk Damage 4-21

4.2.2 Compressor Rim Failure 4-21

4.2.2.1 Compressor Blade Damage From a Rim Failure 4-21
4.2.2.2 Compressor Rim Damage 4-23

4.2.3 Compressor Issues 4-23

4.3 Turbine Analysis 4-23

4.3.1 Turbine Disk Failure 4-24

4.3.1.1 Turbine Blade Damage From a Disk Failure 4-24
4.3.1.2 Turbine Disk Aerodynamic Effects 4-36
4.3.1.3 Turbine Disk Damage 4-36

4.3.2 Turbine Rim Failure 4-36

4.3.2.1 Turbine Blade Damage From a Rim Failure 4-36
4.3.2.2 Turbine Disk Damage From a Rim Failure 4-38

4.3.3 Turbine Blade Failure 4-39

4.3.3.1 Engine Case Penetration Analysis 4-44
4.3.3.2 Nonengine Case Penetration—Helical Analysis 4-45

4.3.4 Turbine Issues 4-45

5. SUMMARY 5-1

6. DEBRIS PENETRATION MODEL CORRELATION 6-1

6.1 Blade Failure Helical Model 6-1
6.2 Fan Disk Event Blade Analysis 6-3

7. RECOMMENDATIONS 7-1

8. REFERENCES 8-1

Appendix A—Modeling of Aerodynamic Effects on Uncontained Engine Debris

LIST OF ILLUSTRATIONS

Figure		Page
1-1	Uncontained Turbine Disk Event	1-1
2-1	Blade Debris Penetration Model for Disk Events	2-2
2-2	Required Inputs for the Barrier Equations	2-3
2-3	General Engine Cowling Layout	2-4
2-4	Blade Debris Penetration Model for Blade Events	2-4
2-5	Turbine Tail Pipe Showing Helical Exit Trajectory	2-5
2-6	Disk Aerodynamic Assumptions	2-6
2-7	Sample Plot of Debris Size Versus Trajectory Angle	2-7
2-8	Disk Rim Segment Versus Fuselage Hole Size	2-7
2-9	Debris Energy Estimation Plot	2-9
2-10	Sample Predicted Skin Thickness Plot	2-10
2-11	Debris Impact Orientation Sensitivity Analysis	2-10
4-1	Typical Engine to Inlet-Nacelle Geometry	4-2
4-2	Fan Disk Failure Debris	4-2
4-3	Fan Blade Damage From a Disk Event	4-3
4-4	Fan Blade Damage From a Disk Event for Fuselage-Mounted Engines	4-3
4-5	Fan Cowl Model for Fan Disk Events	4-4
4-6	Debris Energy Estimation for a 25% HBR Fan Blade	4-5

4-7	Predicted Skin Thickness to Defeat a 25% HBR Fan Blade	4-6
4-8	Debris Energy Estimation for a 25% LBR Fan Blade	4-7
4-9	Predicted Skin Thickness to Defeat a 25% LBR Fan Blade	4-8
4-10	HBR Fan Disk Windage Effects	4-8
4-11	LBR Fan Disk Windage Effects	4-9
4-12	Fan Disk Damage	4-9
4-13	Fan Disk Damage From a Disk Event	4-10
4-14	Fan Blade Damage From a Blade Event	4-10
4-15	Fan Blade Damage From a Blade Event for Wing-Mounted Engine	4-11
4-16	Fan Blade Damage From a Blade Event for Fuselage-Mounted Engines	4-11
4-17	Fan Blade Helical Trajectory	4-12
4-18	Fan Blade Exit Trajectory	4-13
4-19	Fan Blade Helical Trajectory	4-14
4-20	Helical Trajectory	4-14
4-21	Blade Debris Exit and Cowl Damage	4-15
4-22	Compressor Blade Damage From a Disk Event	4-18
4-23	Damage Ratio Versus Trajectory	4-18
4-24	Debris Energy Estimation for a 100% Compressor Blade	4-19
4-25	Disk and Blade Damage From Compressor Disk Event	4-20
4-26	Predicted Skin Thickness to Defeat a 100% Compressor Blade	4-20
4-27	Compressor Disk Windage Effects	4-21
4-28	Compressor Disk Fragment After Passing Through the Fuselage	4-21
4-29	Compressor Disk Damage From a Disk Event	4-22
4-30	Compressor Blade Damage From a Rim Event	4-22
4-31	Compressor Disk Damage From a Rim Event	4-23

4-32	Turbine Blade Damage From a Disk Event	4-24
4-33	Turbine Blade Fuselage Damage From a Disk Event	4-25
4-34	Turbine Blade Wing Damage From a Disk Event	4-25
4-35	Debris Energy Estimation for a 100% HP Turbine Blade	4-26
4-36	Predicted Skin Thickness to Defeat a 100% HP Turbine Blade	4-27
4-37	Debris Energy Estimation for HBR 50% LP Turbine Blade With the Cowl	4-28
4-38	Predicted Skin Thickness to Defeat a HBR 50% LP Turbine Blade With the Cowl	4-29
4-39	Debris Energy Estimation for HBR 50% LP Turbine Blade Without the Cowl	4-30
4-40	Predicted Skin Thickness to Defeat a HBR 50% LP Turbine Blade Without the Cowl	4-31
4-41	Debris Energy Estimation for LBR 50% LP Turbine Blade With the Cowl	4-32
4-42	Predicted Skin Thickness to Defeat a LBR 50% LP Turbine Blade With the Cowl	4-33
4-43	Debris Energy Estimation for LBR 50% LP Turbine Blade Without the Cowl	4-34
4-44	Predicted Skin Thickness to Defeat a LBR 50% LP Turbine Blade Without the Cowl	4-35
4-45	Turbine Disk Aerodynamic Effects	4-36
4-46	Turbine Disk Damage From a Disk Event	4-37
4-47	Trajectory of Rim Failure Event	4-37
4-48	Turbine Rim Fragments From Rim Peal Event	4-38
4-49	Turbine Blade Damage From a Rim Event	4-38
4-50	Fuselage Damage From Turbine Rim Debris	4-39
4-51	Turbine Disk Damage From a Rim Event	4-39
4-52	Turbine Blade Damage From a Blade Event	4-40
4-53	Turbine Blade Damage From a Blade Event for Fuselage-Mounted Engines	4-41
4-54	Turbine Blade Damage From a Blade Event for Wing-Mounted Engines	4-41

4-55 HP Turbine Blade Damage From a Blade Event 4-42

4-56 LP Turbine Blade Damage From a Blade Event 4-42

4-57 Turbine Blade Damage From the Last Stage of Low Bypass Ratio Engines 4-43

4-58 Turbine Blade Damage From the Last Stage of High Bypass Ratio Engines 4-43

4-59 Turbine Overspeed Resulting in Uncontained LPT Blade Release (Near-Field Fuselage Damage) 4-44

6-1 Engine Cowl and Aircraft Model 6-3

LIST OF TABLES

Table Page

1-1 Transport Aircraft Uncontainment History 1-3
3-1 Event Type Summary 3-1
3-2 Percent of Damages Causing Systems Damage 3-2
3-3 Debris Damage Size Ratio 3-2
3-4 Found Debris Database 3-3
3-5 Debris Size Correlated to Damage Bin Size 3-4
4-1 Fifty Percent Fan Debris Residual Velocity Upon Leaving the Engine Cowl 4-13
4-2 HBR Fan Debris—Helical Model 4-15
4-3 LBR Fan Debris—Helical Model 4-16
4-4 HBR Fan Debris—Reingestion Model 4-17
4-5 LBR Fan Debris—Reingestion Model 4-17
4-6 Turbine Blade Residual Velocity (Engine Case and Cowl) 4-44
4-7 Turbine Blade Residual Velocity 4-45
5-1 Debris Characterization Summary 5-1
6-1 Inner Blade Fragment 6-2
6-2 Outer Blade Fragment 6-2
6-3 Blade Root Section, 100% Initial Debris Velocity 6-4
6-4 Blade Root Analysis, 75% Initial Debris Velocity 6-4
6-5 Blade Tip Fragment, 100% Initial Debris Velocity 6-5
6-6 Blade Tip Fragment, 75% Initial Debris Velocity 6-5

EXECUTIVE SUMMARY

FAR/JAR 25.903(d)(1) states that "Design precautions must be taken to minimize the hazards to the airplane in the event of an engine rotor failure...". Minimization of the hazard to the airplane can be accomplished in several ways: (1) minimize the frequency of uncontained disc events, (2) minimization of fragment energies, quantities and related trajectories, and (3) mitigation of the hazard to safe flight through mitigation provided in aircraft design and construction. It is understood that absolute containment is unlikely, thus the minimization of fragment energies and mitigation in the aircraft are the reasonable methods of compliance.

The Aviation Rulemaking Advisory Committee (ARAC) 25.903(d)(1) Task Group is in the process of updating the engine uncontained fragment hazard model as defined in Advisory Circular (AC) 20-128A. The updated model will be implemented in AC 20-128B. The analysis defined herein is a significant part of that effort as it provides a methodology to define fragment energies and defines a generic engine fragment model. Additionally, some preliminary modeling of ballistic penetration of aircraft structures and potential barrier materials is presented.

1. INTRODUCTION.

Uncontained gas turbine engine events, figure 1-1, are a basic threat to aircraft safety. To better defend against this threat, debris characteristics must be accurately defined. Debris characterization includes defining debris size, mass, velocity, trajectory angles, and number of fragments per event type. This report defines these characteristics for different engine types and failure modes. Recommendations for future analysis are also provided.

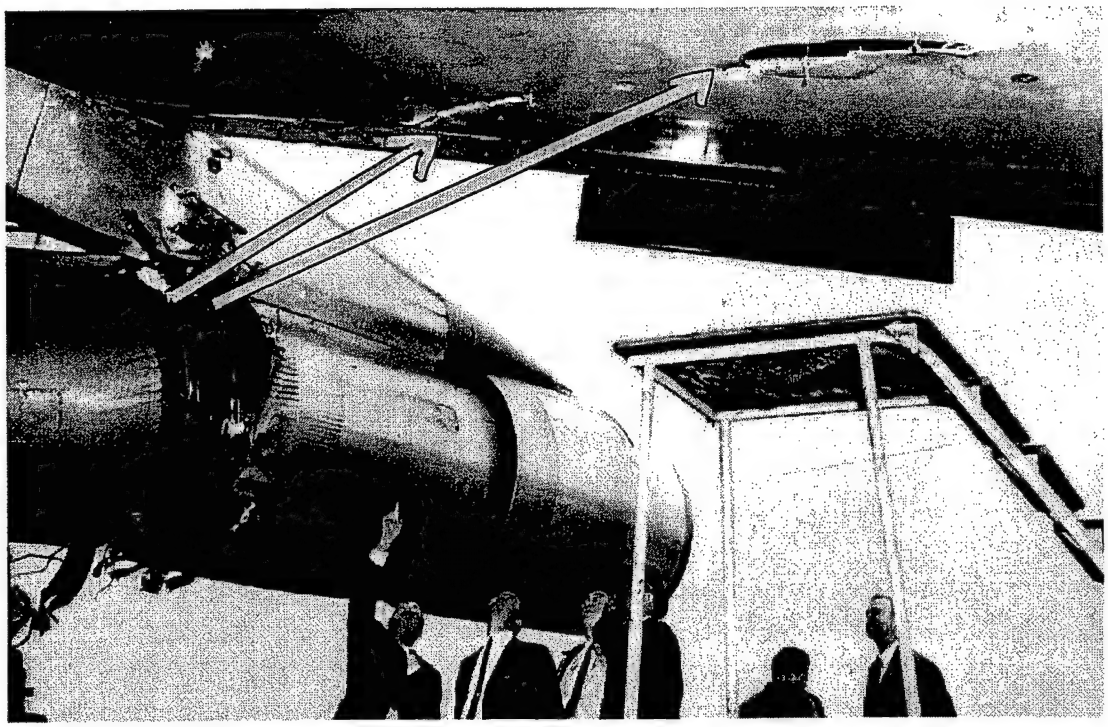

FIGURE 1-1. UNCONTAINED TURBINE DISK EVENT

The Aviation Rulemaking Advisory Committee (ARAC) engine specialists assisted with project direction and reviewed the initial results. Specific recommendations for data analysis and component failure mechanisms from the specialists have been incorporated.

Work began in FY-96 with the collection of data of uncontained engine events. A database was developed that includes details of 65 large engine uncontained events. Large engines are defined as those engines that power narrow- and wide-body commercial transport aircraft. (Commuter and business jet engines are considered small engines.) The database spans the period from November 1961 through the present. The primary sources of information were private sector engine companies and airframe companies. A debris database was established and used to characterize typical debris sizes and trajectory angles for specific component failures. Two groups of debris data were analyzed: (1) small fragments (blades) that may be mitigated with appropriate skin thicknesses and (2) large debris that may only be mitigated with redundancy and separation.

A model was developed to estimate debris kinetic energy as a function of trajectory angle. The presented results are generic in nature to provide an overview of uncontained debris characteristics. If required, the procedures used in this analysis could be applied to a specific engine and a specific aircraft configuration. The basic assumptions and procedures used to generate the data are presented in the next section followed by an overview of results from the debris database and then by specific debris characterization.

A thorough search was conducted for data to be included in the analysis. Despite the relatively small number of data-rich incidents used in the analysis, hundreds of events were reviewed with the support of engine and airframe manufacturers. Additionally, the National Transportation Safety Board was very cooperative, allowing detailed data to be collected on-site for several of the events that took place during the course of this effort. The 65 events in the database are not merely a representative selection of the data but the only events with sufficient information to conduct the type of analysis described herein. Many of the uncontained event records reviewed had details of the component failures but were lacking aircraft damage details. There are many additional fan blade and turbine disk events that are not in the database because of a lack of detailed damage data. For the most part, the lack of such detailed event information is felt to be due either to the lack of aircraft damage being present or the damage being of such a minor nature that on-site repairs were conducted and the aircraft returned to service in less than 24 hours. Specific parameters needed in the analysis include aircraft type, engine model, failed component, engine position, engine component dimensions (disk diameter or blade length), damage location (defined by xyz coordinates relative to the failed component, or aircraft station number), size of the damage (length and width), and any subsequent damage to aircraft structure or subsystems. If the debris that caused the aircraft damage was found, the size and mass of the fragment was included.

The large engine database contains information on narrow- and wide-body commercial transport aircraft, including the Boeing 707, 720, 737, 727, 747, 767; the Douglas DC-8, DC-9, MD-80, MD-88, DC-10; the Lockheed L1011; and the Airbus A300. The engines included were the Pratt & Whitney JT3D, JT4A, JT8D, JT9D, and TF33; the General Electric CF6; the Rolls Royce RB211, and the Conway 508. The reader is reminded that the inclusion of an engine type does not imply that this engine type is any more susceptible to an uncontained failure than any other engine, but that data from such event was available and complete for the purpose of this study. Likewise, the exclusion of an engine type does not imply that the engine type has not had an uncontained failure or is less likely to fail.

1.1 UNCONTAINED EVENT HISTORY.

To get a better understanding of the uncontained engine failure history, a review of two Aerospace Information Reports (AIR) was conducted. These documents, AIR 4003 [1] and AIR 4770 [2], categorize uncontained turbine rotor events between 1976 to 1983 and 1984 to 1989 respectively. This data provides a historical picture of past uncontained engine failures (table 1-1). The presented is the number of events by engine component (fan, compressor and turbine) and failure type (blade and disk) for large engines. This data provides insight to the

components with the most failures and provides a check against recently developed database to ensure that emphasis is placed in the right areas.

TABLE 1-1. TRANSPORT AIRCRAFT UNCONTAINMENT HISTORY

	AIR 4003	AIR 4770	Total
Fan disk	5	9	14
Fan blade	74	53	127
Fan other	9	0	9
Compressor disk	25	10	35
Compressor blade	4	0	4
Compressor other	11	2	13
Turbine disk	22	17	39
Turbine blade	44	39	83
Turbine other	8	10	18
Totals	203*	143*	346*

*(One Unknown in 4003 and three unknowns in 4770)

Most of the events in the "Other" category were the result of component spacer/seal failures.

2. MODEL DEVELOPMENT

To provide a working model for characterizing engine debris, certain assumptions in analyzing the debris database and in predicting debris energy levels were utilized. The assumptions are defined in this section followed by a discussion of the analytical procedure.

2.1 ASSUMPTIONS.

2.1.1 Debris Database Assumptions.

Incident reports provide aircraft damage descriptions, but the actual debris that caused the damage is often unknown. To help provide an estimate of the debris size, the damage locations were normalized to the engine component size. For blade related damage, the normalization factor was maximum blade length; for disk related damage, the normalization factor was disk diameter. The normalized damage size is often referred to as damage ratio within this document.

2.1.2 Debris Energy Assumptions.

Emphasis was placed on analyzing blade debris energy levels, since this debris may be mitigated with appropriate shielding. There are several considerations in estimating blade debris kinetic energy. Two failure modes are addressed: blade debris from disk events and blade debris from blade events. Details of the analysis for each of these failure modes are defined below. A significant factor in each of these failure modes is external aerodynamic drag effects.

2.1.2.1 Blade Debris From Disk Failures.

When evaluating blade debris energy from a disk event, energy loss from penetrating the engine case is NOT estimated. The assumption is most of the debris will exit through an existing hole in the engine case caused by a disk segment. Disk segments generally stay within the plane of rotation, while smaller pieces such as blade debris get deflected to the larger trajectory angles. However, blade debris must still penetrate the engine cowling.

Figure 2-1 summarizes the basic model used for analyzing disk events. Initial debris velocity ($V_{initial}$) is the tangential velocity based on the centroid location ($r_{cg}\omega$). Upon release from within the engine, debris will initially want to travel tangentially outward in the plane of rotation, but through impacts with the engine structure and other debris, some particles may get deflected to their final trajectory angles.

Energy is lost during this deflection process. A conservative model is to assume the debris velocity is proportional to the cosine of the trajectory angle ($V_{debris} = V_{initial} \cos \theta$) as shown in figure 2-1. The assumption is the velocity component normal to the final trajectory path was lost during an impact. This assumption was previously used in reference 3 which examined disk fragment characteristics.

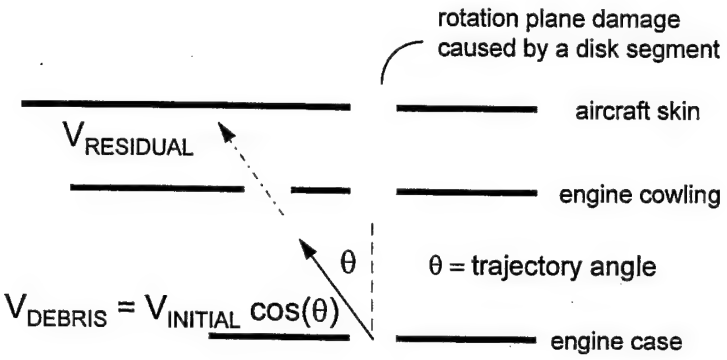

FIGURE 2-1. BLADE DEBRIS PENETRATION MODEL FOR DISK EVENTS

The estimated energy loss from penetrating the cowl is provided by the BARRIER equations. They are empirically based equations for fragment penetration analysis [4]. The equations from reference 4 are used in the vulnerability analysis process to determine the vulnerable area of military aircraft. The required fragment obliquity and orientation parameters for BARRIER are defined in figure 2-2. BARRIER calculates fragment presented area by width*length*cosine (orientation angle). It is important to understand the difference between obliquity angle and orientation angle. The obliquity angle refers to the angle between the debris velocity vector and surface of the plate the debris is impacting. The fragment orientation angle is defined as the angle created between the fragment length and a line normal to the debris velocity vector (figure 2-2(b)). The obliquity angle is used in BARRIER to calculate the relative thickness of the plate that the debris is impacting.

2.1.2.2 Engine Casings and Cowlings.

A generic set of engine casings and cowlings were used in this analysis. The values selected were average values based on data provided by engine and airframe manufacturers (figure 2-3). The cowlings used in this particular analyses are provided in each section.

2.1.2.3 Blade Debris From Uncontained Blade Failures.

For fan, compressor, and turbine blade failures, blade debris energy loss from penetrating the engine case should be considered except in two special cases. For blade debris which must penetrate the engine case and the engine cowl, an edgewise penetration (debris orientation of 80 degrees) through the engine case is assumed followed by a tumbling penetration (debris orientation of 45 degrees) through the cowl (refer to figure 2-4). The engine case was represented by 0.25 inch of hardened steel.

There are two special fan blade failure scenarios where the debris does not penetrate the engine case. First, during a fan blade failure a blade tip fragment is liberated as the blade buckles against the containment ring. The tip fragment travels forward of the containment ring into the inlet in a helical motion. Estimated debris velocity is 75% of the tip velocity. Eventually a fragment edge catches the soft inner wall and penetrates the initial wall edgewise (debris

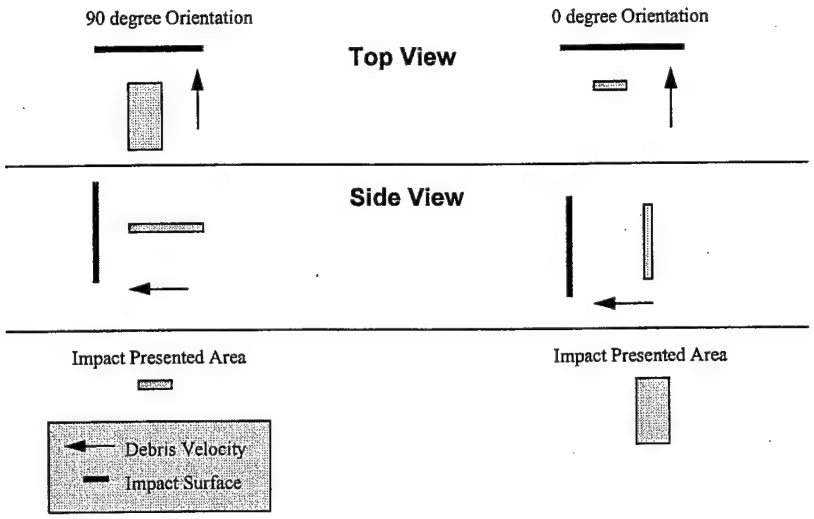

(a) Impact Orientation and Presented Area

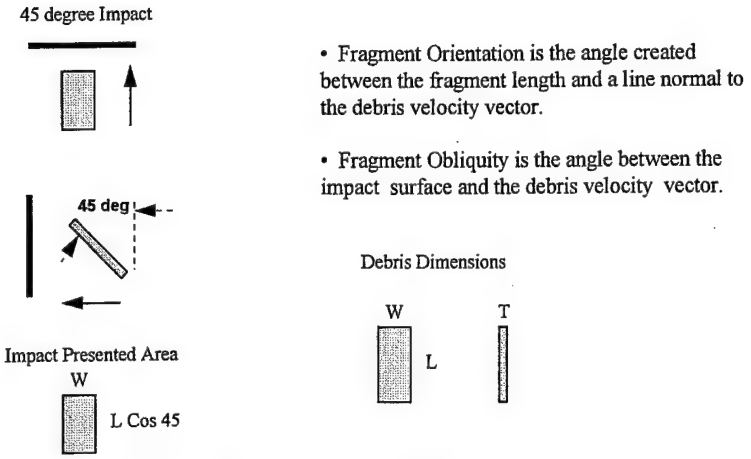

(b) Debris Orientation for a 45 degree Penetration

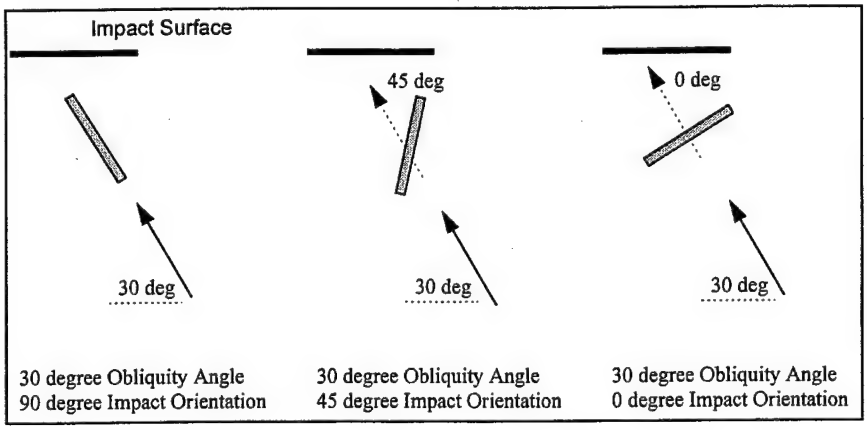

(c) Fragment Obliquity and Orientation

FIGURE 2-2. REQUIRED INPUTS FOR THE BARRIER EQUATIONS

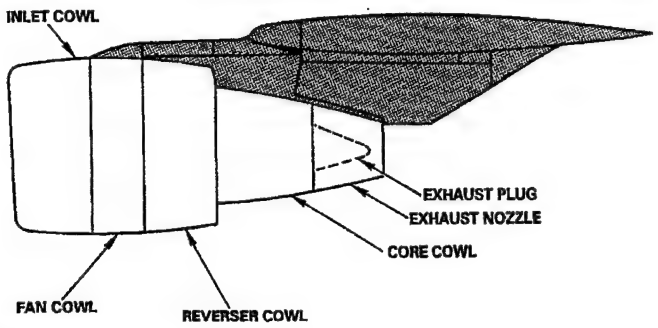

Skin Thickness (in)

Fan/Inlet Cowl	Compressor Cowl	Core / Turbine Cowl
0.025 Al	0.040 Al	0.040 Al
0.025 Al		None
0.040 Al		

Note: Thrust reverser was not modeled because most of the data was for engines without a fan reverser.

FIGURE 2-3. GENERAL ENGINE COWLING LAYOUT

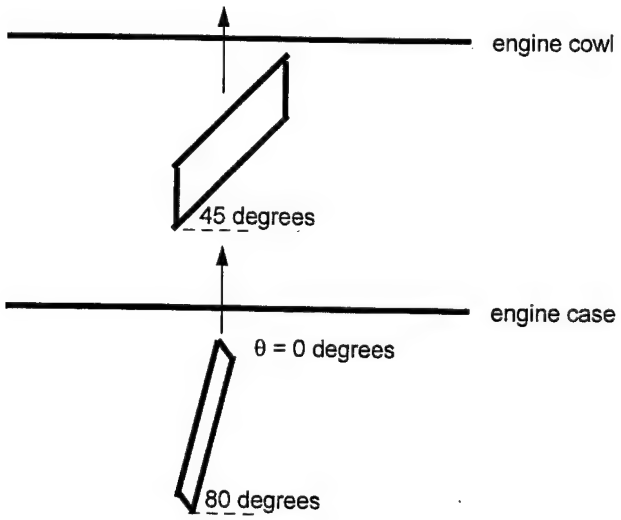

FIGURE 2-4. BLADE DEBRIS PENETRATION MODEL FOR BLADE EVENTS

orientation of 80 degrees). After this initial penetration, the fragment is assumed to be tumbling (debris orientation of 45 degrees). BARRIER is used to estimate the energy loss from penetrating the inlet cowl.

The second scenario involves fan debris that is reingested into the engine and then kicked forward by the fan rotor. Reference 5 provides a method for estimating the debris mass and velocity as a function of trajectory angle for this process. BARRIER is then used to estimate the energy loss from penetrating the inlet cowl. It is assumed the debris is tumbling freely during this time (orientation angle of 45 degrees).

There is also a special turbine blade scenario in which the blade fragments do not penetrate the engine case or cowl. This scenario pertains to last stage turbine blade events where the blade fragments exit the engine out the tailpipe as seen in figure 2-5 but are initially traveling in a helical trajectory similar to the fan blade scenario. For this case, the blade fragment is assumed to lose 25% of its initial velocity due to fictional effects prior to exiting the tailpipe. The initial helical path is influenced by the presence of struts and mixers. Additional discussion about this special case is provided in section 4.3.3.2.

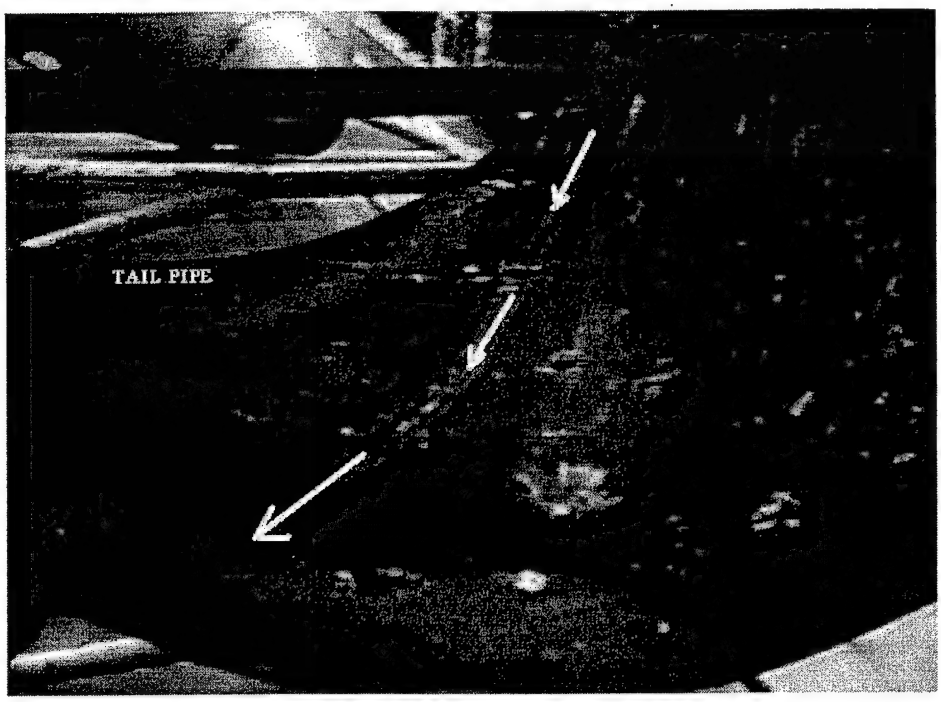

FIGURE 2-5. TURBINE TAIL PIPE SHOWING HELICAL EXIT TRAJECTORY

2.1.2.4 Aerodynamic Effects on Blade Debris.

Once the debris exits the engine, it is subjected to aerodynamic drag. Debris liberated from a wing-mounted engine may experience a significant reduction in kinetic energy before it reaches an aircraft fuselage (far-field effects). According to reference 6, an appropriate drag coefficient for a flat plate in three-dimensional flow is 1.17. A 45 degree orientation is also used to represent the average presented area. Standard equations of motion are used. The analysis was conducted at a flight condition of 35,000 ft, Mach 0.85. The debris is assumed to travel 30 ft from the engine to the impact point. Specific details are presented in appendix A.

2.1.2.5 Aerodynamic Effects on Disk Debris.

Aerodynamic effects on disk debris were estimated using the same routine described in appendix A. To model a disk fragment, a different set of assumptions was used to determine the effect drag has on the debris. The blade debris aerodynamic analysis assumed a purely tumbling fragment. To model a disk fragment, rotation was assumed in the disk plane of rotation, and the

debris was modeled as a flat plate relative to the free stream velocity (figure 2-6). Thus, the reference area is planform of the debris arc segment. A flat plate drag coefficient (cd = 2.0) was used on the fragments. The analysis was conducted at a flight condition of 35,000 ft, Mach 0.85. This flight condition was chosen to provide an upper limit of trajectory shift that can be expected due to aerodynamic drag. The initial trajectory angle is 0 degrees. Disk fragment characteristics (length, width, weight, and initial velocity) are based on the most common fragment size for the given category.

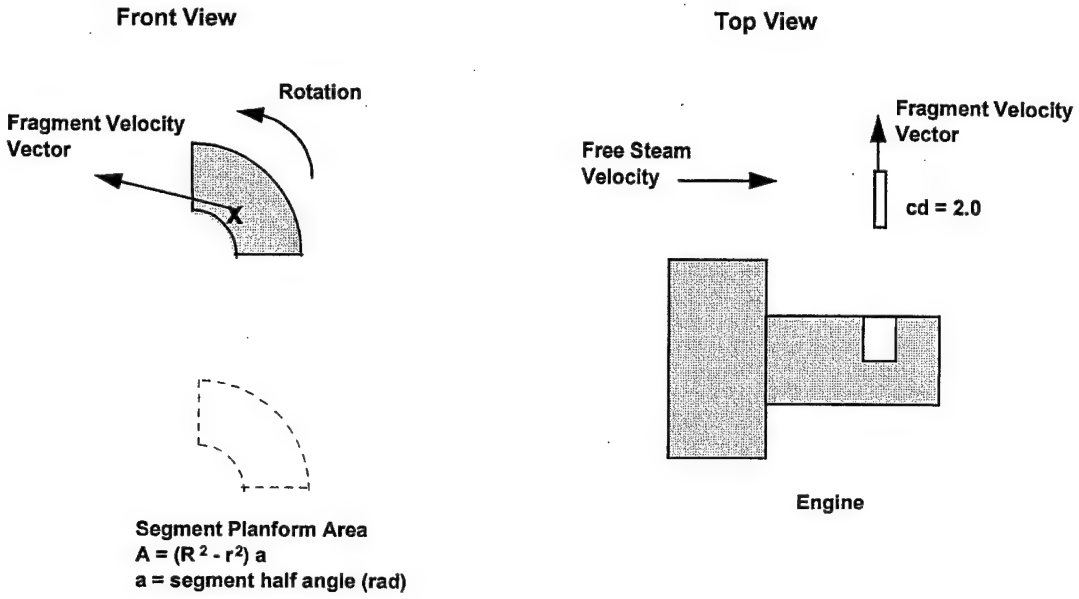

FIGURE 2-6. DISK AERODYNAMIC ASSUMPTIONS

2.2 PROCEDURE.

2.2.1 Analytical Procedure.

There are two constituents that make up the Uncontained Debris Trajectory-Energy Model. The first is the debris trajectory limits, which are defined by sorting the data in the uncontained debris database. The second is the debris penetration analysis, which defines the debris residual velocities and energy estimates. It is the combination of these two analyses that make up the uncontained debris model.

Data plots are generated using the above assumptions. The following section discusses which plots were generated and how they were used.

2.2.1.1 Blade Debris From a Disk Failure.

The debris database is first used to evaluate debris size versus trajectory angle. A sample plot for small fragment (compressor blade) damage is shown in figure 2-7. The chart plots debris damage ratio versus trajectory angle. Damage ratio is the aircraft damage length divided by the

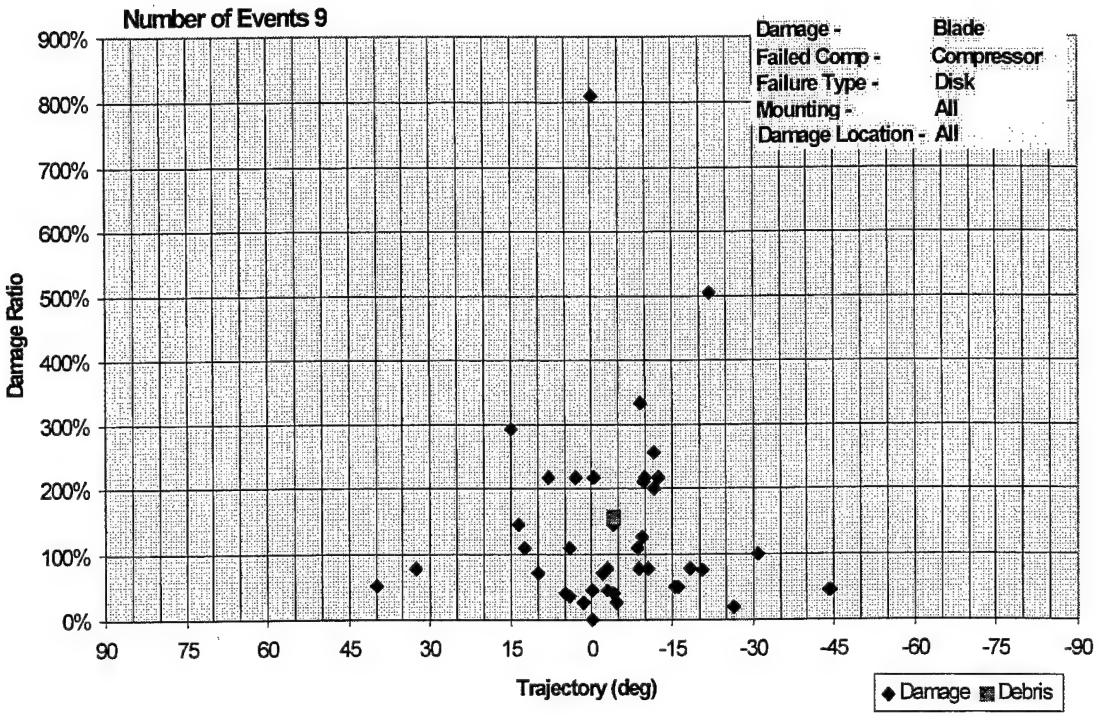

FIGURE 2-7. SAMPLE PLOT OF DEBRIS SIZE VERSUS TRAJECTORY ANGLE

original component length (blade or disk diameter). Figure 2-8 shows the disk rim segment versus fuselage hole size. Positive angles are forward trajectories, negative angles are aft of the rotor plane of rotation. The plot defines the debris size that includes approximately 90% of all fragments and the corresponding trajectory angles. For this example, a 100% compressor blade was selected.

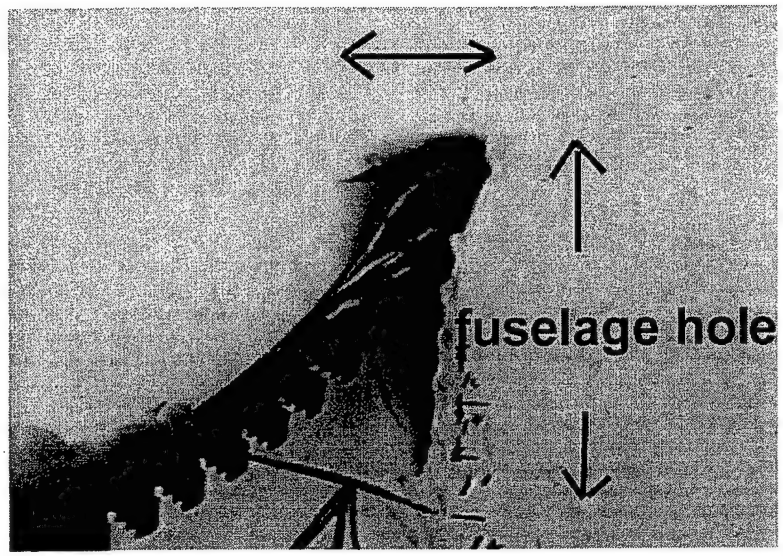

FIGURE 2-8. DISK RIM SEGMENT VERSUS FUSELAGE HOLE SIZE

The energy level of this debris is then estimated using the assumptions in section 2.2. Debris energy upon leaving the engine cowl is shown figure 2-9(a) (sample). The trajectory angle limits from figure 2-7 are also plotted to help focus the analysis. Figure 2-9(a) does not include aerodynamic effects and essentially represents the debris energy upon impact for a fuselage-mounted engine (near-field effects).

Aerodynamic effects are a significant factor for debris liberated from a wing-mounted engine (far-field effects, see appendix A). To provide the relative difference in debris kinetic energy from aerodynamics, figure 2-9(b) (sample) plots residual debris energy after traveling 30 feet from the engine during a cruise flight condition of Mach 0.85 at 35,000 feet.

BARRIER is then used to estimate the required skin thickness to defeat blade debris liberated from fuselage- and wing-mounted engines (see figure 2-10). This provides a means of checking model predictions with empirical data. At some trajectory angle the debris kinetic energy will be insufficient to penetrate the aircraft skin. Fuselage skin thicknesses generally vary between 0.06 and 0.08 inch of 2024 aluminum. These values are then used to estimate where the minimum and maximum trajectory angles should occur and whether they match the values from the debris database.

The maximum trajectory angles are shown in figure 2-9(a) to verify that the angles from the trajectory plot are feasible. For example, the maximum aft trajectory angle (~ -55 degrees) of figure 2-9 is achievable only when aerodynamic forces are considered.

When estimating the required skin thickness to defeat a piece of debris, the debris was assumed to be oriented at 45 degrees, which represents the average tumbling orientation. If the debris entered at angles greater than 45 degrees, which approaches an edgewise penetration, the required skin thickness will increase. Figure 2-11 examines the sensitivity of debris orientation. Essentially, for 60 degrees or less the predictions are relatively clustered together. For orientations greater than 60 degrees, there is a dramatic increase in required skin thickness. Edgewise penetration may have to be considered for debris with large trajectory angles that normally would not have enough energy to penetrate the engine cowl or the fuselage structure.

2.2.1.2 Disk Debris Aerodynamic Effects.

Aerodynamic effects on disk fragments were also estimated. The same equations were used as described for the blade fragment aerodynamic effects. Assumptions for the disk analysis are provided in figure 2-6. The disk fragment is assumed to travel tangentially, initially in the rotor plane of rotation. The disk is assumed to act as a flat plate against the free stream air velocity. The drag coefficient used is 2.0.

2.2.1.3 Blade Debris From a Blade Failure.

A plot similar to figure 2-7 is generated to determine typical blade debris sizes for blade failure events. Using the assumption discussed in section 2.2.2, debris kinetic energy is then estimated. Results are provided in tabular format.

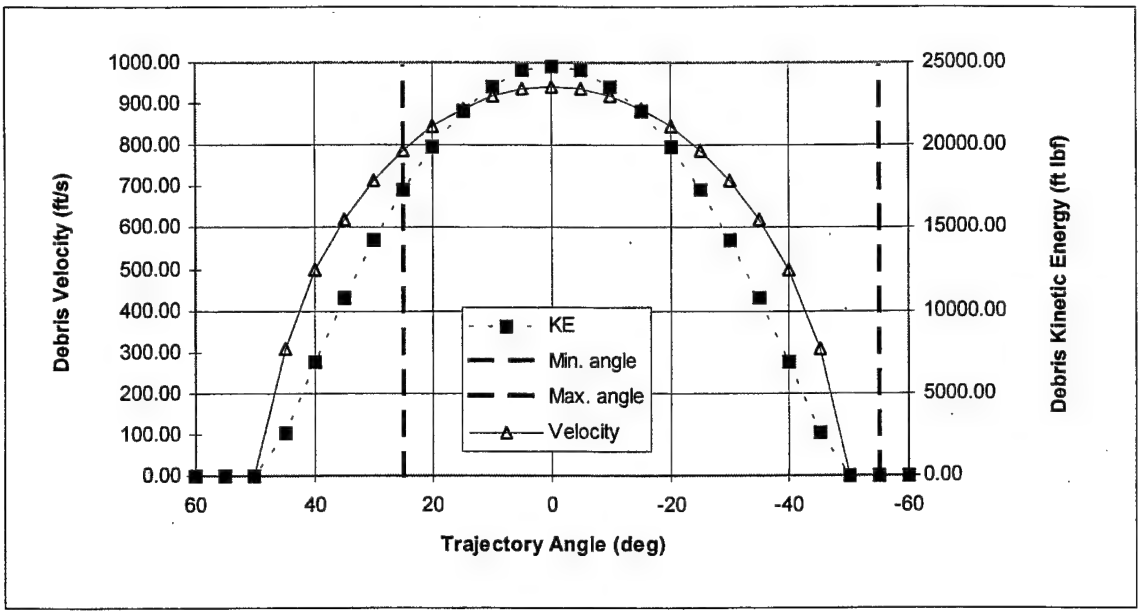

(a) Residual Velocity and Energy Once Outside the Cowl

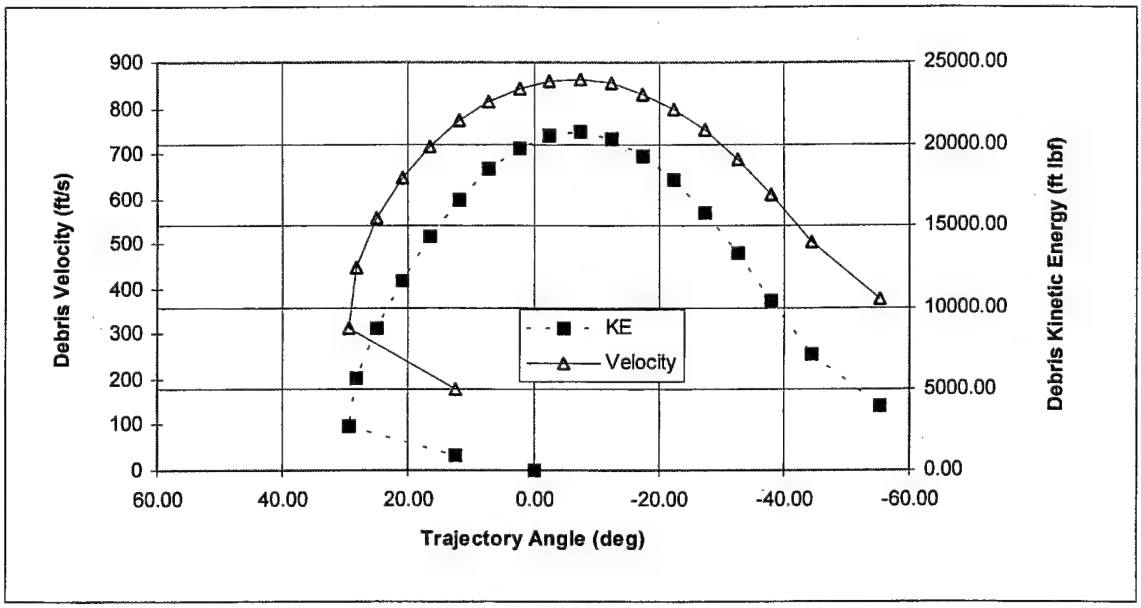

(b) Debris Characteristics After Traveling 30 ft From a Wing-Mounted Engine (Altitude = 35,000, Mach = 0.85)

FIGURE 2-9. DEBRIS ENERGY ESTIMATION PLOT

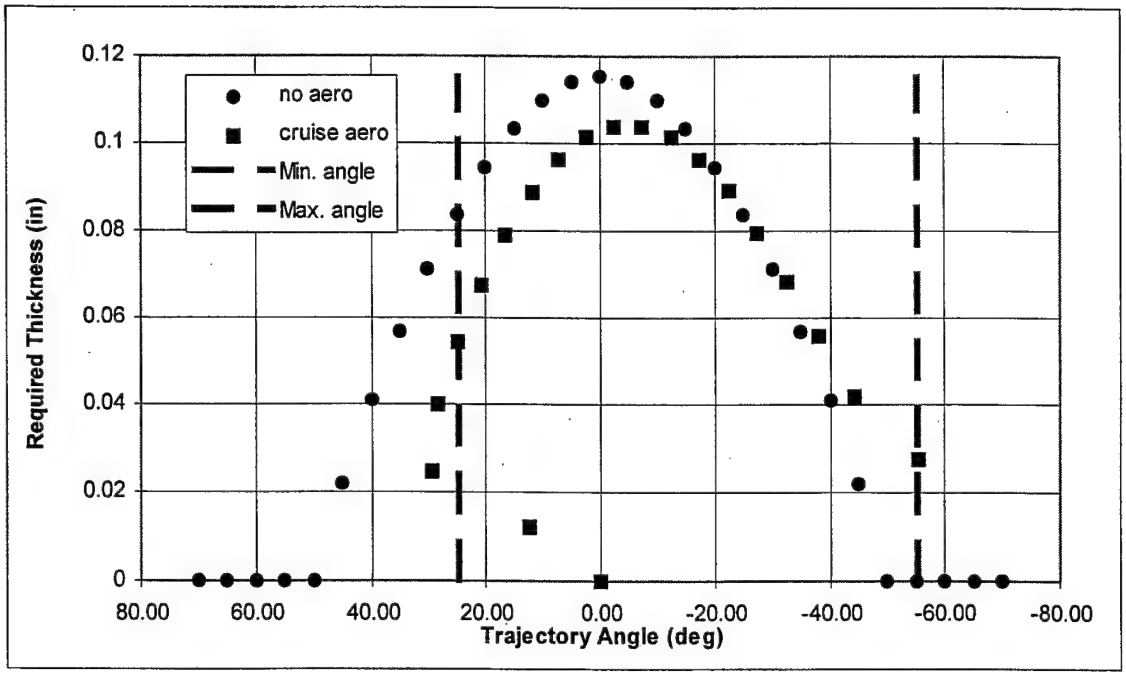

FIGURE 2-10. SAMPLE PREDICTED SKIN THICKNESS PLOT

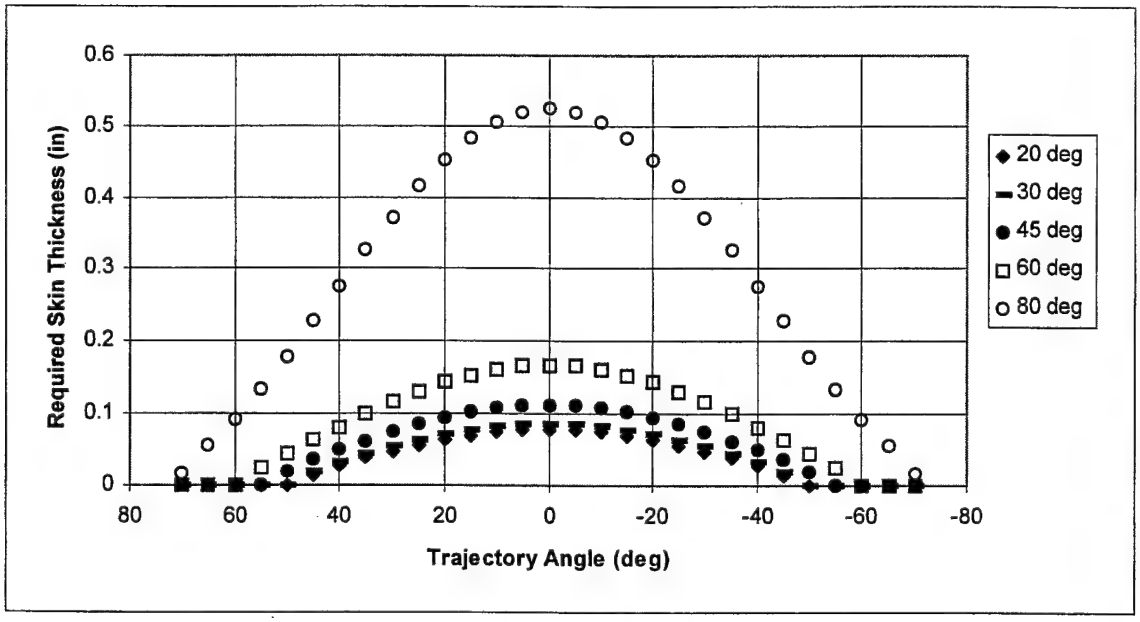

FIGURE 2-11. DEBRIS IMPACT ORIENTATION SENSITIVITY ANALYSIS

3. DEBRIS DATABASE OVERVIEW.

The debris database was used to define debris trajectories and estimated debris size when actual sizes were unknown. Data was normalized and then sorted by failure mode (i.e., blade failure, disk failure, rim failure), damage source (i.e., blade debris, disk debris, rim debris), and engine mounting (wing or fuselage). The data was then plotted versus trajectory angle. Key plots are presented in conjunction with the debris energy estimations in section 4.

The normalized debris analysis does provide clear trends. Table 3-1 lists the different event types with the number of events and average number of aircraft damages per event. A review of table 3-1 shows fan disk events and turbine disk events to generate the largest amount of aircraft damaging debris.

TABLE 3-1. EVENT TYPE SUMMARY

Event Type	Number of Events	Average Number of Damages per Event	Maximum Number of Damages in a Single Event	Minimum Number of Damages in a Single Event
Fan Disk	8	21.9	73	3
Fan Blade	10	8.2	32	2
Compressor Disk	8	8.5	19	1
Compressor Rim	3	6.3	14	2
Turbine Disk	11	17.2	81	5
Turbine Rim	6	10.3	28	3
Turbine Blade	10	8.8	15	2

A tabulation was also conducted to define the number of times another aircraft system (system other than the failed engine) was damaged during an uncontained event (table 3-2). Loss of system includes failure modes like fuel tank penetrations, severed electrical wiring, severed hydraulics, or punctured pressurized cabin. Doing so has provided additional insight to the number of fragments exiting the engine and impacted the aircraft with a "high" energy level. It appears that overall about 10% of all the fragments that exit engine cases do so with sufficient energy to penetrate the aircraft (wing or fuselage) and cause damage to other systems. Compressor disk and rim failures have a higher percentage of systems damage than the other engine components.

The following sections describe the methodology used to define the fragments that have sufficient energy to penetrate the aircraft fuselage or wing skin and cause damage to other structure or systems. The methodology used provides a conservative yet realistic estimate of the debris energy. The energy estimates are not, however, the most conservative estimate.

Table 3-3 shows the estimated component debris size without regard to failure mode. For example, all fan blade fragments are grouped together whether they came from a fan disk event or a fan blade event.

TABLE 3-2. PERCENT OF DAMAGES CAUSING SYSTEMS DAMAGE

Event Type	Number of Damages	Number of Damages to Systems	Percent of Damages with Systems Damaged
Fan Disk	175	13	7.4%
Fan Blade	74	2	2.7%
Compressor Disk	68	11	16.2%
Compressor Rim	19	4	21.1%
Turbine Disk	189	24	12.7%
Turbine Rim	61	5	8.2%
Turbine Blade	88	10	11.4%
TOTAL	709	70	9.9%

TABLE 3-3. DEBRIS DAMAGE SIZE RATIO

Component Type	Percent Blade Length				
	<= 15%	15% to 25%	25% to 50%	> 50%	Totals
Fan Blade	119 52.4%	41 18.1%	35 15.4%	32 14.1%	227.00 100.0%
Compressor Blade	2 3.2%	1 1.6%	12 19.0%	48 76.2%	63.00 100.0%
Turbine Blade	33 10.9%	77 25.5%	124 41.1%	68 22.5%	302.00 100.0%
Component Type	Percent Disk Diameter				
	<25%	25% to 50%	50% to 100%	>100%	Totals
Fan Disk	0 0.0%	0 0.0%	3 50.0%	3 50.0%	6.00 100.0%
Compressor Rim	1 20.0%	1 20.0%	3 60.0%	0 0.0%	5.00 100.0%
Compressor Disk	1 33.3%	1 33.3%	1 33.3%	0 0.0%	3.00 100.0%
Turbine Rim	2 50.0%	1 25.0%	1 25.0%	0 0.0%	4.00 100.0%
Turbine Disk	1 16.7%	1 16.7%	1 16.7%	3 50.0%	6.00 100.0%

Normalized data was grouped into the four bins shown in table 3-3. The purpose was to show the most common debris size for each component (fan blade, compressor blade, turbine blade, etc.). The total number data points are also presented. Table 3-3 proved useful in categorizing blade debris, which represents over 95% of the damage recorded in the database.

A special note must be made concerning the blade damage results from table 3-3. The debris database does include actual debris retrieved from some of the incidents, and the debris sizes are shown in table 3-4. The engine specialist members from the ARAC group noted that in

table 3-3 some hole size data yielded disk particle estimates > 100% of the diameter of the disk. Additionally, it was noted that numerous fan blade events yielded estimates > 50% blade size particles even though no material was missing from the fan rotor of this geometric size. An explanation for the damage data yielding these inflated values is that the damage values were based on cuts, tears, and holes in the fuselage and wing skins. These aircraft surfaces are not flat and the debris impact is not perpendicular to the surface. Debris that impacts an arc section of the skin will produce a hole longer than the debris that causes the damage. The ARAC Group did request data sorts on table 3-4 to compare with the bin results shown in table 3-3. Unfortunately, the amount of actual blade debris data is too scarce for accurate comparisons.

TABLE 3-4. FOUND DEBRIS DATABASE

Component Type	Percent Blade Length				
	< 15%	15% to 25%	25% to 50%	> 50%	Totals
Fan Blade	0 0.0%	2 40.0%	1 20.0%	2 40.0%	5
Compressor Blade	1 100.0%	0 0.0%	0 0.0%	0 0.0%	1
Compressor Blade	0 0.0%	1 7.7%	10 76.9%	2 15.4%	13
Component Type	Percent Disk Diameter				
	< 25%	25% to 50%	50% to 100%	> 100%	Totals
Fan Disk	1 11.1%	0 0.0%	4 44.4%	4 44.4%	9
Compressor Rim	8 66.7%	4 33.3%	0 0.0%	0 0.0%	12
Compressor Disk	0 0.0%	4 57.1%	2 28.6%	1 14.3%	7
Turbine Rim	2 33.3%	2 33.3%	1 16.7%	1 16.7%	6
Turbine Disk	1 25.0%	1 25.0%	1 25.0%	1 25.0%	4

Representative debris sizes for the respective bins in table 3-3 are shown in table 3-5. For the fragment types within the bins identified in table 3-3, average debris dimensions, debris mass, and initial debris velocities were used from the database of known debris (table 3-4). When actual data was unavailable, component information was obtained from engine drawings. Sizes were based on the actual debris found and the typical engine sizes within the debris database. Table 3-5 provides these estimates as well as the initial debris velocity upon release. (It is understood that for the analysis of a specific engine, debris size and weight will be based on the engine dimensions, materials, and operating speeds of each stage of the engine. If that data is unavailable, the data in table 3-5 provides a good starting point.)

TABLE 3-5. DEBRIS SIZE CORRELATED TO DAMAGE BIN SIZE

		15%	25%	50%	100%			
Fan Blade								
HBR	Length (in)	4.8	8.0	16.0	32.0		Blade Tip Dia	90
	Width (in)	4.8	8.0	8.0	8.0		Fan RPM	3600
	Thickness (in)	0.2	0.2	0.3	0.4			
	Weight (lb)	0.6	1.8	4.5	9.0			
	Velocity (ft/sec)	1338	1288	1162	911			
LBR								
	Length (in)	2.5	4.0	7.5	15.5		Blade Tip Dia	45
	Width (in)	2.5	4.0	5.0	5.0		Fan RPM	8100
	Thickness (in)	0.2	0.2	0.3	0.4			
	Weight (lb)	0.2	0.4	1.5	3.0			
	Velocity (ft/sec)	1502	1449	1325	1043			
Compressor Blade								
	Length (in)	*1*	*2*	*3*	*4*		Disk Dia	20
	Width (in)	*1*	*2*	*2*	*2*		RPM	10000
	Thickness (in)	*0.15*	*0.15*	*0.15*	*0.15*			
	Weight (lb)	*0.03*	*0.13*	*0.19*	*0.25*			
	Velocity (ft/sec)	916	960	1004	1047			
HPT Turbine Blade								
	Length (in)		*1.2*	*2*	4		Disk Dia	27
	Width (in)		*1.2*	*2*	2		RPM	10000
	Thickness (in)		*0.15*	*0.15*	0.15			
	Weight (lb)		*0.05*	*0.13*	0.25			
	Velocity (ft/sec)		1475	1440	1353			
LPT Turbine Blade								
	Length (in)	*1.2*	*2.0*	4.0	8.0		Disk Dia	27
	Width (in)	*1.2*	*2.0*	2.0	2.0		LBR RPM	8100
	Thickness (in)	*0.2*	*0.2*	0.2	0.2		HBR RPM	3600
	Weight (lb)	*0.05*	*0.13*	0.25	0.68			
LBR	Velocity (ft/sec)	1477	1449	1378	1237			
HBR	Velocity (ft/sec)	657	644	613	550			
HBR Fan Disk		54.0	90.0	162.0	180.0			
	Length (in)	6.0	16.1	14.0	25.8		Disk Dia	30
	Width (in)	3.0	10.1	4.2	13.4		Bore Dia	25
	Thickness (in)	6.7	6.7	6.7	6.7		RPM	3600
	Weight (lb)	10.0	27.8	45.0	84.5		Ti.	
	Centroid	13.28	12.41	9.63	8.78		Wt. ~120 lb.	
	Velocity (ft/sec)	417	390	303	276			
LBR Fan Disk		54.0	90.0	162.0	180.0			
	Length (in)	6.0	16.1	14.0	25.8		Disk Dia	16
	Width (in)	3.0	10.1	4.2	13.4		Bore Dia	9
	Thickness (in)	5.0	5.0	5.0	5.0		RPM	8100
	Weight (lb)	10.0	27.8	41.0	71.0		Ti.	
	Centroid	6.18	5.77	4.48	4.08		Wt. ~100 lb.	
	Velocity (ft/sec)	437	408	317	289			

TABLE 3-5. DEBRIS SIZE CORRELATED TO DAMAGE BIN SIZE (Continued)

Compressor Rim		54.0	90.0	162.0	180.0			
	Length (in)	4.8	*15.7*	*20.0*	*20.0*		Disk Dia	20
	Width (in)	1.3	*3.0*	*10.0*	*1.0*		Bore Dia	17
	Thickness (in)	1.0	*0.5*	*1.0*	*1.0*		RPM	10000
	Weight (lb)	0.6	*4.7*	*6.0*	*7.0*		Ni	
	Centroid	8.9	8.3	6.5	5.9		Wt. ~ 20	
	Velocity (ft/sec)	779	728	565	515			
Compressor Disk		54.0	90.0	162.0	180.0			
	Length (in)	7.7	13.5	14.5	17.8		Disk Dia	20
	Width (in)	4.1	7.0	4.0	6.1		Bore Dia	6
	Thickness (in)	0.8	0.7	0.3	0.8		RPM	10000
	Weight (lb)	3.9	6.0	3.55 / 9.00	6.4 / 10.0		Ni	
	Centroid	6.9	6.4	5.0	4.5		Wt. ~ 20	
	Velocity (ft/sec)	599	560	435	396			
Turbine Rim		54.0	90.0	162.0	180.0			
	Length (in)	8.0	18.3	22.0	*20.0*		Disk Dia	27
	Width (in)	3.0	1.7	1.5	*1.0*		Bore Dia	24
	Thickness (in)	1.0	1.3	1.5	*1.0*		RPM	10000
	Weight (lb)	11.3	6.3	9.7	*20.0*		Ni	
	Centroid	12.3	11.5	8.9	8.1		Wt. ~ 20	
	Velocity (ft/sec)	1073	1003	778	709			
Turbine Disk		54.0	90.0	162.0	180.0			
	Length (in)	10.3	15.5	24.3	*26.0*		Disk Dia	27
	Width (in)	2.3	7.5	11.5	*13.0*		Bore Dia	6
	Thickness (in)	1.3	1.0	3.8	*4.0*		RPM	10000
	Weight (lb)	10.5	19.0	70.0	*81.6*		Ni	
	Centroid	9.0	8.4	6.5	6.0		Wt. ~ 120	
	Velocity (ft/sec)	787	736	571	520			

4. DEBRIS CHARACTERIZATION.

Component analysis is presented in the following order: fan analysis, compressor analysis, and turbine analysis. Different failure modes such as disk failure and blade failure are discussed within each section. Table 3-5 provides the debris sizes and initial debris velocities used in the energy analysis. The analysis has been conducted in such a fashion to define the 90^{th} percentile fragment. That is, 90 percent of the fragments that exit the engine for the defined event types will have an energy level less than or equal to the fragment characteristics defined. As discussed in section 3, only 10 percent of the fragments penetrate the aircraft and damage aircraft structure or subsystems. Thus, this analysis characterizes the fragment most capable of causing damage to the aircraft structure or subsystems. Most fragments will be smaller than that defined, have less energy, and pose a lesser threat to the aircraft.

4.1 FAN ANALYSIS.

For the fan section, an inlet-nacelle skin model was developed based on typical design characteristics (figure 4-1). Below are the skin thicknesses used for the associated components. The selected thicknesses are the thinnest encountered, making them a conservative choice.

a.	Inner barrel—Inlet-Nacelle wall 1	0.025" Al-2024
b.	Inner barrel—Inlet-Nacelle wall 2	0.025" Al-2024
c.	Outer barrel—Fan Cowl wall	0.040" Al-2024

The penetrated inlet-nacelle structure is based on the different failure scenarios. Fan events are divided into disk failures and blade failures. For blade failures, three scenarios are considered: Blade failure with fan case penetration, helical blade trajectory, and fan blade reingestion.

4.1.1 Fan Disk Failure.

For a disk failure as seen in figure 4-2, the aircraft is subject to disk fragments and high-energy blade fragments. As described above, the blade fragments do not always penetrate the containment structure on their way out of the engine. The fan disk failure analysis defines both the fan blade fragments as well as the disk fragments.

4.1.1.1 Fan Blade Damage From a Disk Failure.

For fan blade damage from a disk event, figure 4-3 shows a vast majority of the debris to be under 25% in size. The associated trajectory angles range from 25 degrees to -55 degrees. A total of nine events are shown in figure 4-3; five of them were fuselage-mounted engines which produced trajectory angles between 25 degrees and -35 degrees as shown in figure 4-4. Both high bypass ratio engines and low bypass ratio engines are represented.

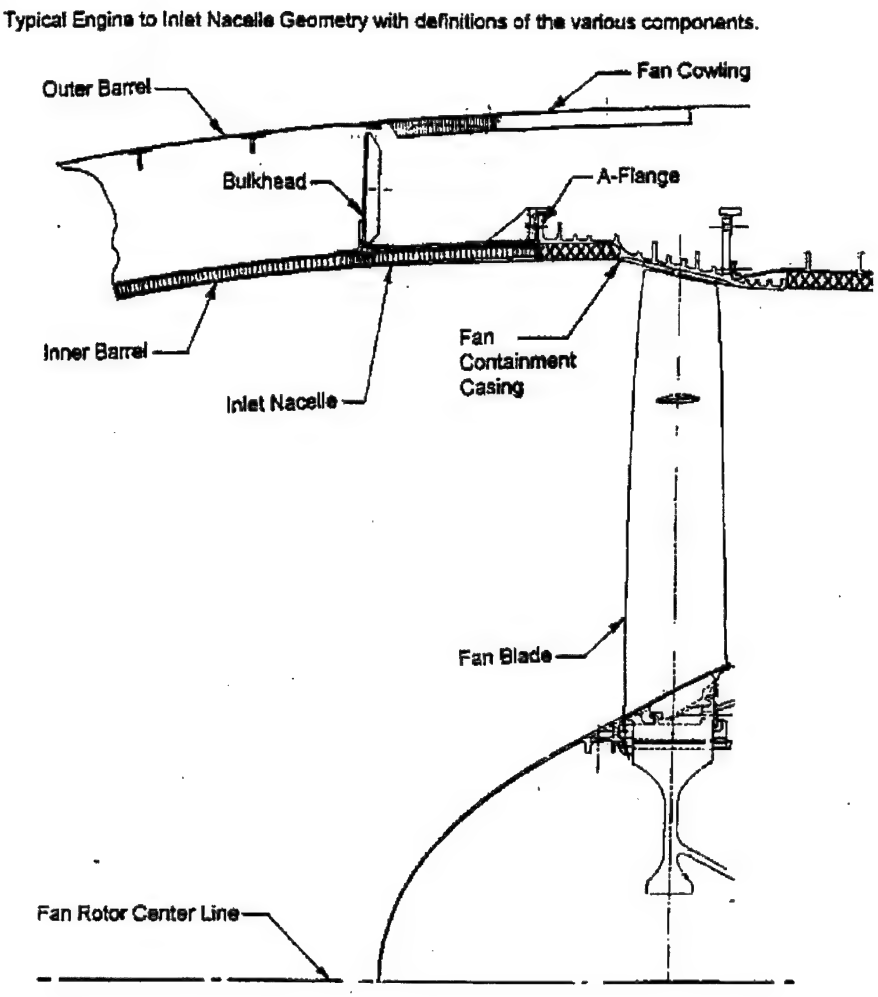

FIGURE 4-1. TYPICAL ENGINE TO INLET-NACELLE GEOMETRY

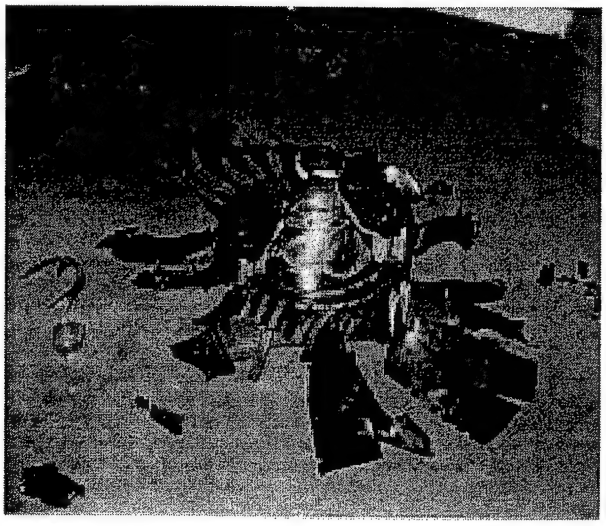

FIGURE 4-2. FAN DISK FAILURE DEBRIS

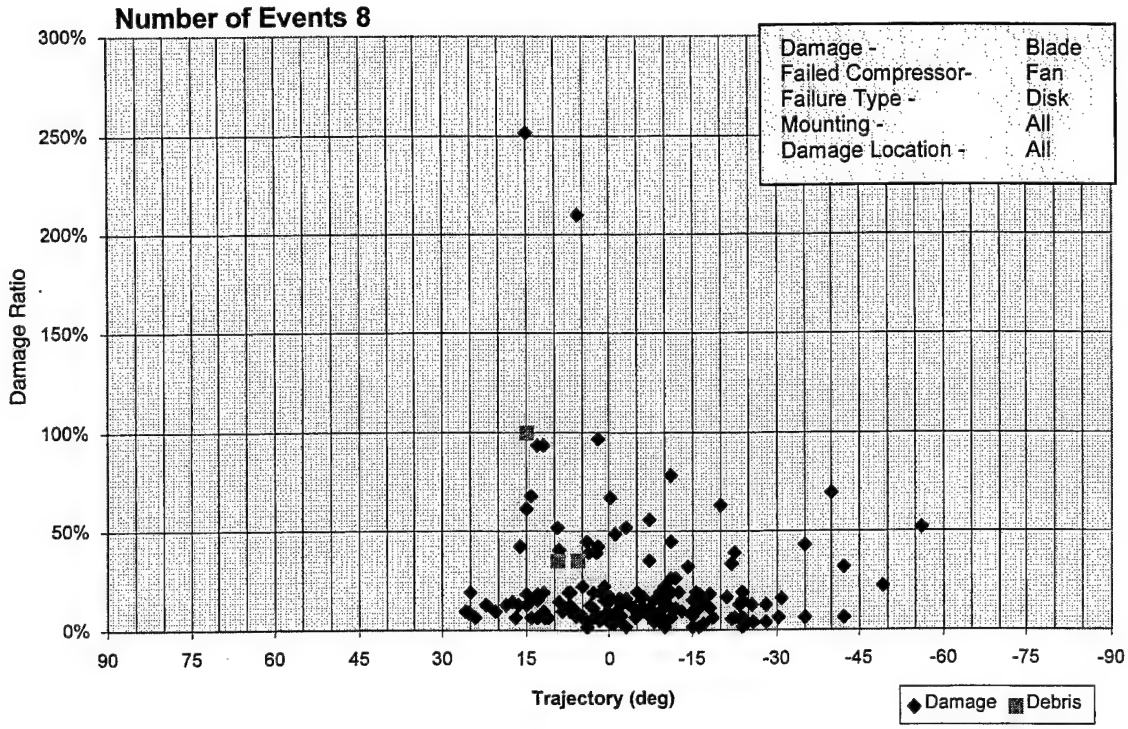

FIGURE 4-3. FAN BLADE DAMAGE FROM A DISK EVENT

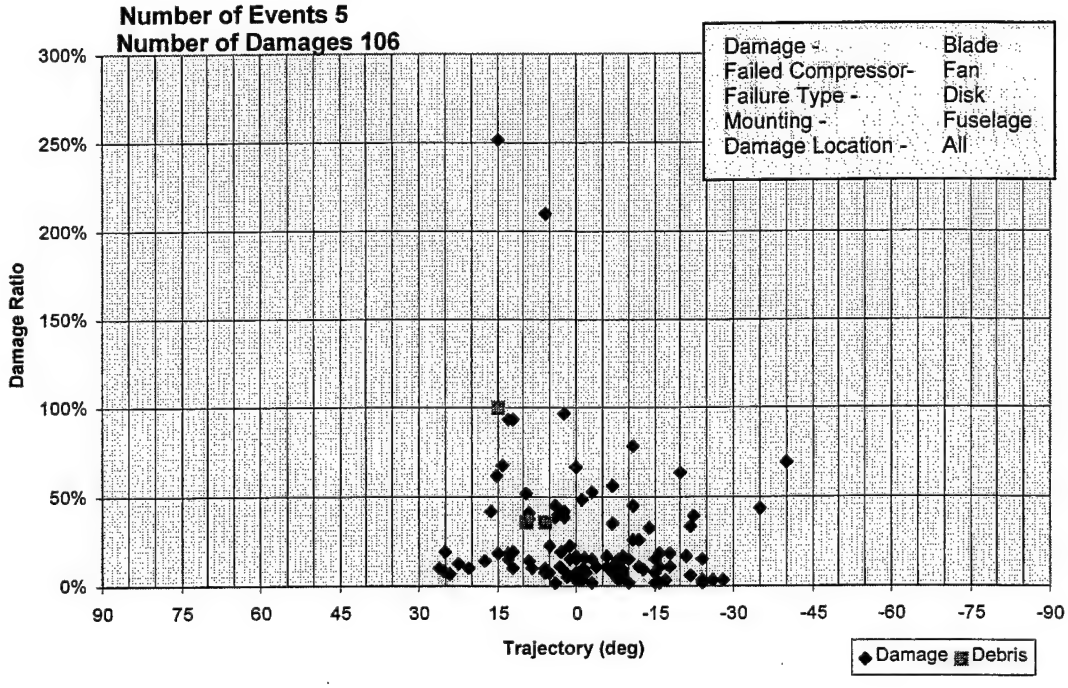

FIGURE 4-4. FAN BLADE DAMAGE FROM A DISK EVENT FOR FUSELAGE-MOUNTED ENGINES

To model the fan blade debris in a disk event, it was assumed that 25% of the debris initial velocity was lost due to impact with the case and other blade fragments prior to impacting the fan cowl. Additionally, the assumption was subsequently verified by analysis of a fan disk event where debris fragments were found imbedded in fuselage structure and the debris penetration was finite (i.e., the debris stayed within the aircraft fuselage). An incident summary is provided in section 6.2. The fan cowl used in this analysis was a 0.040-inch aluminum plate (figure 4-5). As previously mentioned, the engine containment structure was assumed to have been compromised by the disk fragment and thus was not modeled in the analysis.

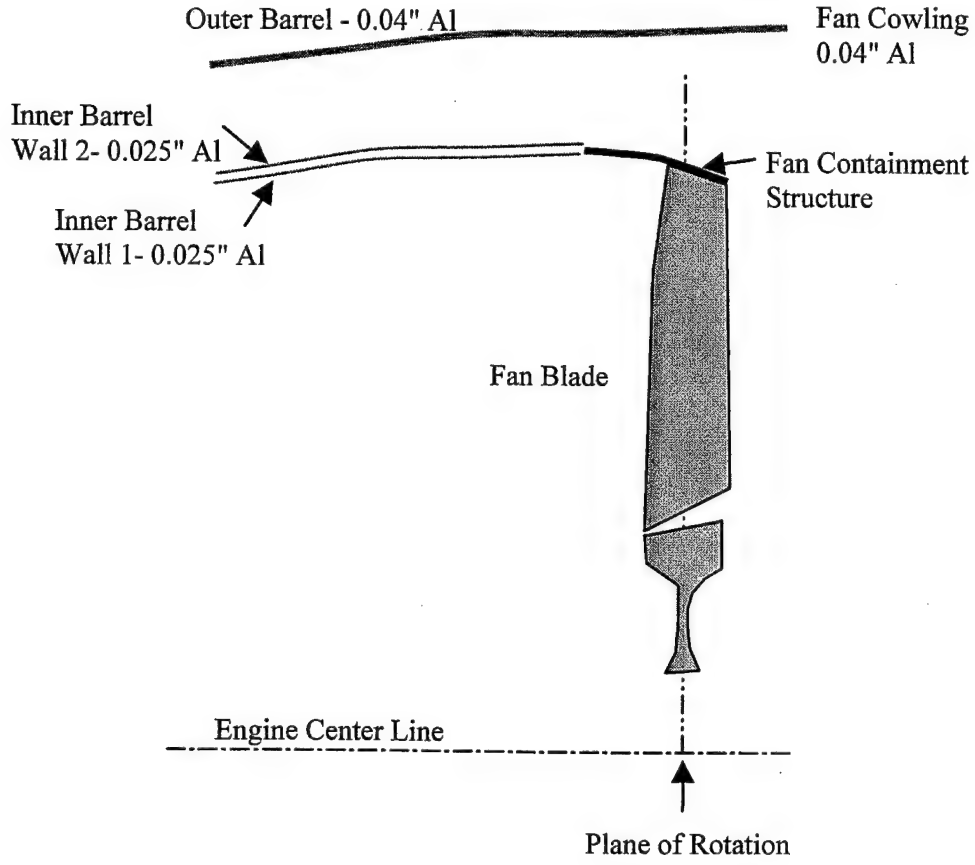

FIGURE 4-5. FAN COWL MODEL FOR FAN DISK EVENTS

For the high bypass ratio engine, estimated debris energy upon exiting the fan cowl is presented in figure 4-6(a). Based on this analysis, the debris has no (0) energy beyond angles of -50 degrees, but figure 4-3 shows damage to -55 degrees. As discussed in appendix A, this disparity is because aerodynamic effects have not been included. To provide a qualitative trend for aerodynamic effects, figure 4-6(b) plots debris residual energy after traveling 30 feet from the engine during a flight condition of Mach 0.85 at 35,000 feet. This type of presentation will be done for the remainder of the report.

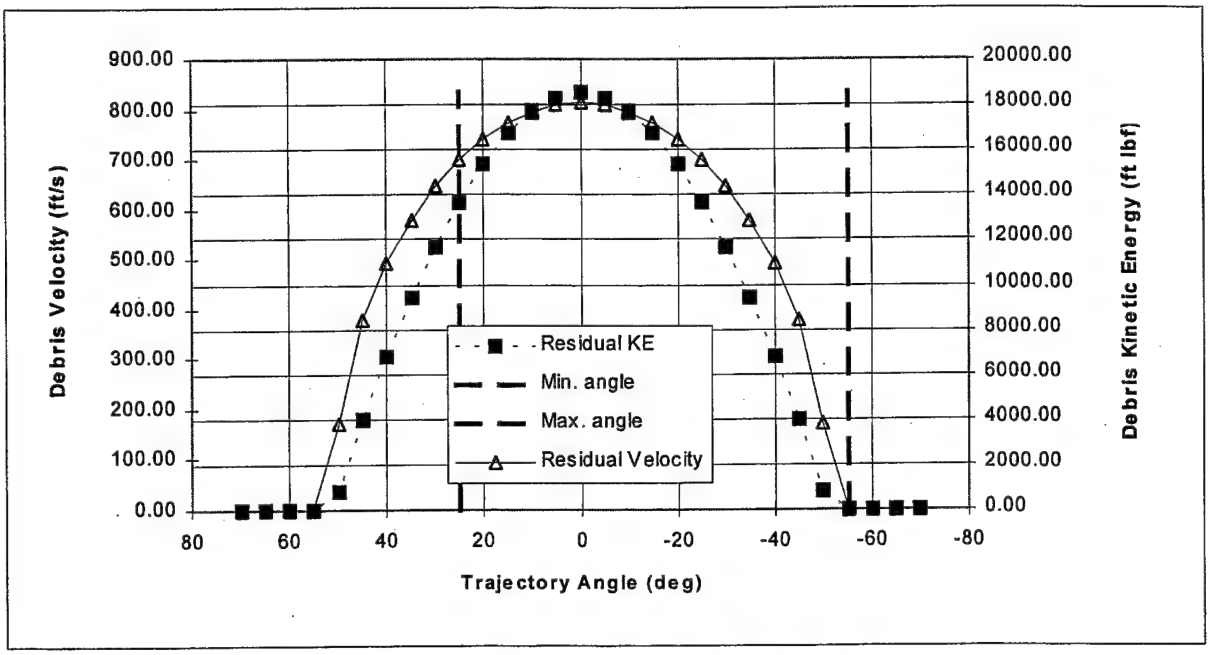

(a) Residual Velocity and Energy Once Outside the Cowl

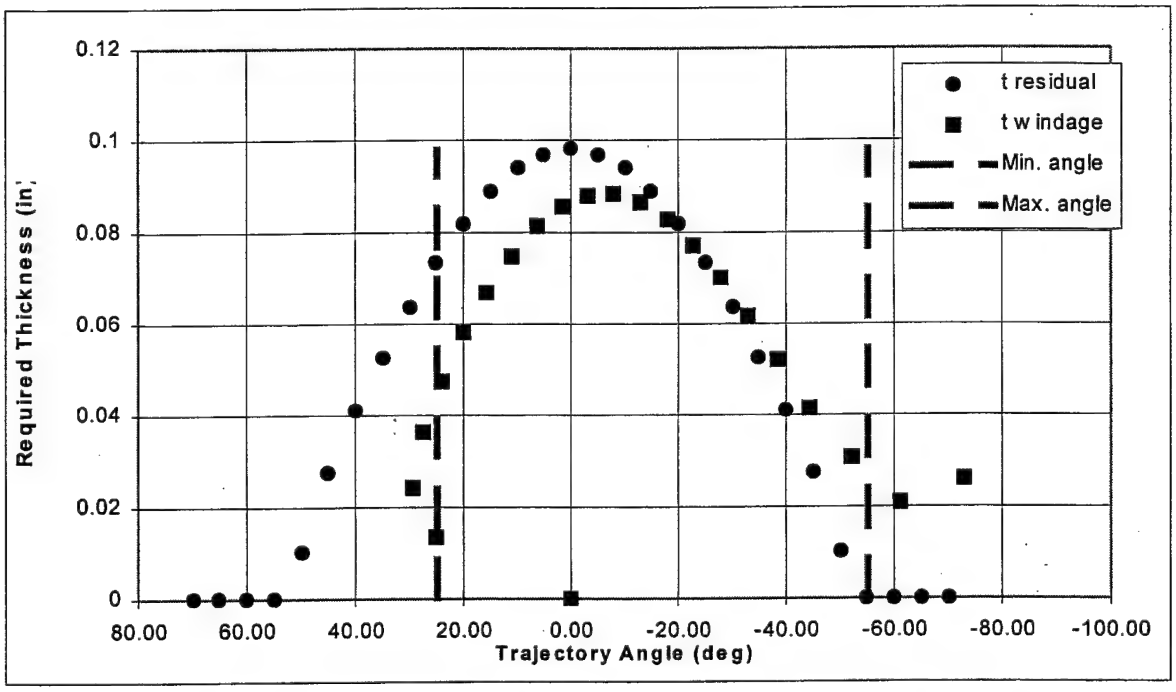

(b) Debris Characteristics After Traveling 30 ft From a Wing-Mounted Engine
(Altitude = 35,000, Mach = 0.85)

FIGURE 4-6. DEBRIS ENERGY ESTIMATION FOR A 25% HBR FAN BLADE

Figure 4-7 shows predicted thicknesses to defeat debris. Aircraft fuselage skin thickness varies between 0.06 and 0.08 inch and wing skins vary from 0.1 to 0.75 inch. Using these numbers show an excellent agreement in maximum forward trajectory angle between the predicted debris energy and the database. As mentioned, the far aft trajectory angles from the debris database are achievable if aerodynamic effects are included but most of the data is within -35 degrees (see figure 4-3) which agrees well with predicted debris energy levels.

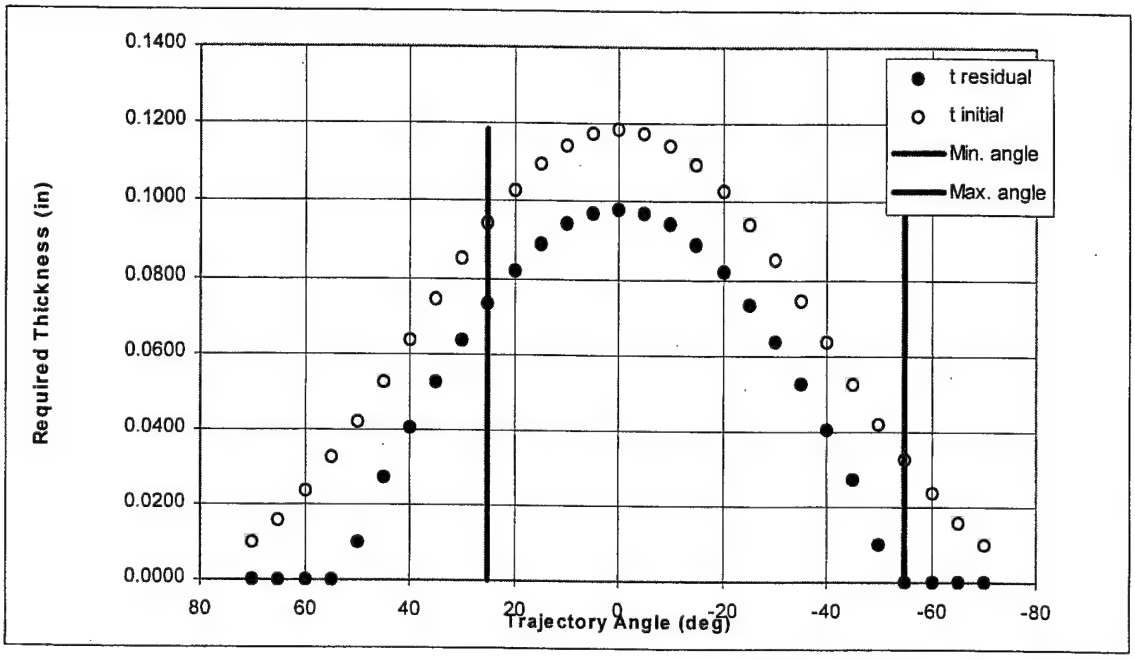

FIGURE 4-7. PREDICTED SKIN THICKNESS TO DEFEAT A 25% HBR FAN BLADE

For low bypass ratio engines, debris energy levels and required skin thicknesses are shown in figures 4-8 and 4-9, respectively. The energy levels for low bypass engine debris are significantly smaller, which indicates a reduced chance for penetration, but the debris presented area is also smaller, which offsets the reduction in energy.

4.1.1.2 Fan Disk Aerodynamic Effects.

The effect of windage on a disk fragment trajectory was estimated. The calculations were conducted at 35,000 ft, Mach 0.85 flight conditions. The disk characteristics used were based on the 100% disk fragment, specifics can be found in table 3-5. The analysis was conducted for a debris fragment traveling 30 feet radially from the engine centerline. For a high bypass ratio (HBR) engine, the disk has traveled 1.6 ft aft, resulting in a change in trajectory angle about -4.2 degrees (figure 4-10). For a low bypass ratio (LBR) engine, the disk fragment has traveled 1.1 feet, resulting in a change in trajectory of about 3 degrees (figure 4-11).

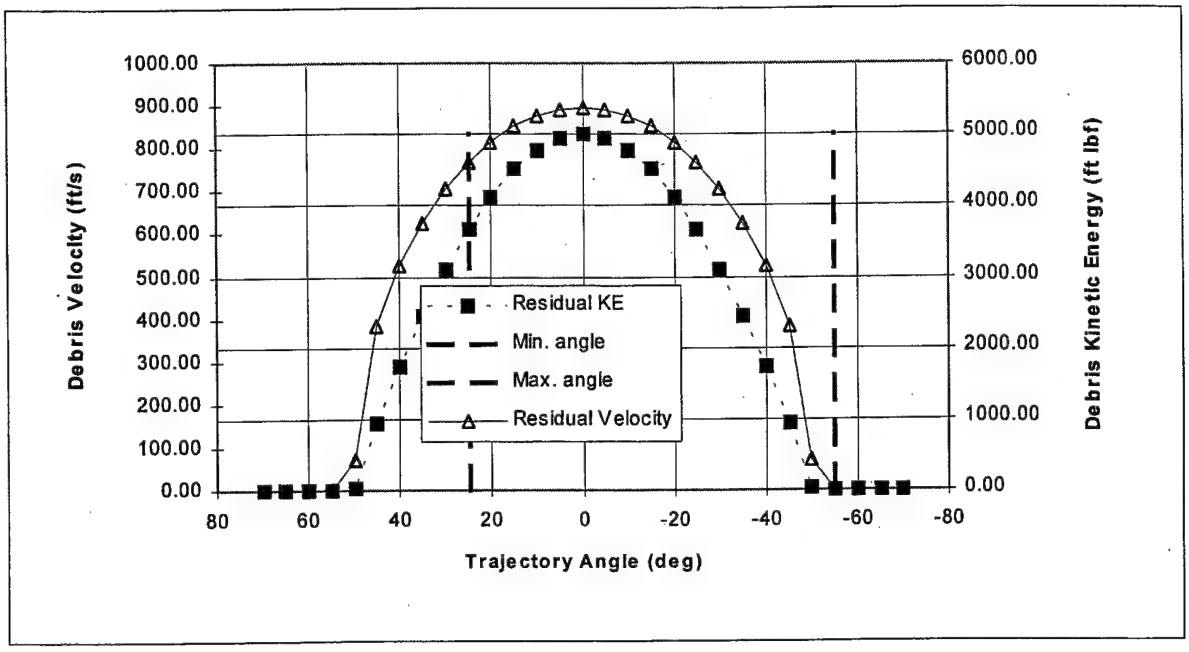

(a) Residual Velocity and Energy Once Outside the Cowl

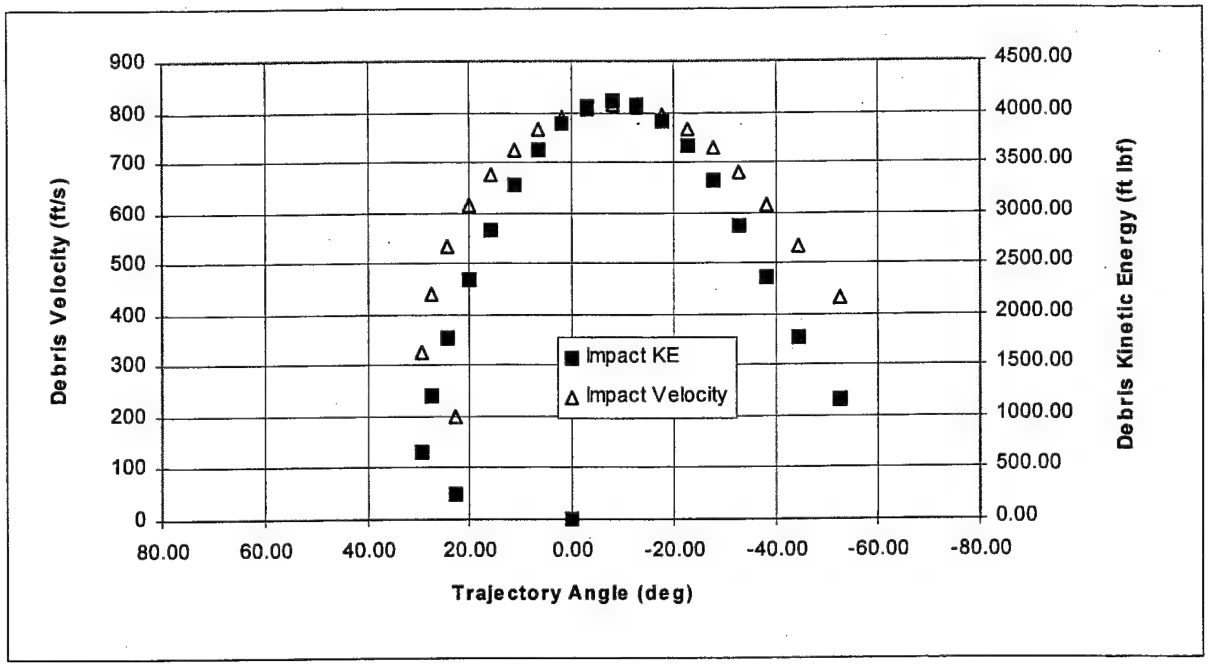

(b) Debris Characteristics After Traveling 30 ft From a Wing-Mounted Engine
(Altitude = 35,000, Mach = 0.85)

FIGURE 4-8. DEBRIS ENERGY ESTIMATION FOR A 25% LBR FAN BLADE

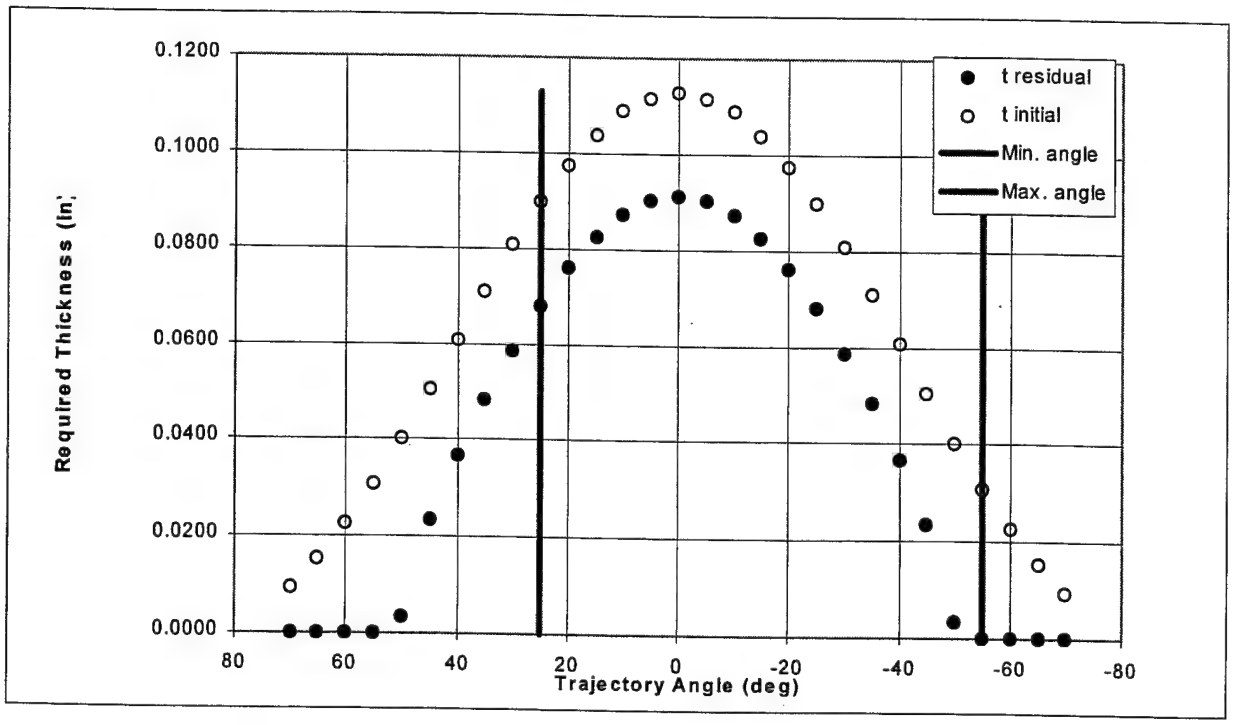

FIGURE 4-9. PREDICTED SKIN THICKNESS TO DEFEAT A 25% LBR FAN BLADE

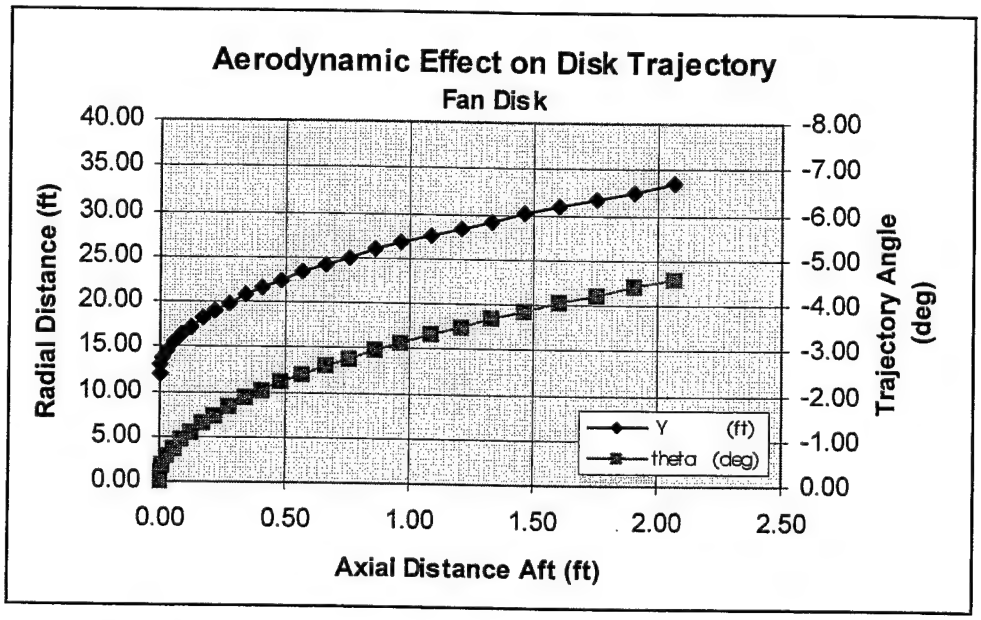

FIGURE 4-10. HBR FAN DISK WINDAGE EFFECTS

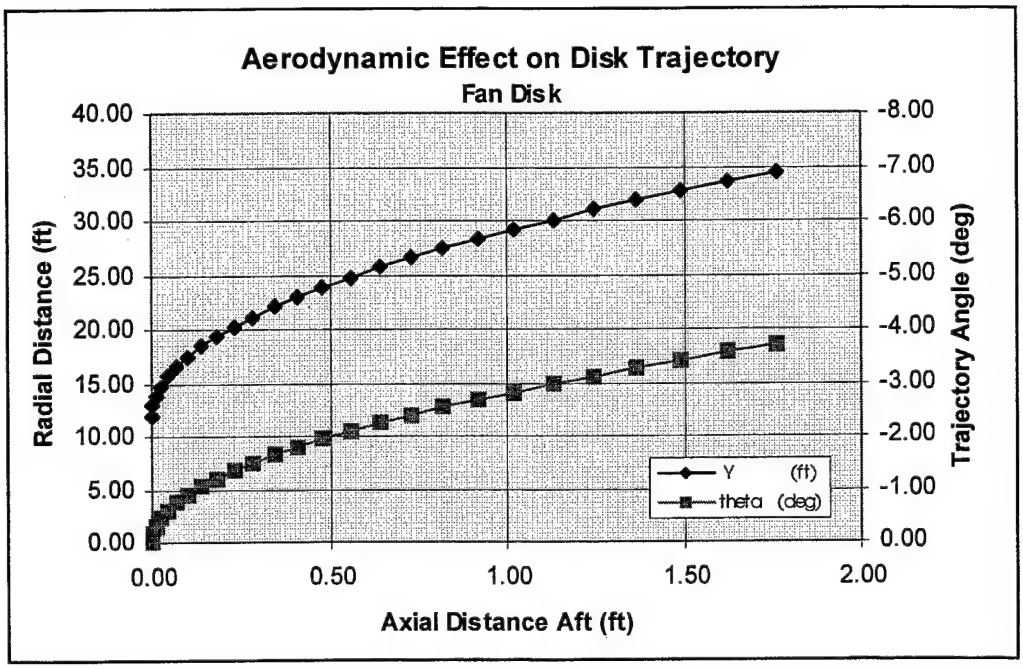

FIGURE 4-11. LBR FAN DISK WINDAGE EFFECTS

4.1.1.3 Fan Disk Damage.

For fan disk damage from a disk failure (shown in figure 4-12), figure 4-13 shows the basic trajectory angles to range from +5 and -5 degrees. A 100% normalized disk fragment is used to model fan disk debris. Initial energy levels are near 100,000 ft lbf.

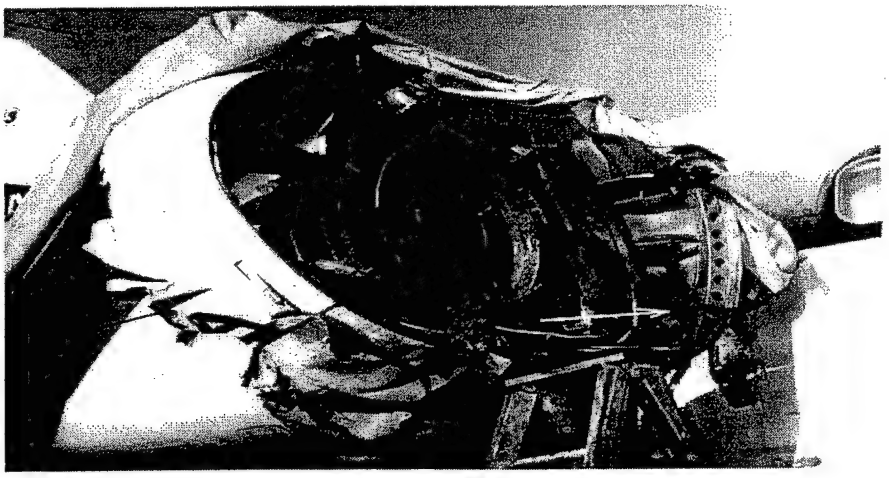

FIGURE 4-12. FAN DISK DAMAGE

Attempts to estimate the residual energy upon leaving the engine are not presented since the disk debris size is far beyond BARRIER's capability. Debris size including tumbling should be coupled with the trajectory angles to estimate the debris hazard zone.

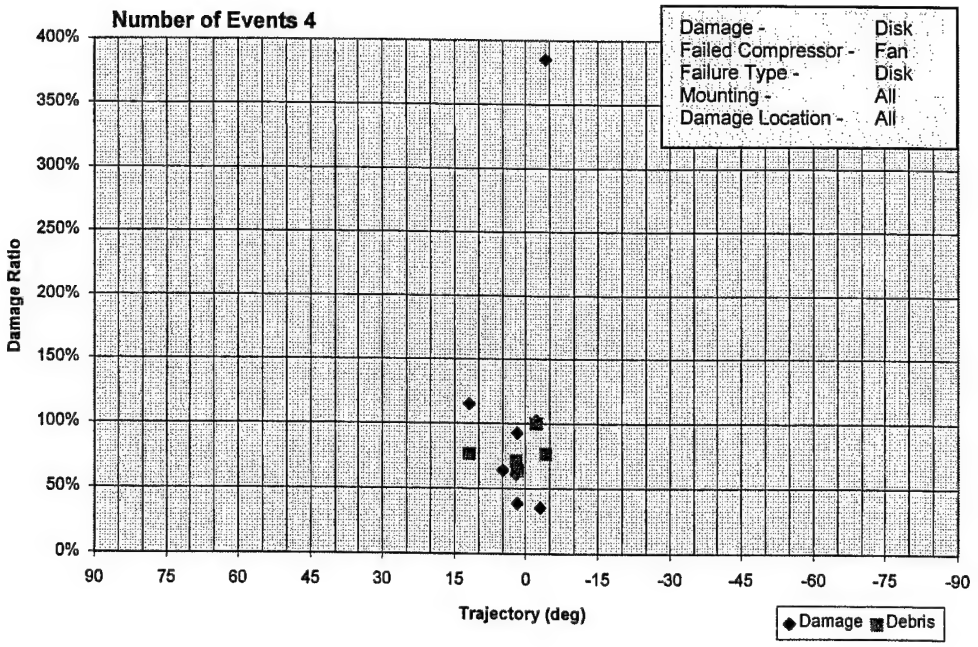

FIGURE 4-13. FAN DISK DAMAGE FROM A DISK EVENT

4.1.2 Fan Blade Failure.

Debris from fan blade failures have trajectory angles from 20 to -35 degrees as shown in figure 4-14. Most of the data are below 50% damage ratio. The cluster of points between 70% to 90% are from one event (fuselage mounted). Events from wing-mounted engines are shown in figure 4-15 while events from fuselage-mounted engines are shown in figure 4-16.

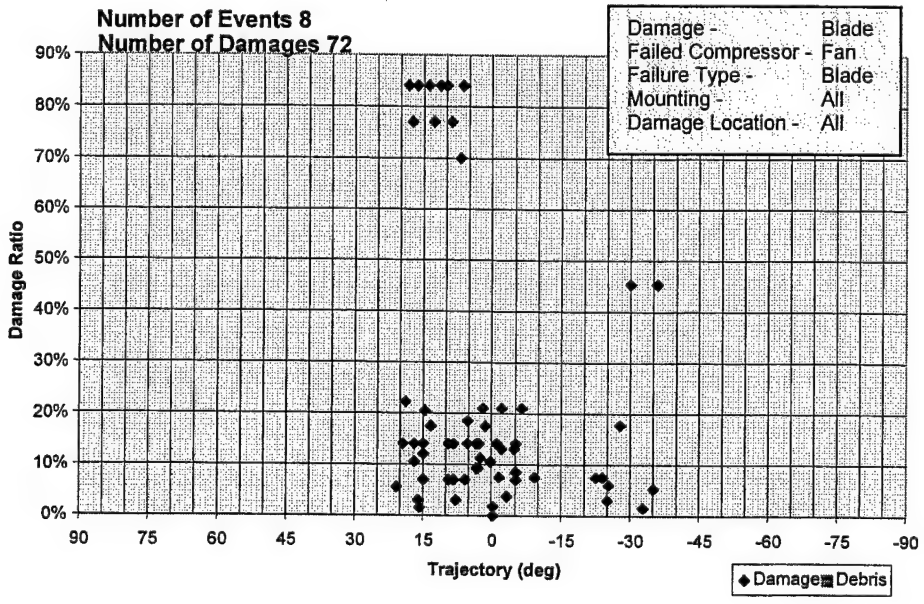

FIGURE 4-14. FAN BLADE DAMAGE FROM A BLADE EVENT

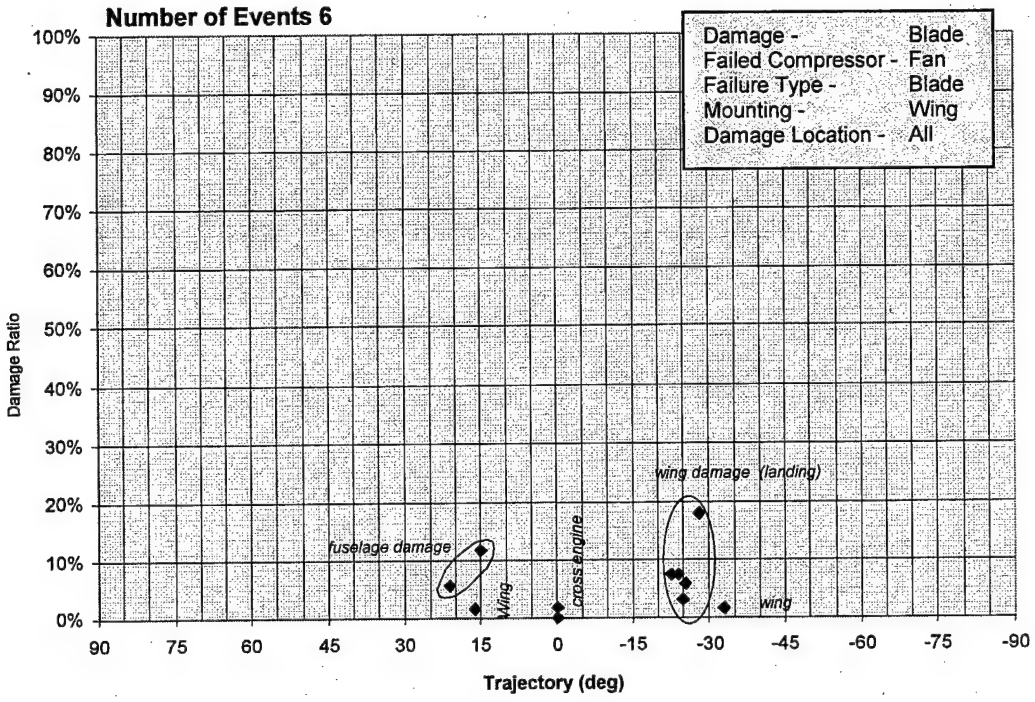

FIGURE 4-15. FAN BLADE DAMAGE FROM A BLADE EVENT FOR WING-MOUNTED ENGINE

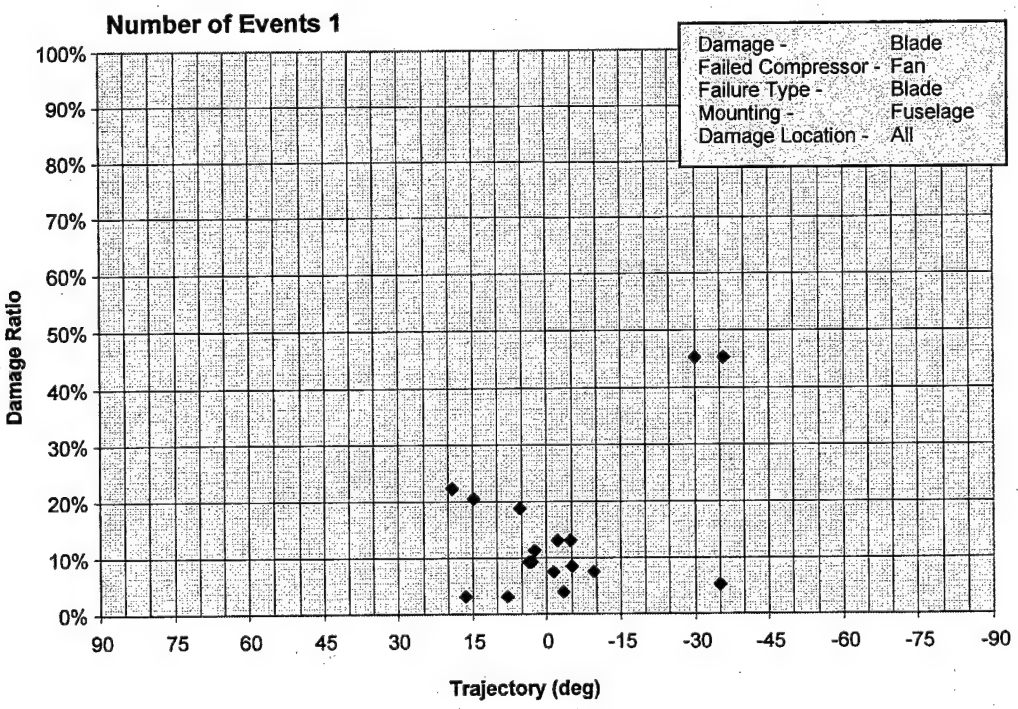

FIGURE 4-16. FAN BLADE DAMAGE FROM A BLADE EVENT FOR FUSELAGE-MOUNTED ENGINES

For the aft trajectory angles, the debris must pass through the engine case and cowl. For the forward trajectories, however, there are two primary failure modes to consider: (1) helical motion of a blade tip upon fracturing against the containment ring and (2) particles which are reingested and then kicked forward after impacting the fan rotor (figure 4-17).

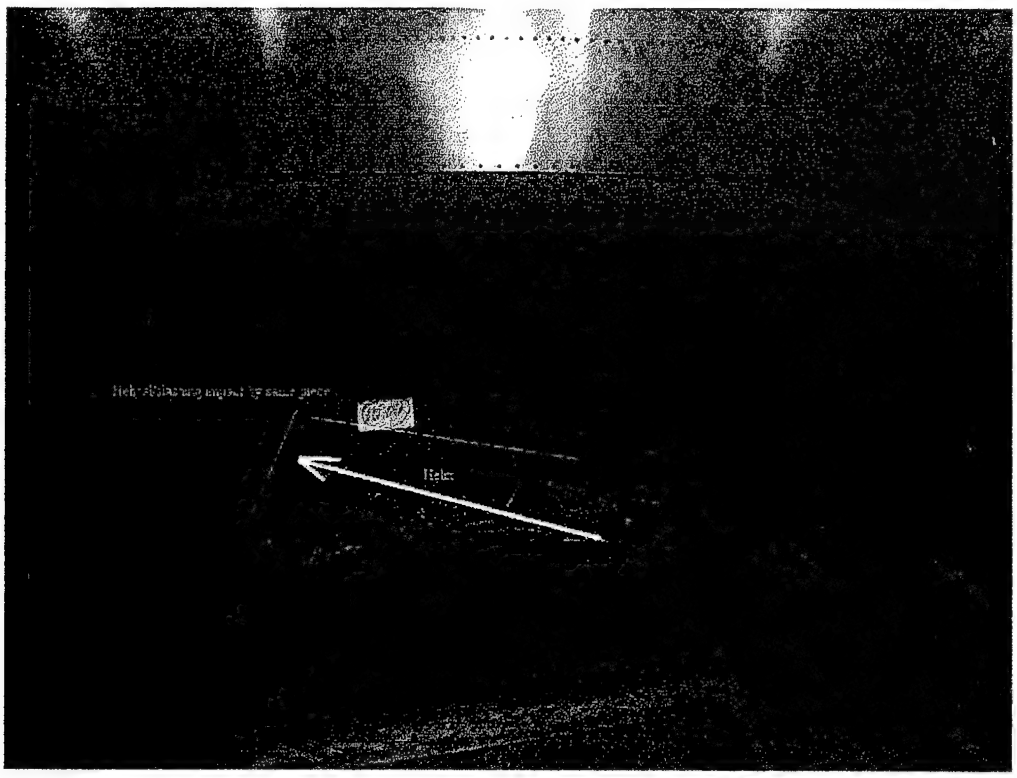

FIGURE 4-17. FAN BLADE HELICAL TRAJECTORY

4.1.2.1 Aft Trajectory Angles—Engine Case Penetration.

In a typical fan blade failure event where a large (> 50%) section of the blade is released, the blade tip section fragments and slides forward resulting in a helical trajectory while the root section of the blade is caught by the trailing blade and swept aft. This aft moving debris is assumed to impact the fan containment structure. Typically, a single blade release is contained; however, when multiple blades are released, blade fragments have exited through the containment structure as seen in figure 4-18.

For fan debris that impacts the fan containment case and fan cowl, residual velocities of a 50% fan blade are shown in table 4-1. The residual velocities listed are for an 80 degree impact orientation with the fan case and a 45 degree impact orientation with the fan cowl. The analysis used a 0.25-inch steel fan case and a 0.04-inch Al fan cowl.

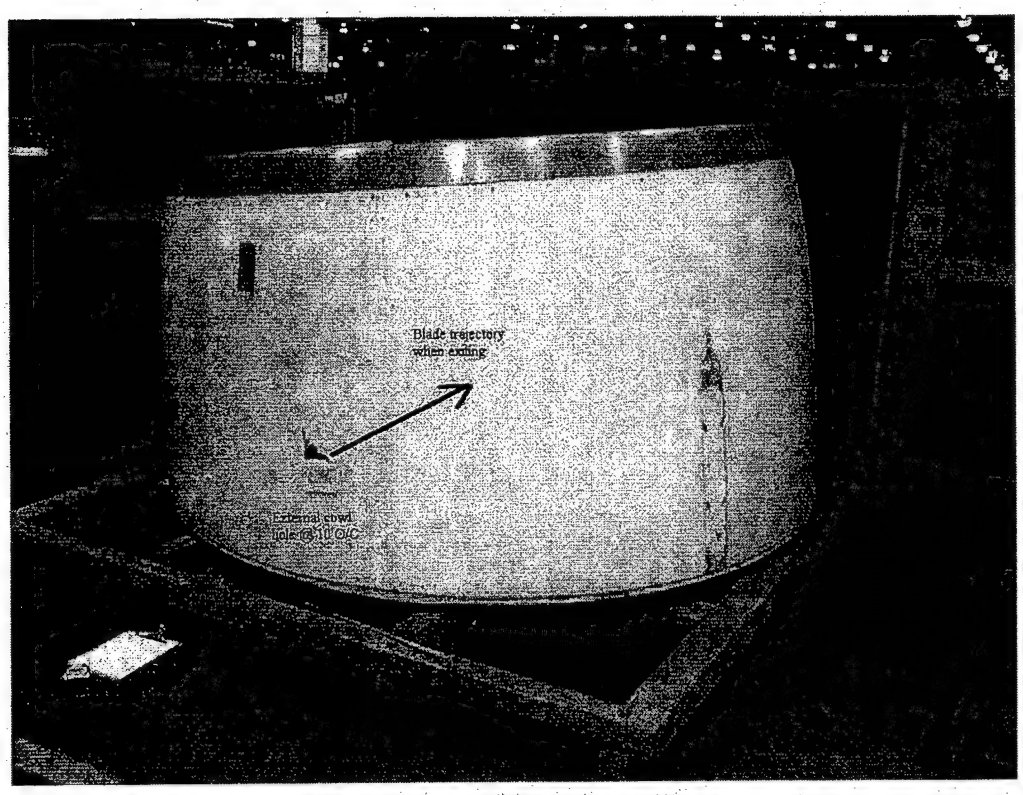

FIGURE 4-18. FAN BLADE EXIT TRAJECTORY

TABLE 4-1. FIFTY PERCENT FAN DEBRIS RESIDUAL VELOCITY UPON LEAVING THE ENGINE COWL

Debris	Residual Velocity
HBR Fan Debris (16" x 8", 4.50 lbm)	452 ft/s
LBR Fan Debris (7.5" x 5", 1.50 lbm)	697 ft/s

4.1.2.2 Forward Trajectory Angles—Helical Model.

In the helical scenario, the blade tip fractures upon impact with the containment structure and moves forward in a spiraling path (figure 4-19). Based on film data concerning the helical trajectory as shown in figure 4-20, approximately 10% to 25% of the outer blade is liberated as the blade buckles against the containment ring. The estimated debris velocity is 75% (1060 ft/s) of the tip velocity due to frictional effects of the fragment sliding along the inlet cowl as seen in figure 4-21. In order for the debris to penetrate the inlet cowl, a corner must catch the cowl; this assumes the debris penetrates edgewise (80 degrees) through the first inner barrel wall. For the remaining layers, the standard 45 degree orientation angle is assumed.

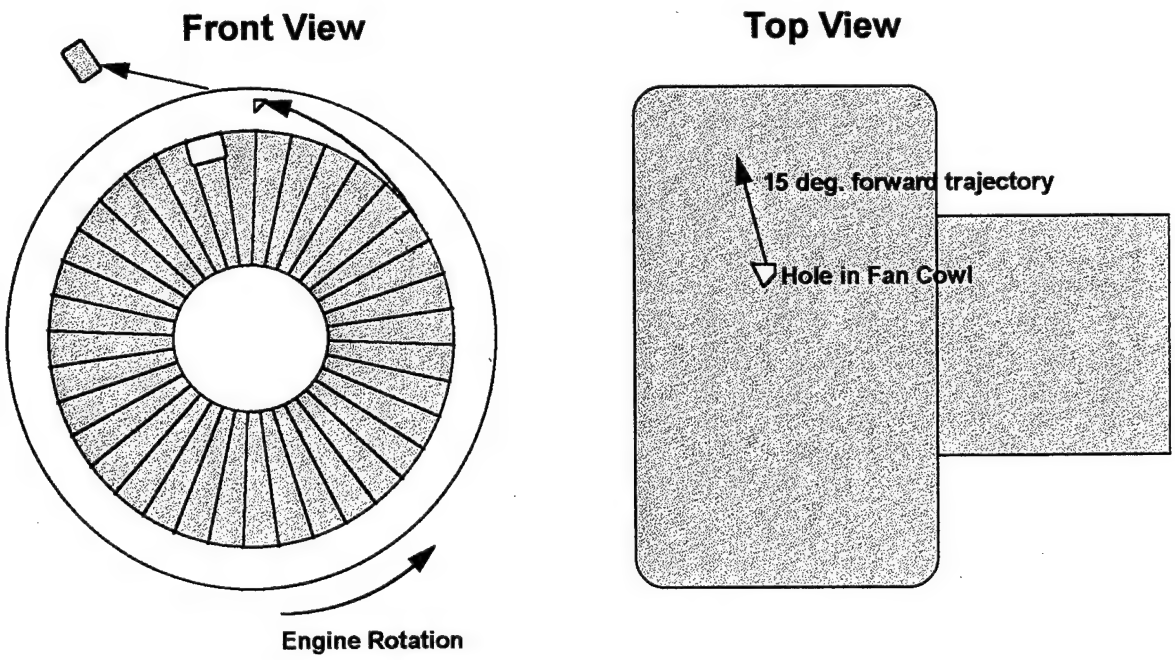

FIGURE 4-19. FAN BLADE HELICAL TRAJECTORY

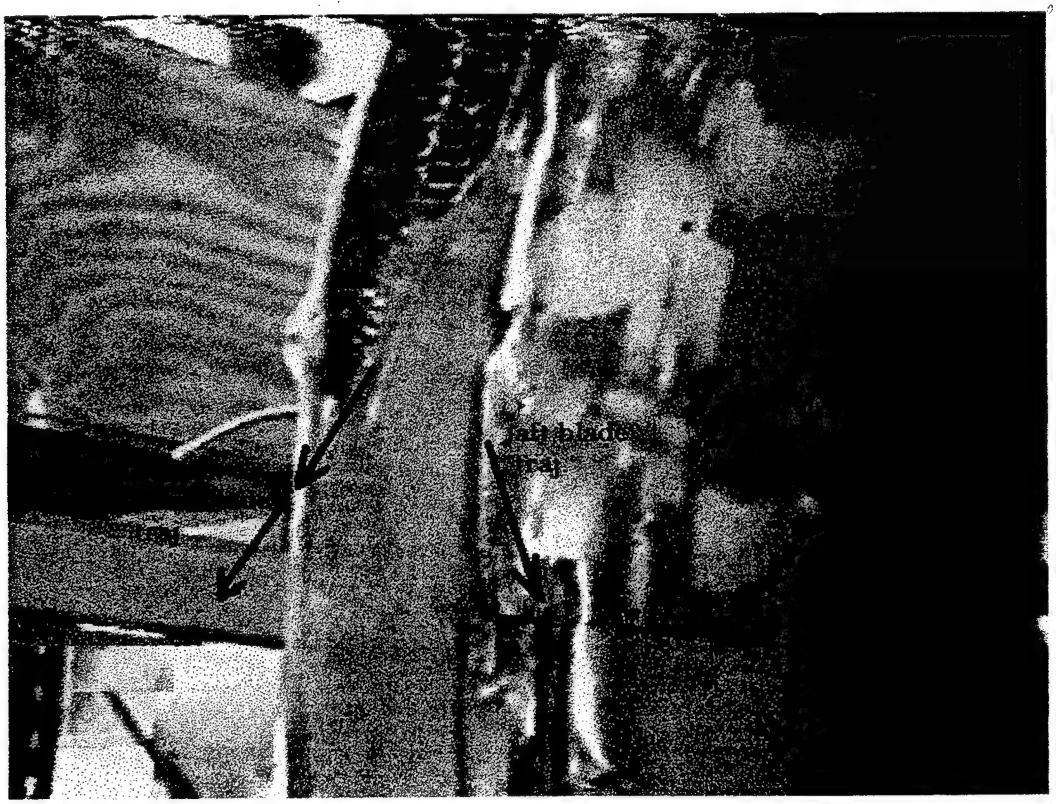

FIGURE 4-20. HELICAL TRAJECTORY

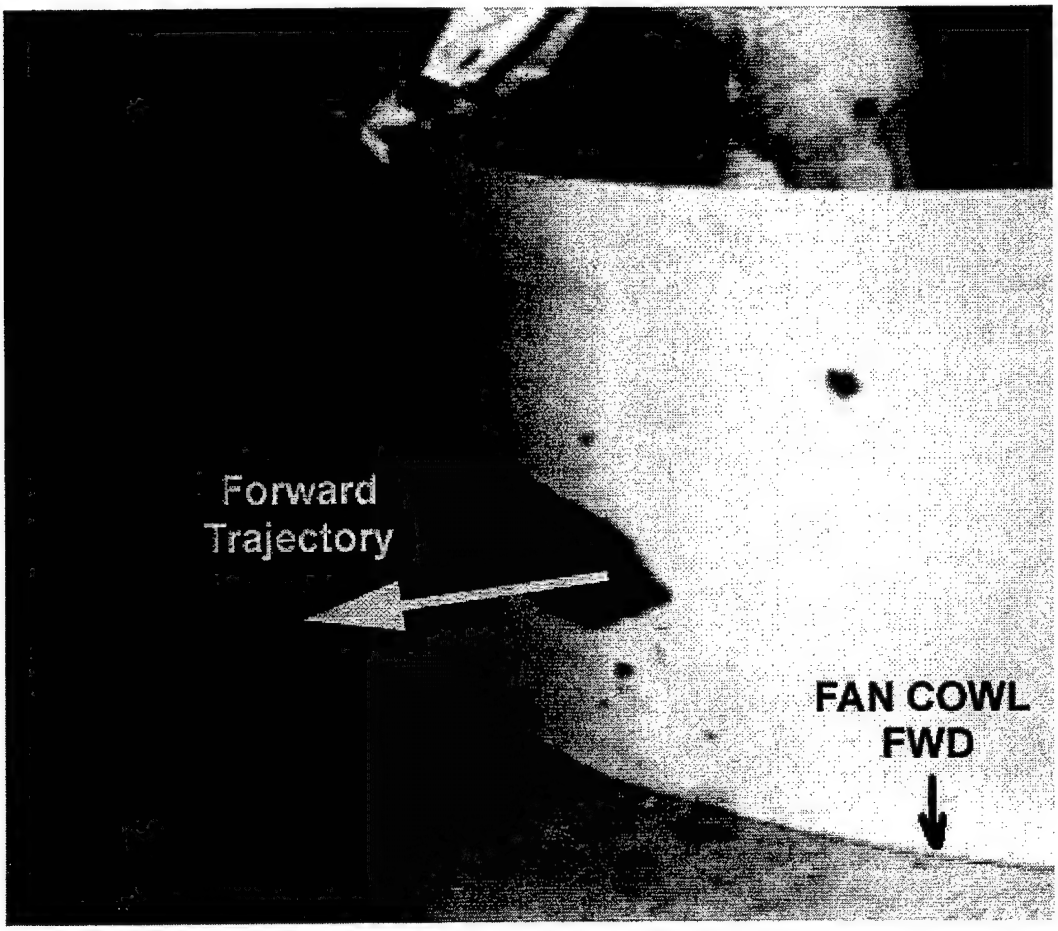

FIGURE 4-21. BLADE DEBRIS EXIT AND COWL DAMAGE

Debris residual velocity and energy are summarized in tables 4-2 and 4-3, assuming either a 15% or a 25% blade tip fragment is liberated. The exit velocity values using the thinner cowl were felt to be too high by members of the ARAC group. As a result, residual velocities are shown for two fan cowl arrangements to show the effect on residual velocity. The thicker cowl configuration was taken from reference 5.

TABLE 4-2. HBR FAN DEBRIS—HELICAL MODEL

	15% Blade Length (0.65 lbm) Residual Velocity (ft/s)		25% Blade Length (1.8 lbm) Residual Velocity (ft/s)	
Theta (degrees)	Cowl of 0.025", 0.025", and 0.04"	Cowl of 0.06", 0.03", and 0.06"	Cowl of 0.025", 0.025", and 0.04"	Cowl of 0.06", 0.03", and 0.06"
5	794	623	801	639
10	790	615	797	631
15	782	601	790	618
20	771	579	779	598

TABLE 4-3. LBR FAN DEBRIS—HELICAL MODEL

	15% Blade Length (0.15 lbm) Residual Velocity (ft/s)		25% Blade Length (0.39 lbm) Residual Velocity (ft/s)	
Theta (degrees)	Cowl of 0.025", 0.025", and 0.04"	Cowl of 0.06", 0.03", and 0.06"	Cowl of 0.025", 0.025", and 0.04"	Cowl of 0.06", 0.03", and 0.06"
5	859	632	875	666
10	853	620	869	656
15	843	600	860	638
20	829	570	847	612

Finally, the edgewise penetration assumption through the first inner barrel wall may also be reevaluated. If the debris actually tumbles through this wall, the residual velocity estimates are drastically reduced (they are not presented).

The residual velocity levels are lower than the levels shown in figures 4-6 and 4-8 for fan blade damage from a blade out event. Hence, if a fuselage were designed to mitigate debris energy levels from figure 4-6, the helical escape would also be mitigated.

4.1.2.3 Forward Trajectory Angles—Reingestion Model.

Debris may also be reingested (the debris spirals forward then is swept by inlet airflow back into the remaining fan blades) and then kicked forward by the fan rotor. A model for predicting debris velocity and mass as a function of trajectory angle was prepared by Mr. H. J. Pinsent (reference 5). The generic model developed was applied to the normalized debris from table 3-5. Since the rotor impacted the debris, the debris was assumed to be freely tumbling. Hence, the average debris orientation of 45 degrees was used.

The resulting residual velocity and energy predictions for high bypass ratio engines and low bypass ratio engines are shown in tables 4-4 and 4-5.

The residual velocity levels are less than the helical model and significantly less than the predicted levels in figures 4-6 and 4-8 for a disk event.

4.1.3 Fan Issues.

The fan blade debris energy levels from a disk event (figures 4-6 and 4-8) are predicted to be greater than the debris energy levels from a blade event (tables 4-1 through 4-5) regardless of the blade failure mode. The energy values in figures 4-6 and 4-8 may be too conservative since energy absorption from the case is not estimated.

TABLE 4-4. HBR FAN DEBRIS—REINGESTION MODEL

Theta (degrees)	Debris Mass	Initial Velocity	Residual Velocity
5	4.85 lbm	534 ft/s	312 ft/s
10	4.44 lbm	550 ft/s	326 ft/s
15	3.65 lbm	576 ft/s	346 ft/s
20	2.29 lbm	658 ft/s	424 ft/s

TABLE 4-5. LBR FAN DEBRIS—REINGESTION MODEL

Theta (degrees)	Debris Mass	Initial Velocity	Residual Velocity
5	1.21 lbm	608 ft/s	381 ft/s
10	1.11 lbm	626 ft/s	400 ft/s
15	0.91 lbm	656 ft/s	420 ft/s
20	0.57 lbm	749 ft/s	504 ft/s

4.2 COMPRESSOR ANALYSIS.

For uncontained compressor events, the selected cowling arrangement is as follows.

- Core cowl 0.040" 2024 Al

In the initial analysis the thrust reverser barrel was also included as recommended by the ARAC Group. This approach was eventually changed to not include the reverser barrel for several reasons: (1) only one incident in the debris database had the reverser barrel over the compressor, (2) by eliminating the barrel there was a better match between the predicted trajectory angles and the empirical trajectory angles from the debris database, and (3) estimated energy levels are more conservative. This does not suggest that a thrust reverser should not be modeled when it is present on an installed engine configuration. In fact, the thrust reverser has been proven to be a good energy absorber, significantly reducing the hazard of uncontained compressor failures. The thrust reverser was not modeled in this analysis because the majority of the data was from engines where the fan duct thrust reverser was not impacted.

4.2.1 Compressor Disk Failure.

4.2.1.1 Compressor Blade Damage From a Disk Failure.

Figure 4-22 shows compressor blade damage from a disk event. Figure 4-23 shows the damage ratio versus trajectory. There is a large amount of scatter in debris size from 25% to 800%. A significant portion of this debris, especially for those greater than 100%, is probably from impacts by debris other than the blades themselves (e.g., the compressor case). This analysis does not attempt to model released static structure.

A satisfactory method of estimating this debris mass was not obtained, thus the best selection to characterize this debris is a full blade (100%).

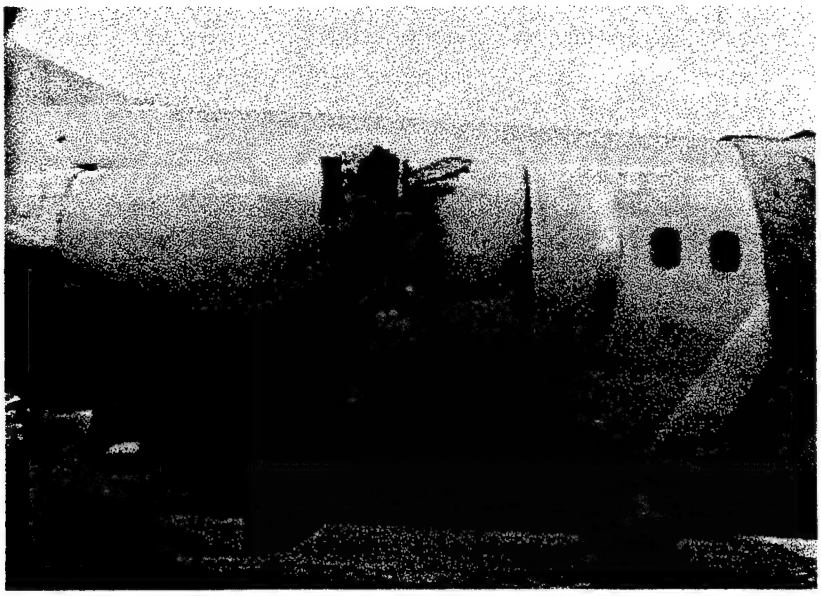

FIGURE 4-22. COMPRESSOR BLADE DAMAGE FROM A DISK EVENT

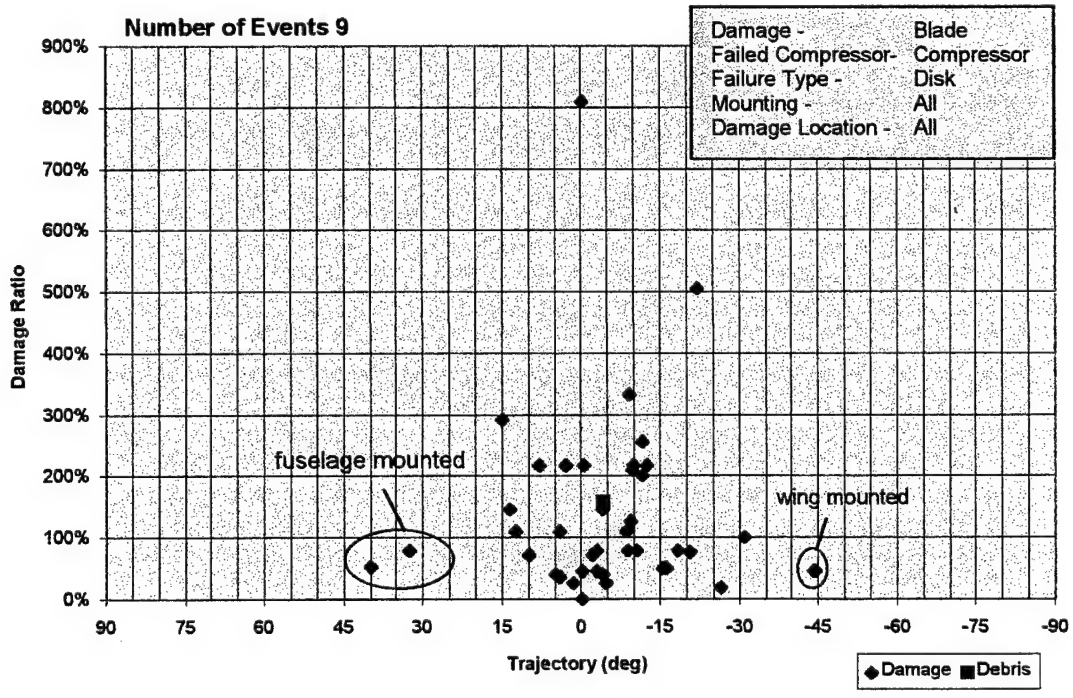

FIGURE 4-23. DAMAGE RATIO VERSUS TRAJECTORY

For debris less than 100% damage ratio, the trajectory angles range from 40 to -45 degrees with most of the damage between 15 and -30 degrees. There are two specific comments in figure 23. First, the debris that impacted at -45 degrees originated from a wing-mounted engine during cruise. Second, the two points beyond 30 degrees (forward direction) originated from a fuselage-mounted engine during takeoff and roll. The model supports both extremes.

Figure 4-24 a plots debris residual velocity and residual energy upon exiting the cowl. For a fuselage-mounted engine during takeoff, the plot shown in figure 4-24(a) would be virtually unchanged. As previously discussed, figure 4-23 shows a penetration point at 40 degrees from a fuselage-mounted engine. At 40 degrees the residual energy is roughly 400 ft-lbf.

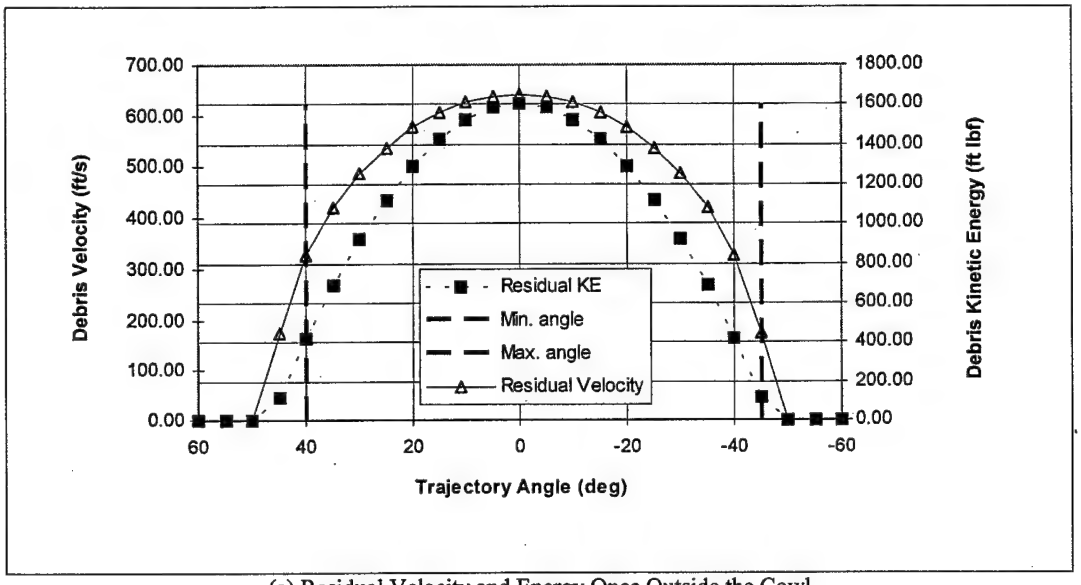

(a) Residual Velocity and Energy Once Outside the Cowl

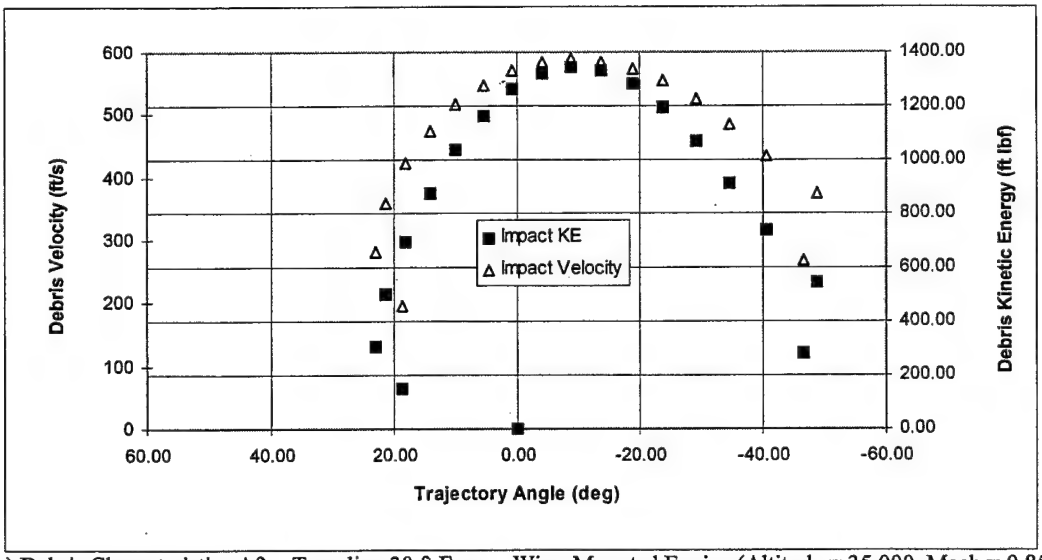

(b) Debris Characteristics After Traveling 30 ft From a Wing-Mounted Engine (Altitude = 35,000, Mach = 0.85)

FIGURE 4-24. DEBRIS ENERGY ESTIMATION FOR A 100% COMPRESSOR BLADE

The other extreme from figure 4-23 includes penetrations at -45 degrees from a wing-mounted engine. Figure 4-24(b) plots the debris impact energy after including the aerodynamic forces, resulting in an aft shift of the energy plot. At -45 degrees the debris energy is also near 400 ft-lbf, thus indicating how compressor blade damage can have a wide trajectory angle. Figure 4-25 shows the disk and blade damage from a compressor disk event.

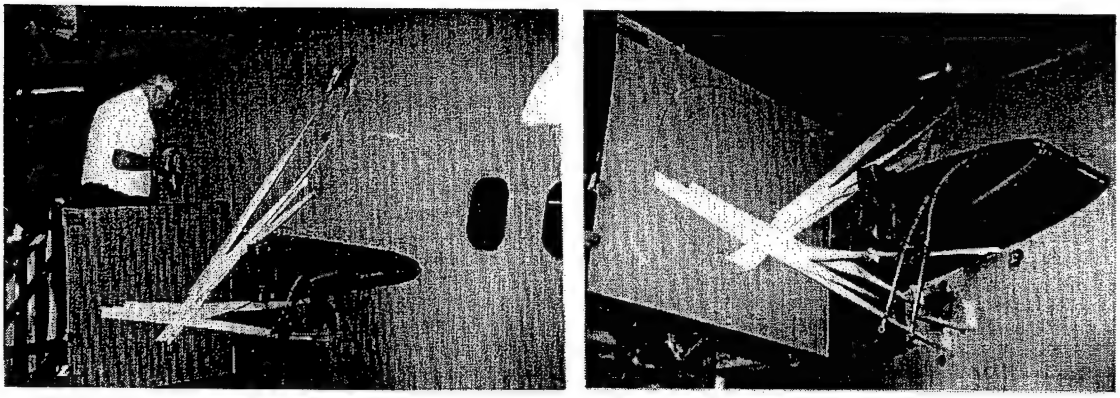

FIGURE 4-25. DISK AND BLADE DAMAGE FROM COMPRESSOR DISK EVENT

Figure 4-26 plots required skin thickness to defeat the debris versus trajectory angle. While there is compressor damage from 40 to -45 degrees, most of the data is between 15 and -30 degrees. This agrees very well when a typical fuselage thickness of 0.04 to 0.08 inch is considered.

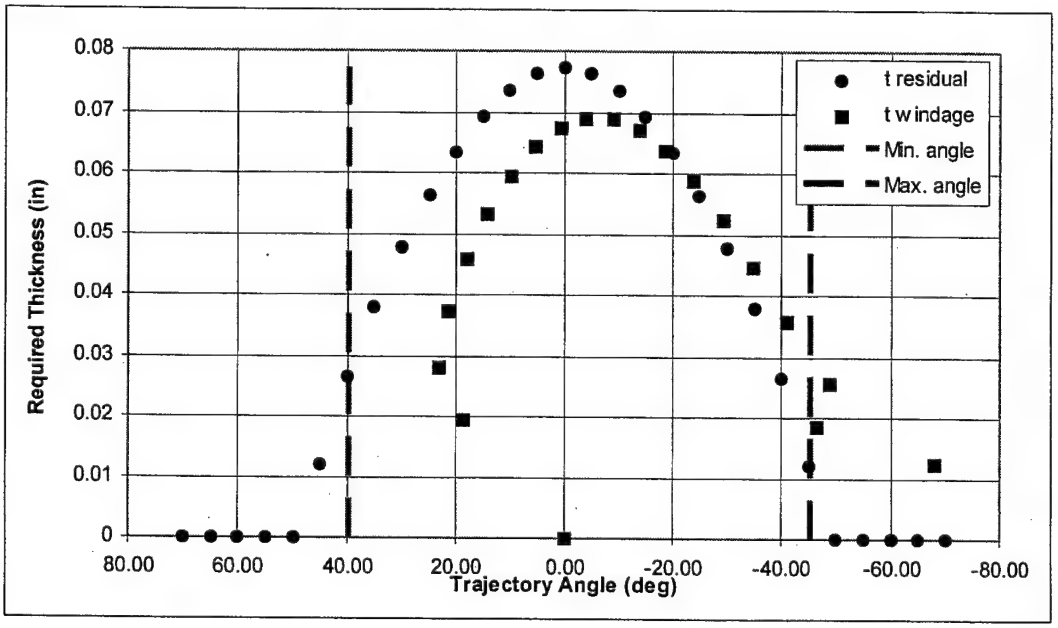

FIGURE 4-26. PREDICTED SKIN THICKNESS TO DEFEAT A 100% COMPRESSOR BLADE

4.2.1.2 Compressor Disk Aerodynamic Effects.

The effect of windage on a disk fragment trajectory was estimated. The sensitivity calculations were conducted at 35,000 ft, Mach 0.85 flight conditions. The disk characteristics used were based on the 50% disk fragment, specifics can be found in table 3-5. The analysis was conducted for a debris fragment traveling 30 feet radially from the engine centerline. At this point, the disk has traveled 8.5 ft aft resulting in a change in trajectory angle of about-22 degrees (figure 4-27).

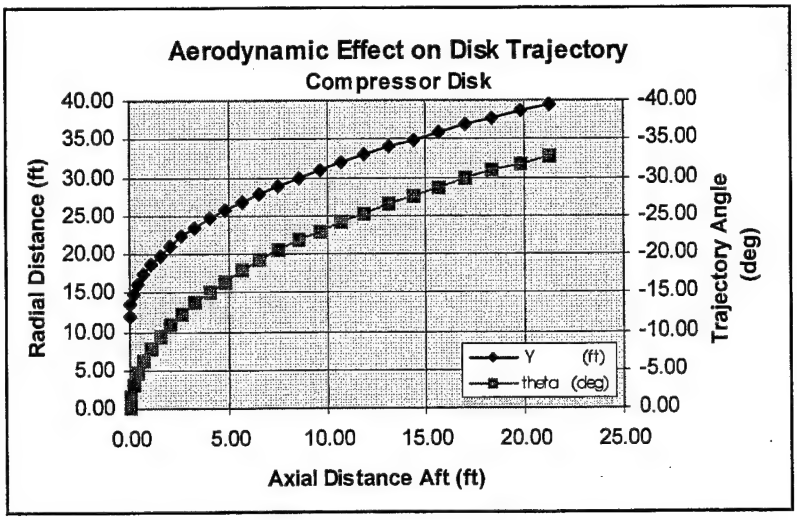

FIGURE 4-27. COMPRESSOR DISK WINDAGE EFFECTS

4.2.1.3 Compressor Disk Damage.

Figure 4-28 shows a compressor disk fragment after passing through the fuselage. Figure 4-29 shows a very tight trajectory band of 5 to -5 degrees for disk debris. Initial energy levels are near 25,000 ft-lbf. These levels are similar to the fan blade energy levels presented earlier (figure 4-6). Disk pieces, however, often enter the fuselage edgewise making them far more likely to penetrate aircraft structure.

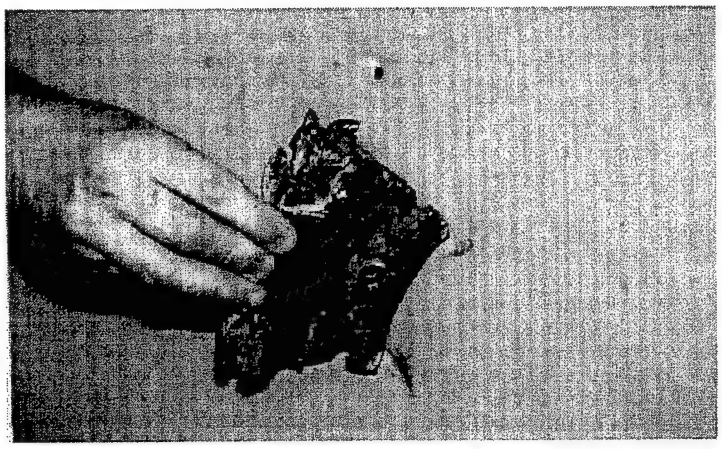

FIGURE 4-28. COMPRESSOR DISK FRAGMENT AFTER PASSING THROUGH THE FUSELAGE

4.2.2 Compressor Rim Failure.

4.2.2.1 Compressor Blade Damage From a Rim Failure.

Figure 4-30 shows blade damage from a rim event. Notice most of the damage clusters near the 100% damage ratio. Hence, the debris energy estimates from figure 4-24 still apply. For the rim

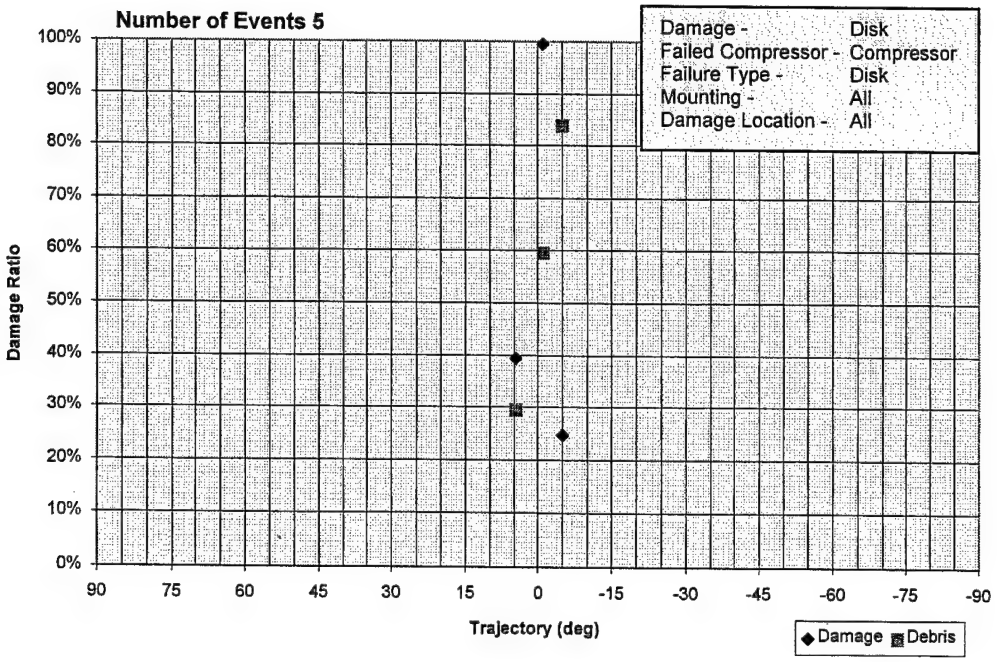

FIGURE 4-29. COMPRESSOR DISK DAMAGE FROM A DISK EVENT

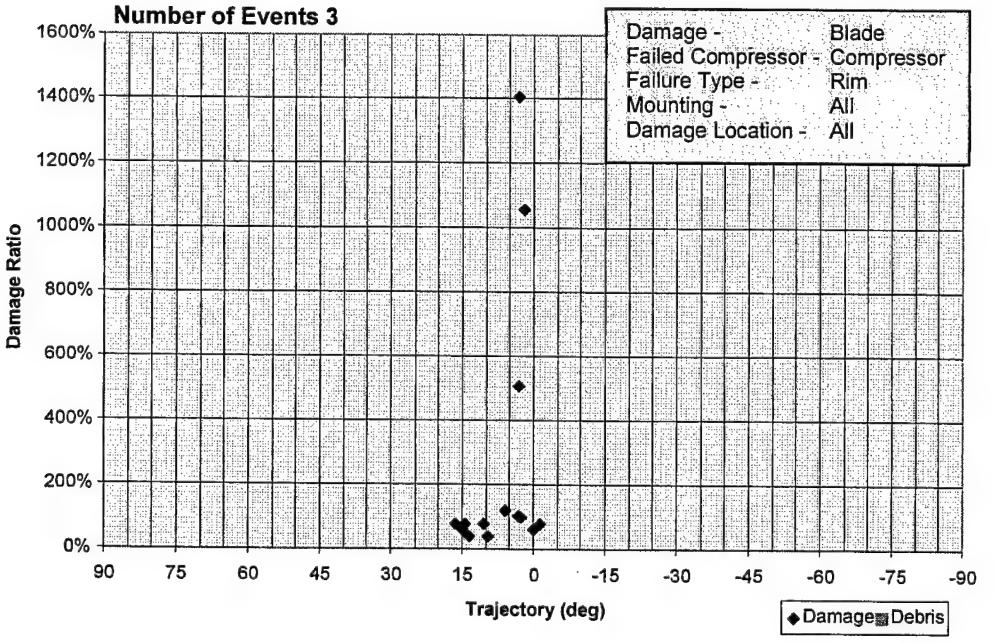

FIGURE 4-30. COMPRESSOR BLADE DAMAGE FROM A RIM EVENT

events, the trajectory angles are from 0 to 15 degrees, but only three events are cataloged. Additional events may expand the trajectory angles to the limits shown in figure 4-23.

4.2.2.2 Compressor Rim Damage.

Figure 4-31 shows the trajectory range for compressor rim events. Estimated initial energy levels approach 30,000 ft-lbf, but these components also enter edgewise making them difficult to defeat. Component size of a 100% rim piece should be used.

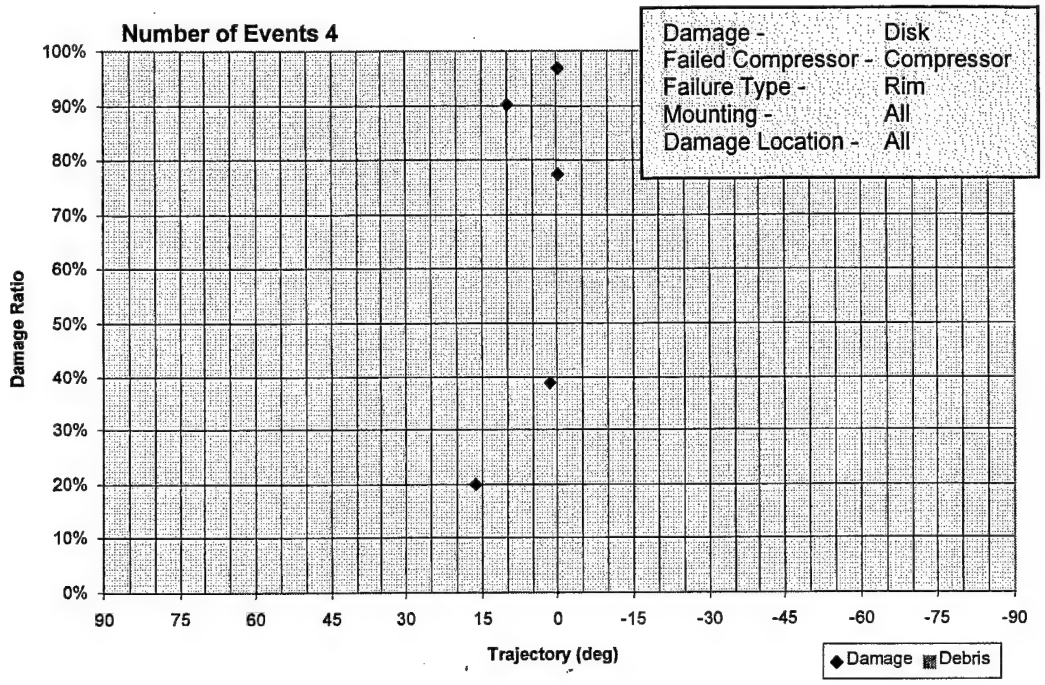

FIGURE 4-31. COMPRESSOR DISK DAMAGE FROM A RIM EVENT

4.2.3 Compressor Issues.

As noted in section 4.3.1.1, a significant portion of the near-field debris from a compressor disk event is probably from the compressor case or other engine components. Methods for characterizing this debris size and energy levels should be evaluated.

4.3 TURBINE ANALYSIS.

Turbine analysis was broken into high-pressure turbine (HPT) blade analysis and low-pressure turbine (LPT) blade analysis. HPT analysis holds for HBR and LBR engines as the core speeds are comparable. LPT analysis was conducted using rotor speeds representative of HBR and LBR engines respectively. Within the LPT analysis, two sets of debris energy calculations were conducted. One with a 0.04-inch cowl and one without. The latter was performed to investigate the large aft trajectory angles which are encountered in the trajectory plots.

4.3.1 Turbine Disk Failure.

4.3.1.1 Turbine Blade Damage From a Disk Failure.

Figure 4-32 shows a representative turbine blade debris size to be 50% or less. The trajectory angles are between 15 and -75 degrees, which are quite extreme. Every event shown in figure 4-32 was a wing-mounted engine; no fuselage-mounted turbine disk events are in the debris database. Figure 4-33 shows fuselage damage from a wing-mounted engine from 15 degrees to -45 degrees. Figure 4-34 shows the near-field wing damage from a wing-mounted engine to vary from 10 to -75 degrees. These two charts indicate that there is a significant difference in trajectories from near field to far field. A possible explanation, as has been seen in the residual velocity and kinetic energy plots, is that the debris traveling to the fuselage at smaller angles has higher energy than the debris traveling at the large aft trajectories. For the purpose of the turbine blade damage from disk failure the trajectories of interest will be 15 to -45 degrees.

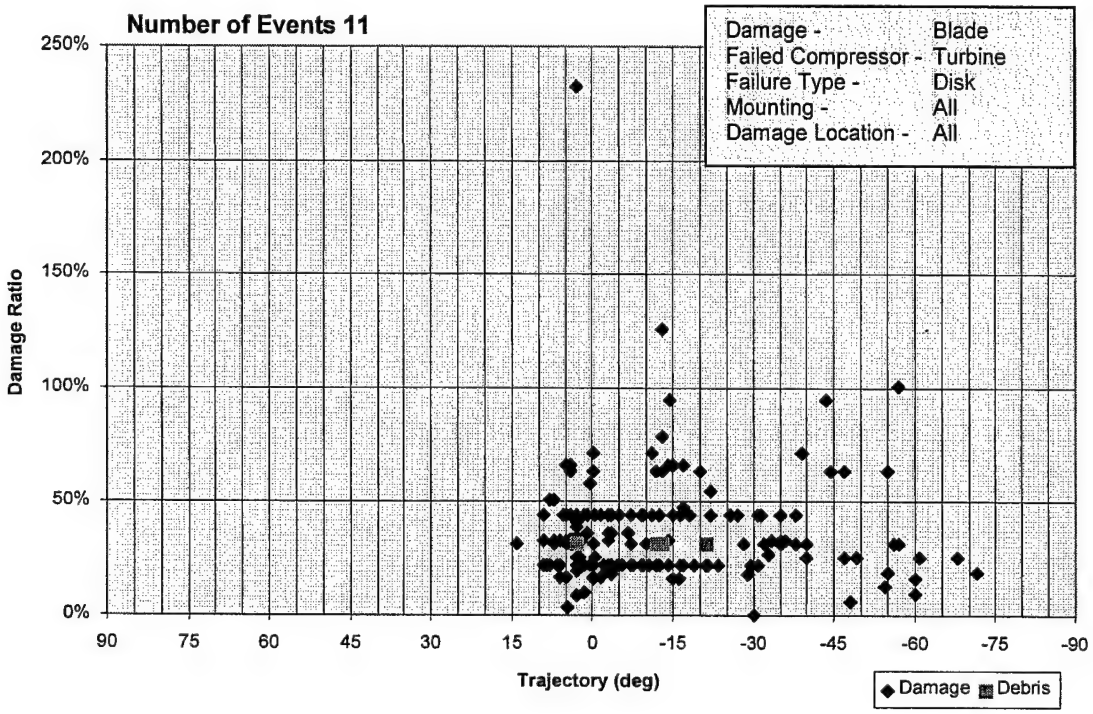

FIGURE 4-32. TURBINE BLADE DAMAGE FROM A DISK EVENT

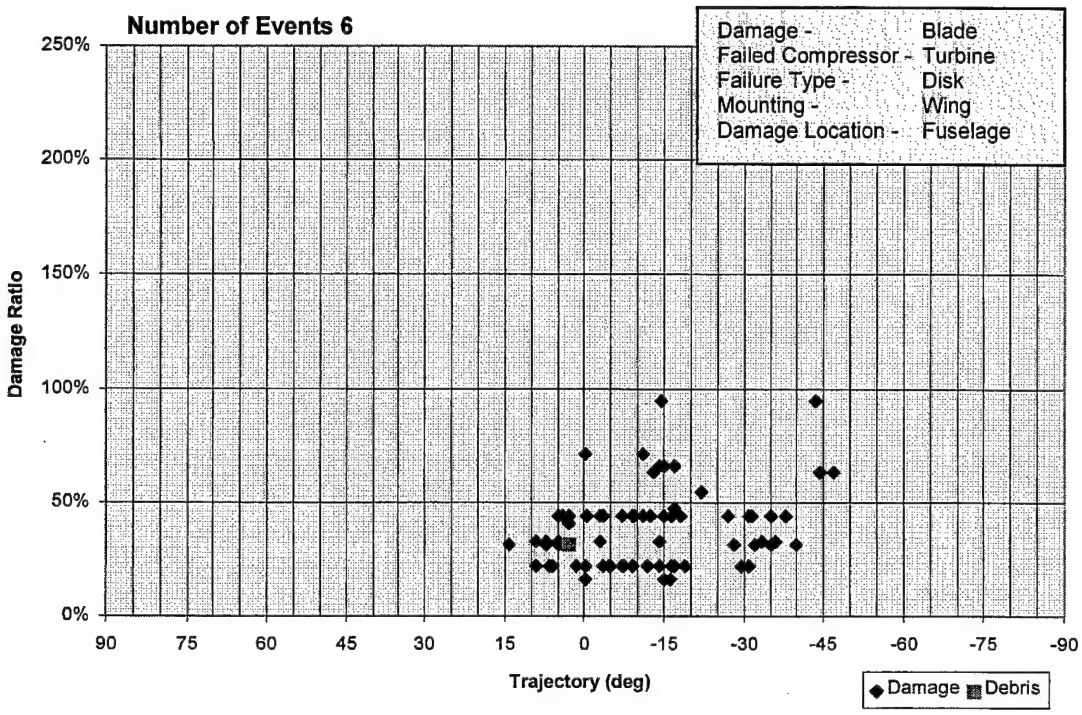

FIGURE 4-33. TURBINE BLADE FUSELAGE DAMAGE FROM A DISK EVENT

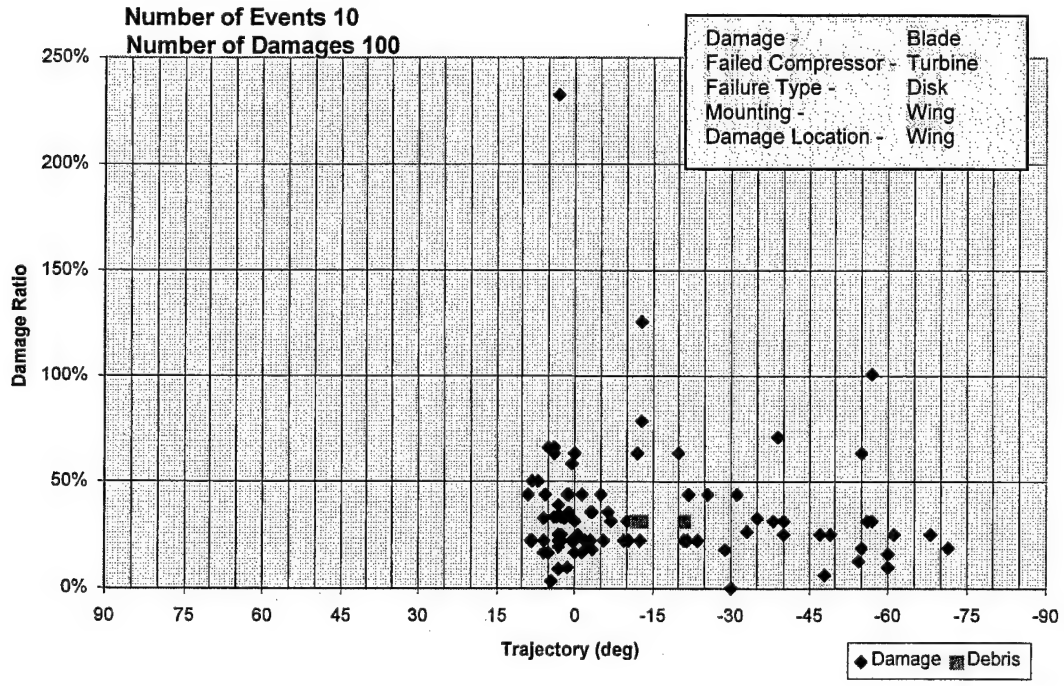

FIGURE 4-34. TURBINE BLADE WING DAMAGE FROM A DISK EVENT

4.3.1.1.1 High-Pressure Turbine (HPT).

In keeping with the debris energy model presented in figure 2-1, a debris energy analysis was performed using a 0.04 inch cowl over the turbine. Debris characteristics are provided in table 3-5. Seventy-five percent of the debris initial velocity was used in this analysis. The results for the 100% HPT blade are shown in figure 4-35. Figure 4-36 shows the required skin thickness to defeat the associated energy levels (figure 4-35). The analysis indicates that there is sufficient energy for a fragment to penetrate a 0.040-inch aluminum skin from approximately 30 degrees forward to -40 degrees aft.

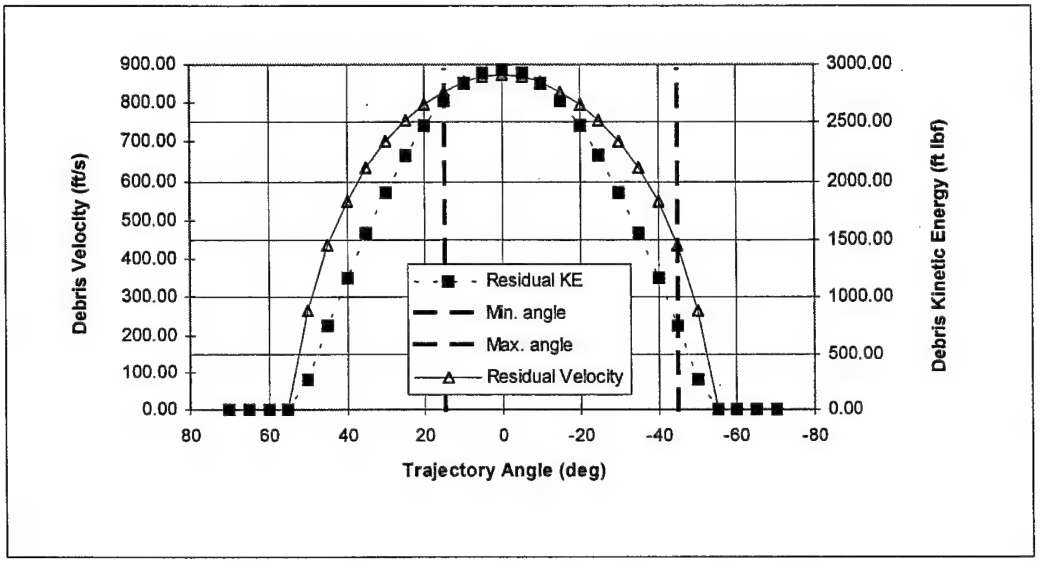

(a) Residual Velocity and Energy Once Outside the Cowl

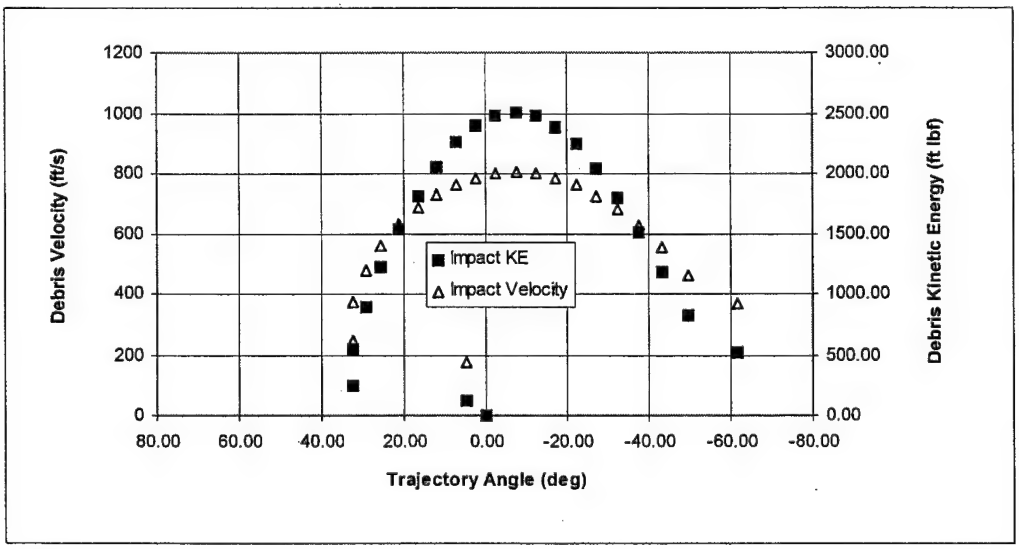

(b) Debris Characteristics After Traveling 30 ft From a Wing-Mounted Engine (Altitude = 35,000, Mach = 0.85)

FIGURE 4-35. DEBRIS ENERGY ESTIMATION FOR A 100% HP TURBINE BLADE

4.3.1.1.2 Low-Pressure Turbine (LPT).

The majority of the LPT uncontained blade data is associated with the last rotating stage that has no downstream nozzle vanes. This coupled with blade debris exiting the nozzle and aerodynamic effects results in an aft skew of the aircraft damage data.

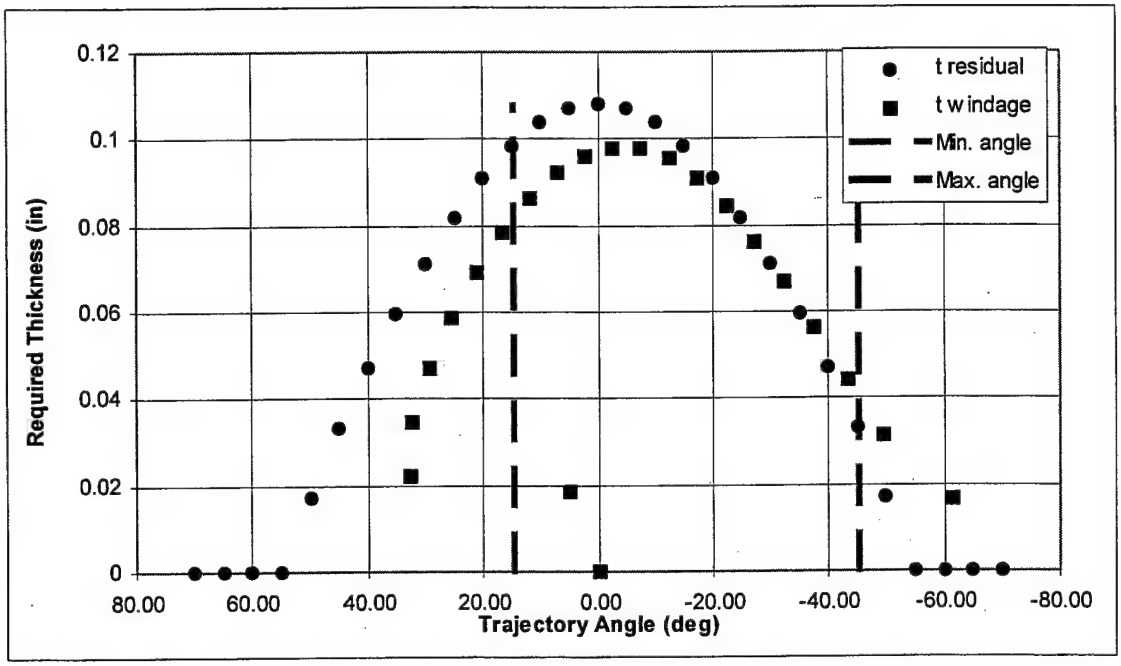

FIGURE 4-36. PREDICTED SKIN THICKNESS TO DEFEAT A 100% HP TURBINE BLADE

4.3.1.1.2.1 High Bypass Ratio Engine, Low-Pressure Turbine.

A similar analysis was conducted on high bypass ratio LPT blade debris. Figures 4-37 and 4-38 define the debris residual energy levels and plate thickness required to stop the fragment. This analysis shows that there is very low debris residual energy if the debris is to pass through the cowl. An additional analysis was conducted to define the highest debris energy level. This analysis was conducted such that there was no energy loss from the debris passing through the cowling (i.e., the cowl had a pre-existing hole). The initial velocity used is 75% of that shown in table 3-5. Results of this analysis (figures 4-39 and 4-40) show that although the energy levels are higher than the case with the cowl, the residual energies are still low and likely would not be a significant hazard to the aircraft.

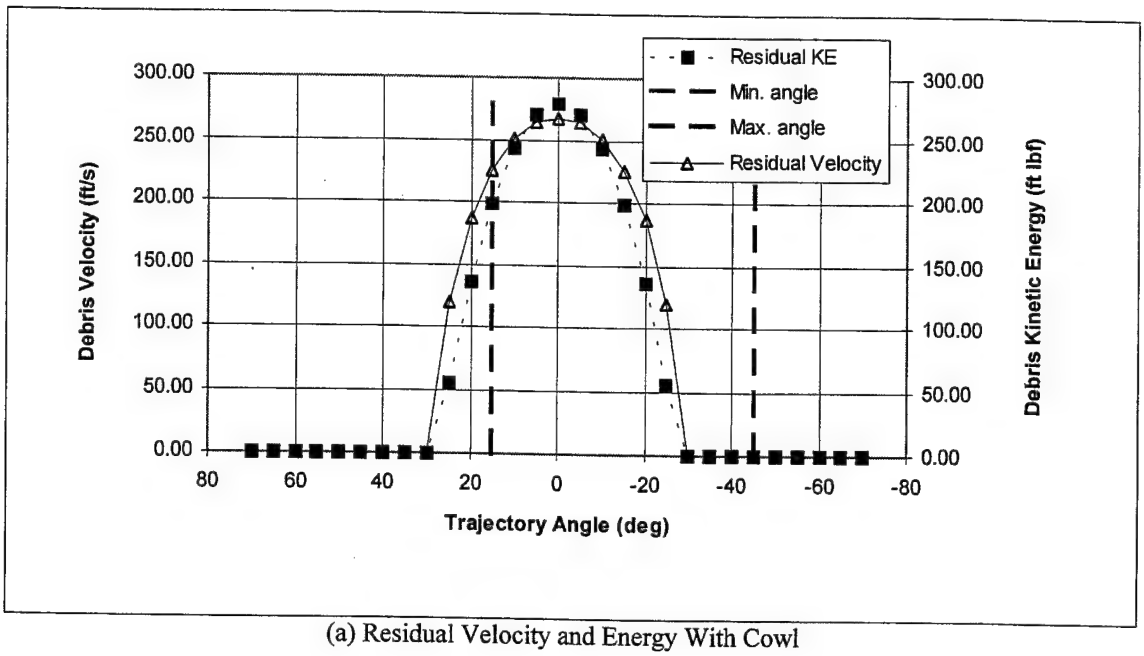

(a) Residual Velocity and Energy With Cowl

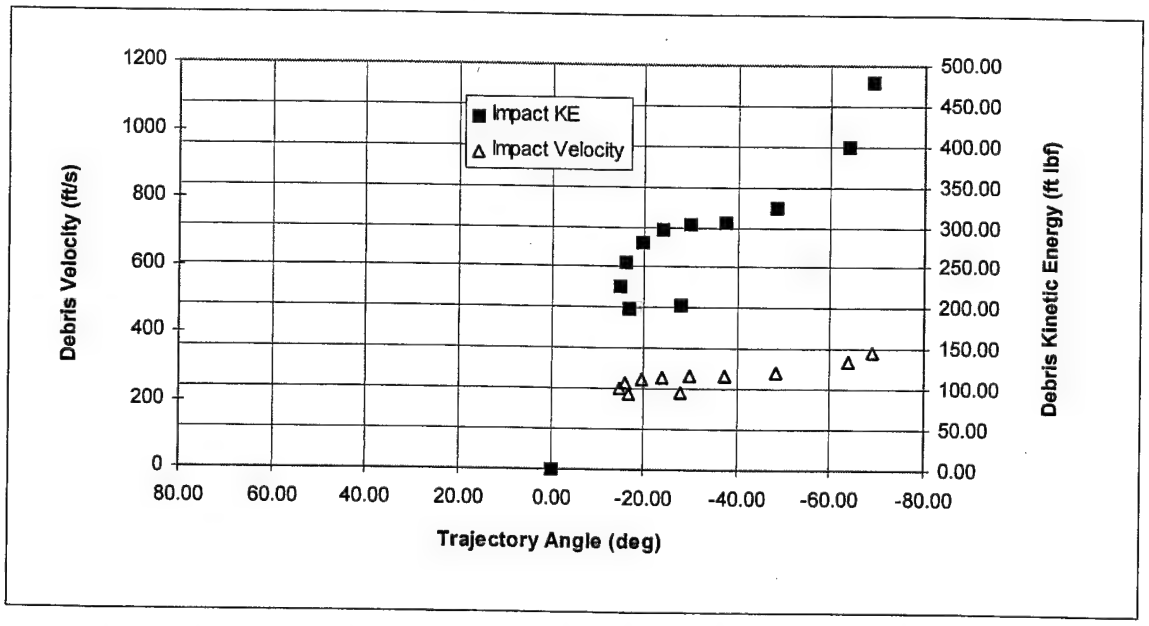

(b) Debris Characteristics After Traveling 30 ft From a Wing-Mounted Engine With Cowl Loss (Altitude = 35,000, Mach = 0.85)

FIGURE 4-37. DEBRIS ENERGY ESTIMATION FOR HBR 50% LP TURBINE BLADE WITH THE COWL

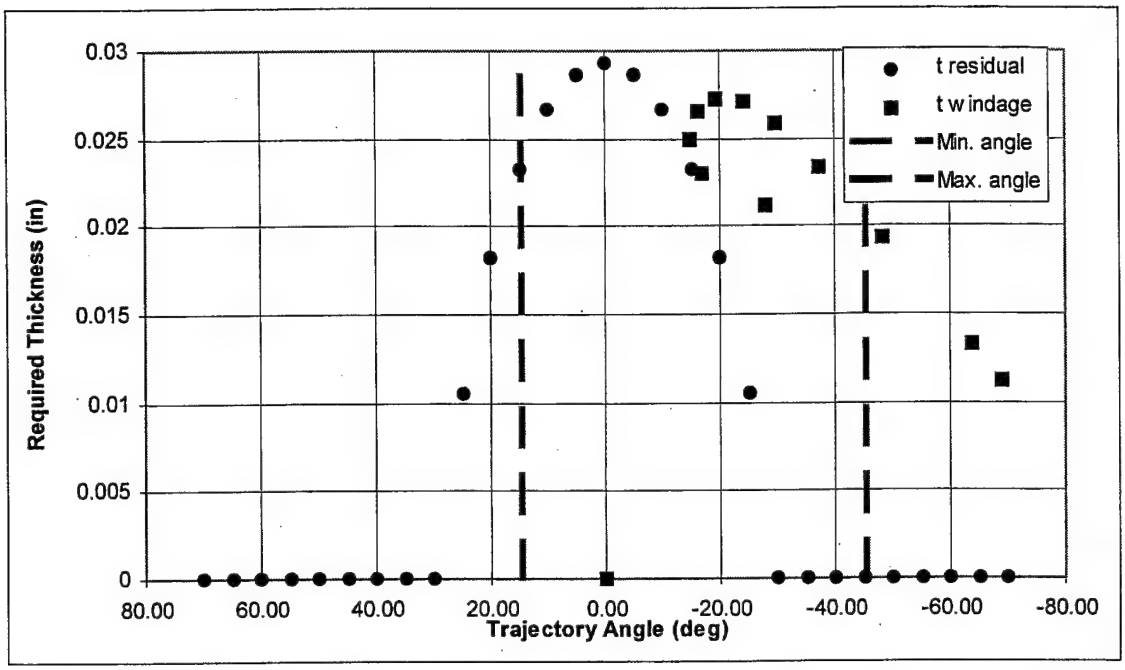

FIGURE 4-38. PREDICTED SKIN THICKNESS TO DEFEAT A HBR 50% LP TURBINE BLADE WITH THE COWL

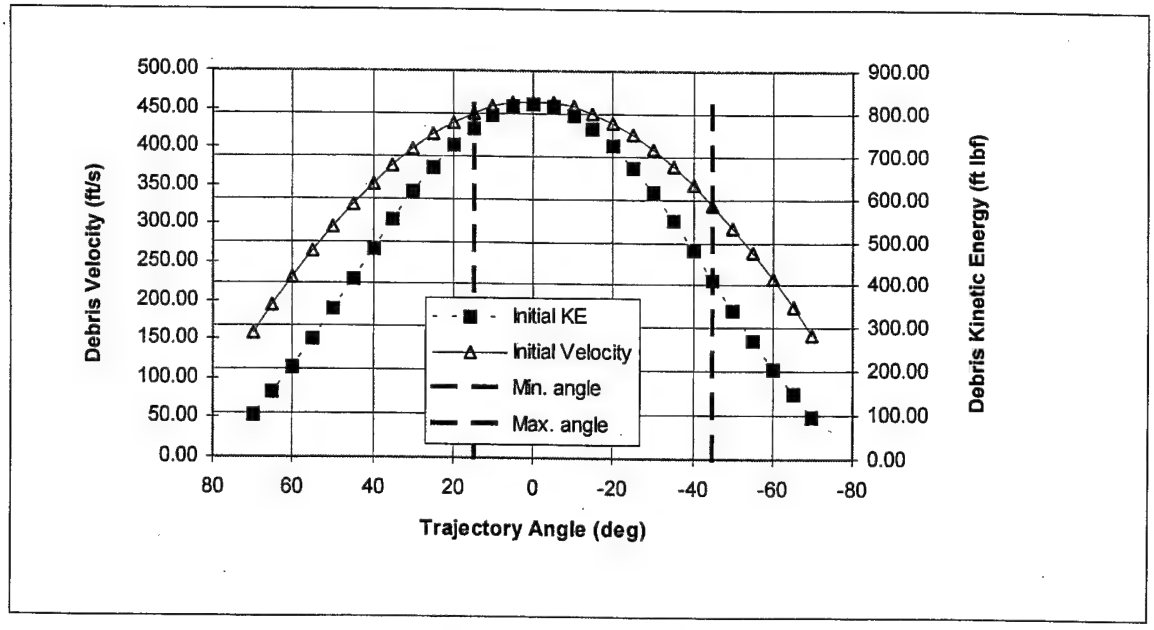

(a) Residual Velocity and Energy Without Cowl

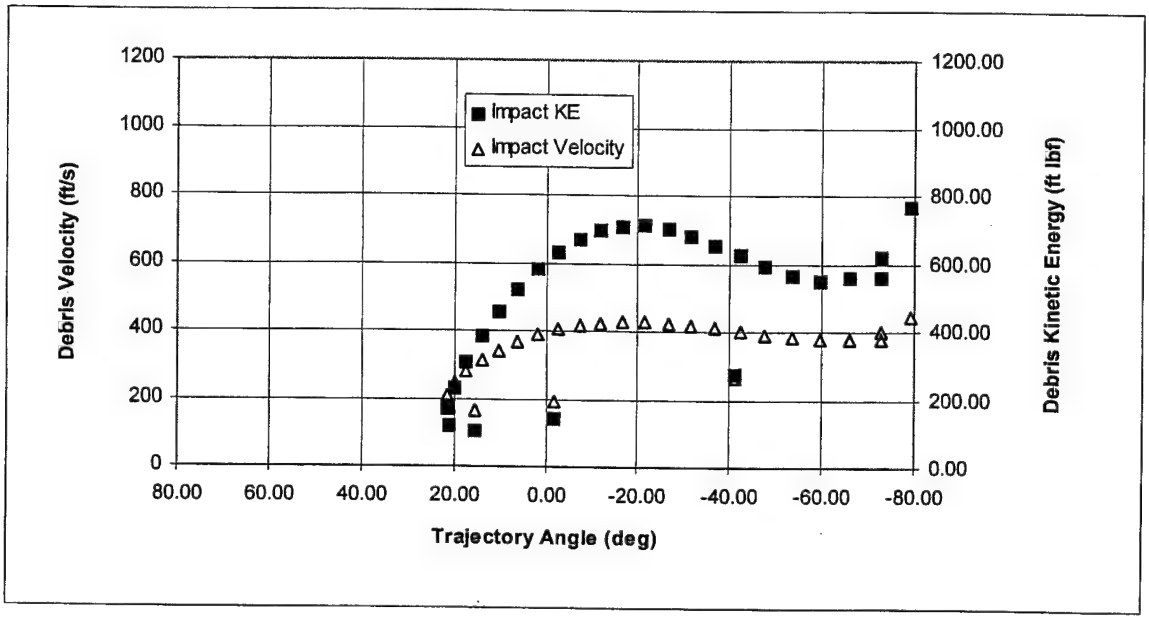

(b) Debris Characteristics After Traveling 30 ft From a Wing-Mounted Engine Without Cowl Loss (Altitude = 35,000, Mach = 0.85)

FIGURE 4-39. DEBRIS ENERGY ESTIMATION FOR HBR 50% LP TURBINE BLADE WITHOUT THE COWL

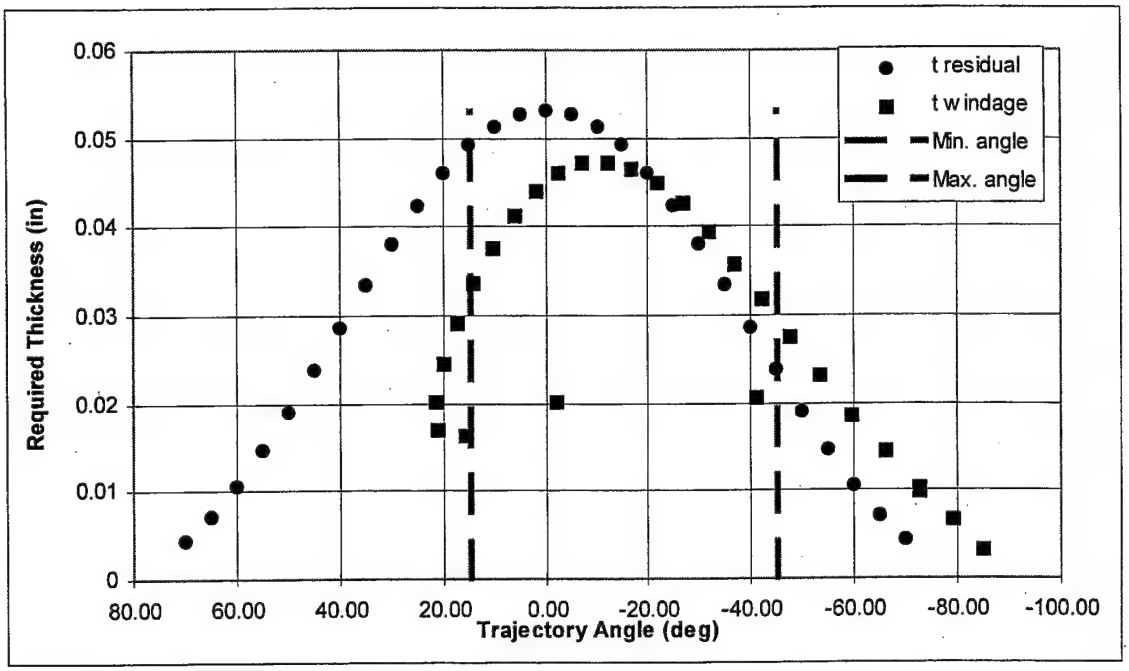

FIGURE 4-40. PREDICTED SKIN THICKNESS TO DEFEAT A HBR 50% LP TURBINE BLADE WITHOUT THE COWL

4.3.1.1.2.2 Low Bypass Ratio Engine, Low-Pressure Turbine.

This analysis was conduct in the same fashion as the HBR LPT analysis. Due to the significant increase in rotor speed and thus initial velocity (table 3-5), debris energy levels are considerably higher (figures 4-41 and 4-42). Peak kinetic energy (KE) values of over 3000 ft-lbf could pose a threat to the aircraft if the impact occurred at a high impact orientation (edge on). Penetration of a 0.040-inch skin would occur between 35 and -45 degrees. An additional analysis was conducted without the cowl and peak energies of over 4000 ft-lbf (figures 4-43 and 4-44).

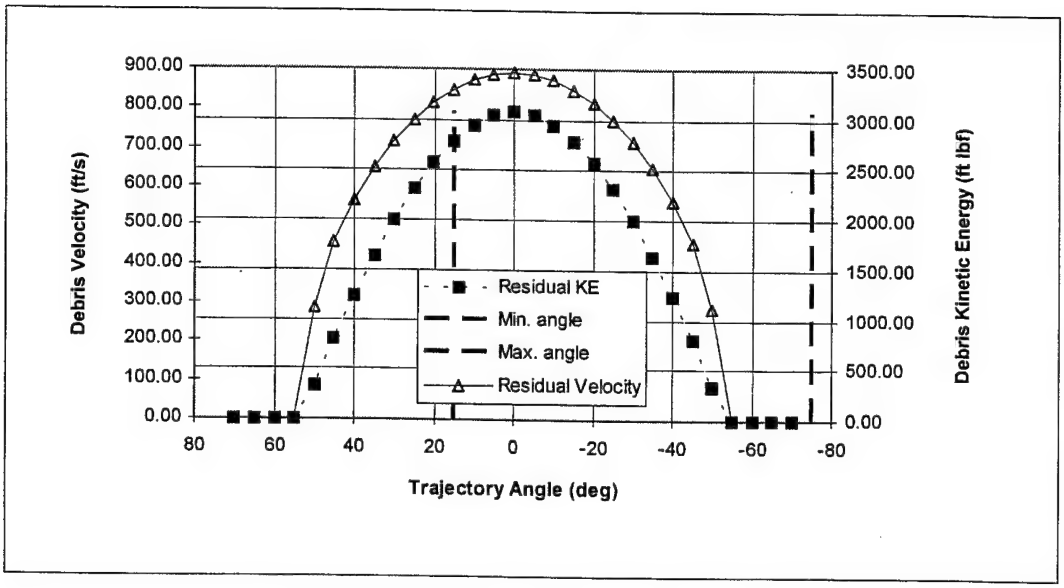

(a) Residual Velocity and Energy With Cowl

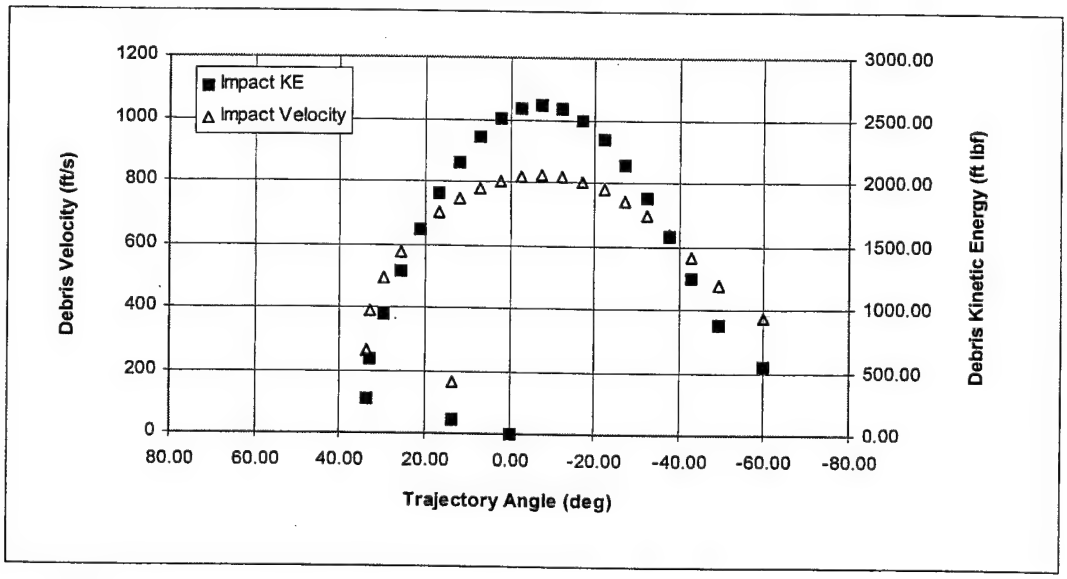

(b) Debris Characteristics After Traveling 30 ft From a Wing-Mounted Engine With Cowl Loss (Altitude = 35,000, Mach = 0.85)

FIGURE 4-41. DEBRIS ENERGY ESTIMATION FOR LBR 50% LP TURBINE BLADE WITH THE COWL

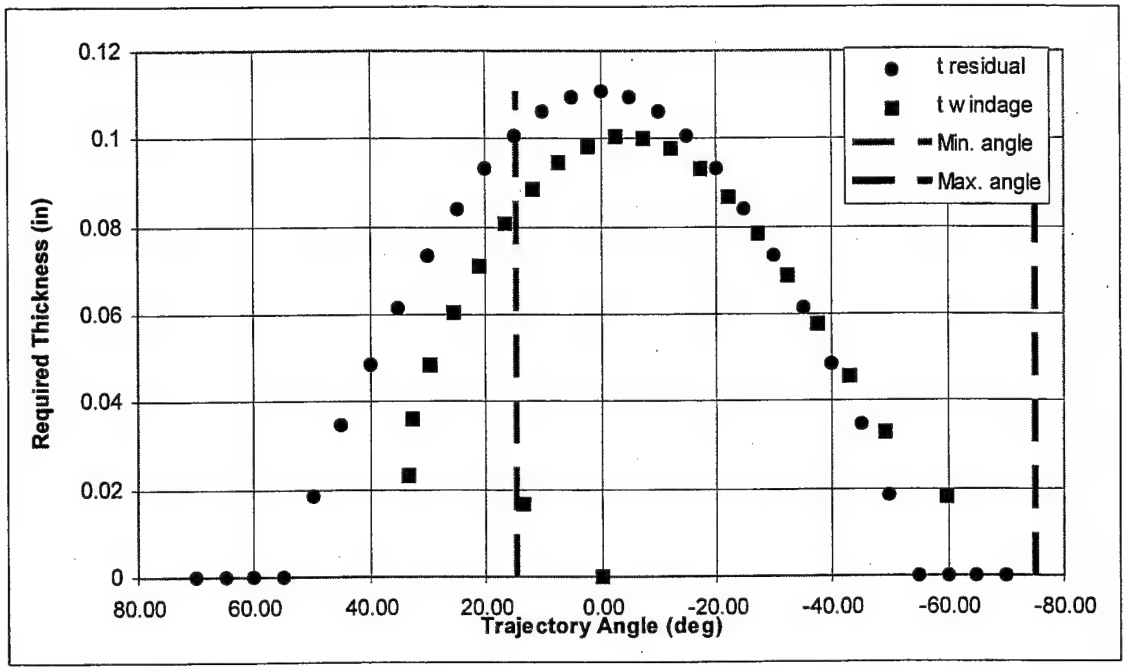

FIGURE 4-42. PREDICTED SKIN THICKNESS TO DEFEAT A LBR 50% LP TURBINE BLADE WITH THE COWL

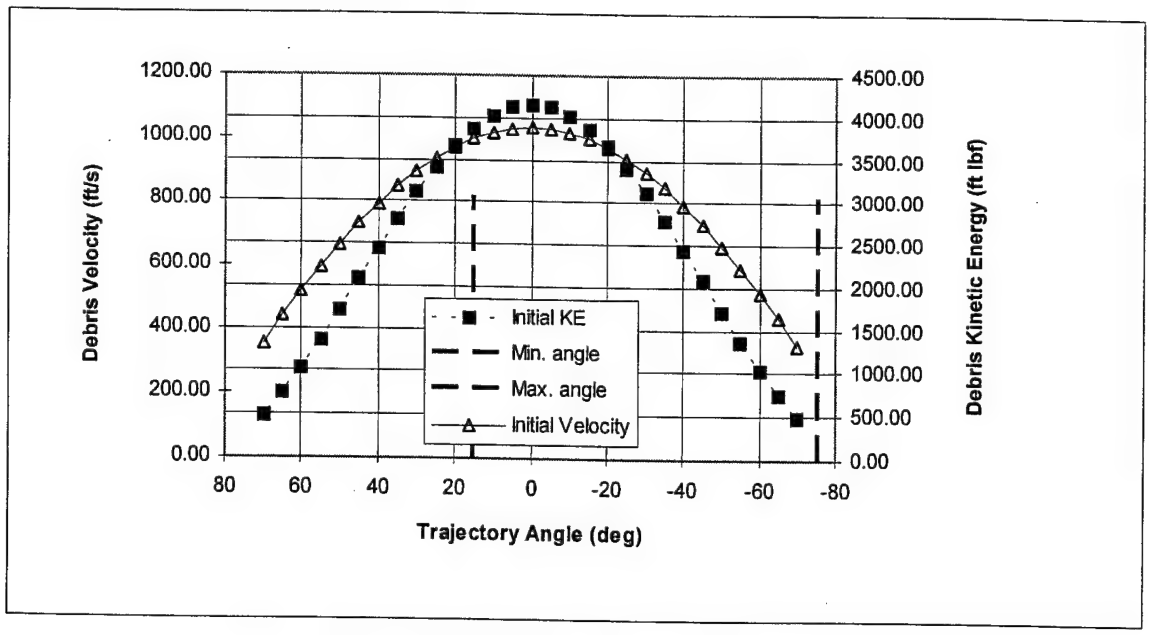

(a) Residual Velocity and Energy With Cowl

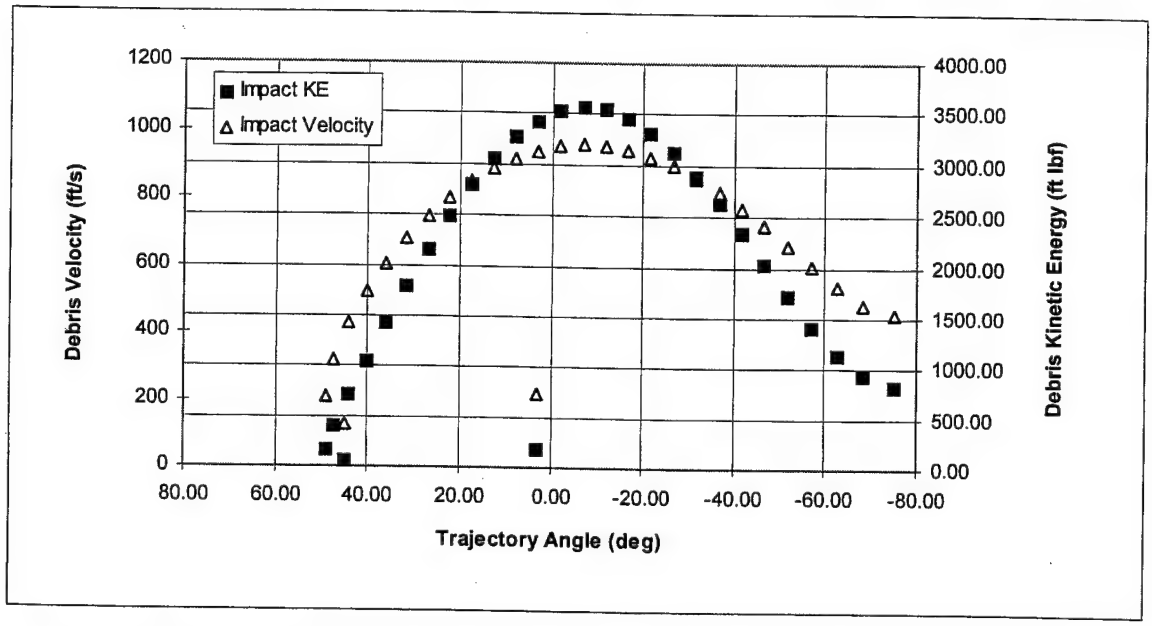

(b) Debris Characteristics After Traveling 30 ft From a Wing-Mounted Engine Without Cowl Loss (Altitude = 35,000, Mach = 0.85)

FIGURE 4-43. DEBRIS ENERGY ESTIMATION FOR LBR 50% LP TURBINE BLADE WITHOUT THE COWL

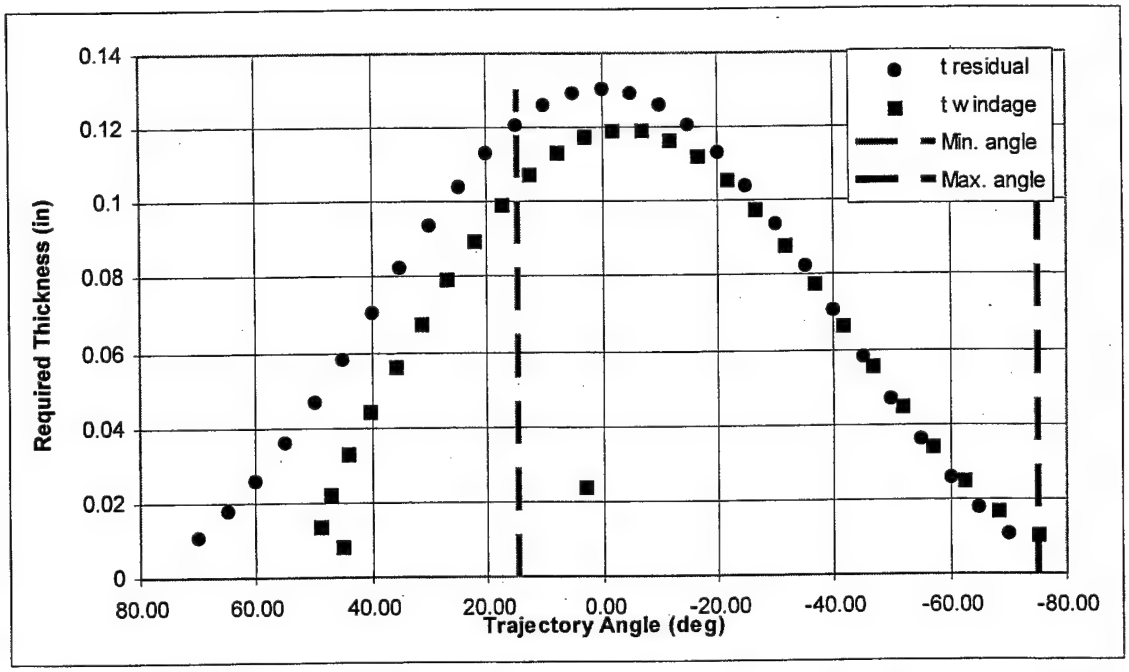

FIGURE 4-44. PREDICTED SKIN THICKNESS TO DEFEAT A LBR 50% LP TURBINE BLADE WITHOUT THE COWL

4.3.1.1.2.3 Turbine Disk Event, Blade Damage Summary.

To summarize the blade damage from disk events, there are several points of consideration. Based on a typical fuselage skin thickness of 0.04 inch, the model predicts debris has sufficient energy to damage the aircraft up to 35 degrees forward, but the debris database only shows damage to 15 degrees. There may be an inherent reason related to a turbine case design that limits the forward trajectories of blade debris. Using the same 0.04-inch skin thickness, it provides an excellent match with the -45 degree trajectory angle shown in figure 4-33 for fuselage damage. The model predicts there is not enough debris energy to penetrate at -75 degrees when the debris exits the side of the engine.

Turbine blade fragments that exit in a helical trajectory should be considered to account for the larger aft trajectories. For turbine events, there is typically static engine structure aft of the rotor that will effect the blade debris' ability to exit out the tailpipe in a helical fashion. However, last stage events of turbines without turbine frame struts have demonstrated this helical debris trajectory. For this special case, debris cannot only exit the side of the engine/cowl but also the tailpipe with significant tangential velocity component. Further discussion is provided in section 4.3.3.2.

An additional explanation of the large aft trajectories is the difference between the engine position with respect to the wing surface (for the most part, forward of the lower wing surface). Also a factor is the relatively thinner skins of the wing aerodynamic surfaces (i.e., leading edge and trailing edge devices) that are easily penetrated.

4.3.1.2 Turbine Disk Aerodynamic Effects.

The effect of windage on a disk fragment trajectory was estimated. The calculations were conducted at 35,000 ft, Mach 0.85 flight conditions. The disk characteristics used were based on the 100% disk fragment, specifics can be found in table 3-5. The analysis was conducted for a debris fragment traveling 30 feet radially from the engine centerline. At this point, the disk has traveled 1.3 ft aft resulting in a change in trajectory angle of about -3.5 degrees (figure 4-36).

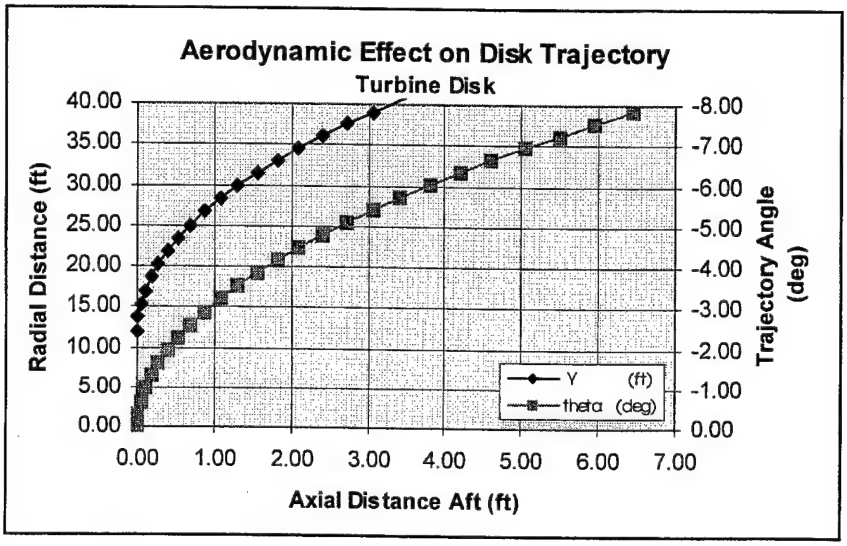

FIGURE 4-45. TURBINE DISK AERODYNAMIC EFFECTS

4.3.1.3 Turbine Disk Damage.

Figure 4-46 shows tight trajectory angles from 5 to -5 degrees for turbine disk damage. The aft trajectory angle extends to -13 degrees when runway rebound is included. Initial kinetic energy is near 340,000 ft-lbf for half a disk. Debris residual energy estimates after penetrating the engine casing are not presented.

4.3.2 Turbine Rim Failure.

4.3.2.1 Turbine Blade Damage From a Rim Failure.

Figure 4-47 shows the trajectory of a rim failure event. Figure 4-48 shows the turbine rim fragments. Figure 4-49 plots turbine blade damage from a rim failure event. This figure shows trajectory angles skewed to the aft direction for a disk failure mode commonly referred to as a "rim-peal." This failure mode occurs for at least two reasons: (1) a spacer or thin-wall sealing ring attached to the disk may fracture in such a way that it "unpeals" from the rotor, and (2) a circumferential fracture under the rim of some disk designs which progress circumfrentially up to 180 degrees before terminating in a radial fracture that releases a portion of the rim. This particle presents itself as a edge-on threat as it passes through the engine cowling. This type of debris has a long length, equivalent to the diameter of the rotor disk and a tumbling action which permits it to be significantly affected by windage effects.

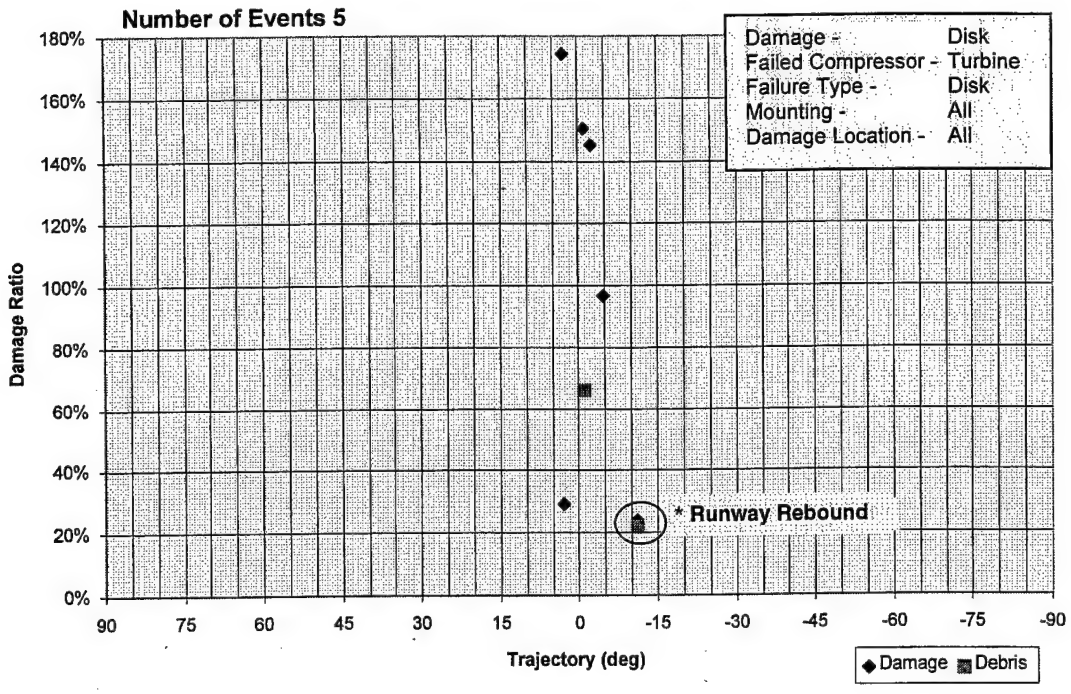

FIGURE 4-46. TURBINE DISK DAMAGE FROM A DISK EVENT

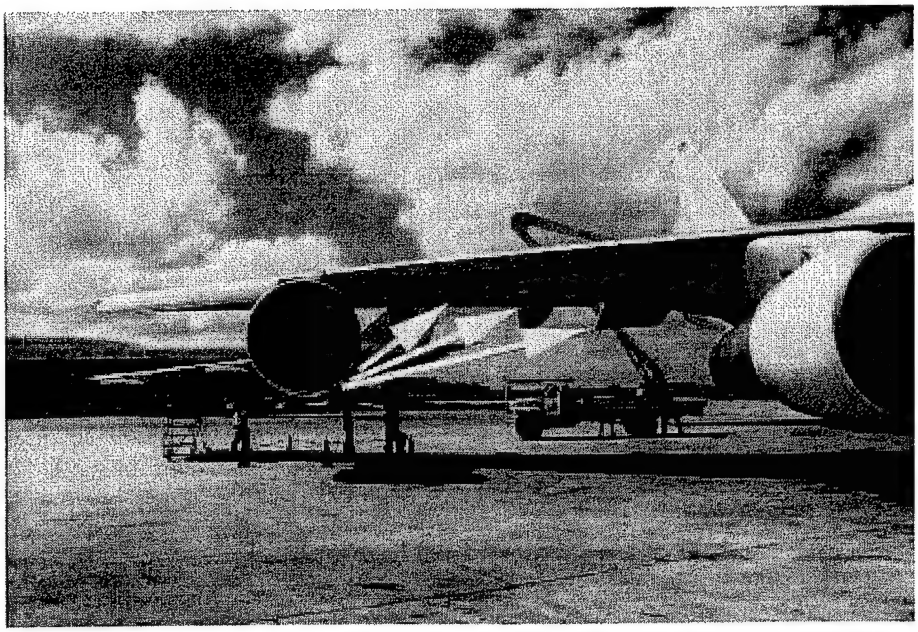

FIGURE 4-47. TRAJECTORY OF RIM FAILURE EVENT

Most of the damage is below the 100% damage ratio allowing figures 4-35, 4-37, and 4-41 to be used for debris energy estimation of HPT and LPT blades respectively. Trajectory angles are from 20 to -45 degrees. Noticeably absent are the large aft trajectory angles. All of this data was also from wing-mounted engines.

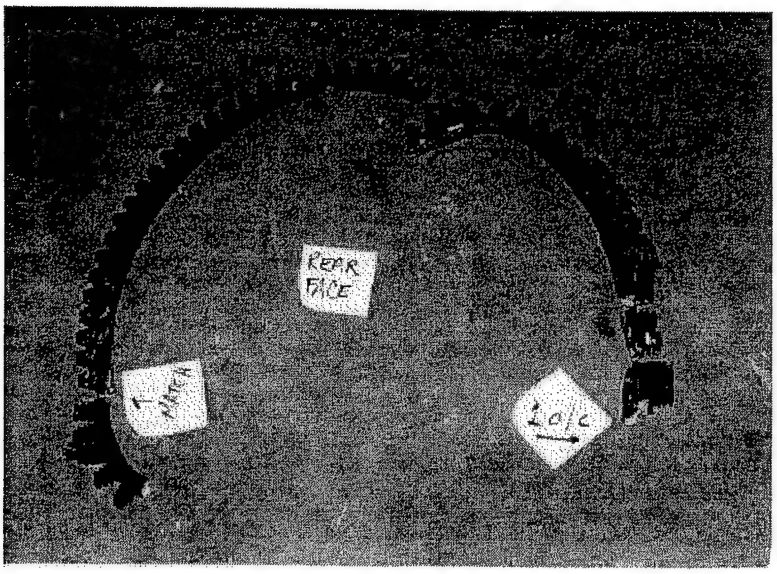

FIGURE 4-48. TURBINE RIM FRAGMENTS FROM RIM PEAL EVENT

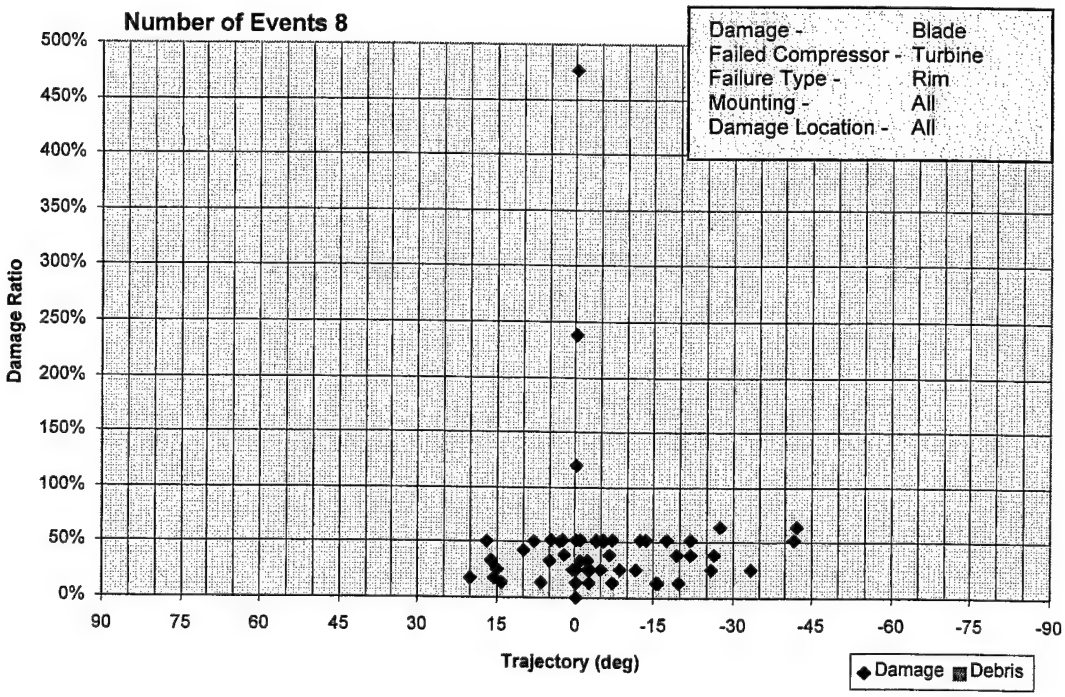

FIGURE 4-49. TURBINE BLADE DAMAGE FROM A RIM EVENT

4.3.2.2 Turbine Disk Damage From a Rim Failure.

Figure 4-50 shows the fuselage damage from turbine rim debris. Figure 4-51 shows the trajectory angles to range from 0 to -30 degrees. A 50% damage ratio should be used to characterize the piece. Initial energy approaches 160,000 ft-lbf.

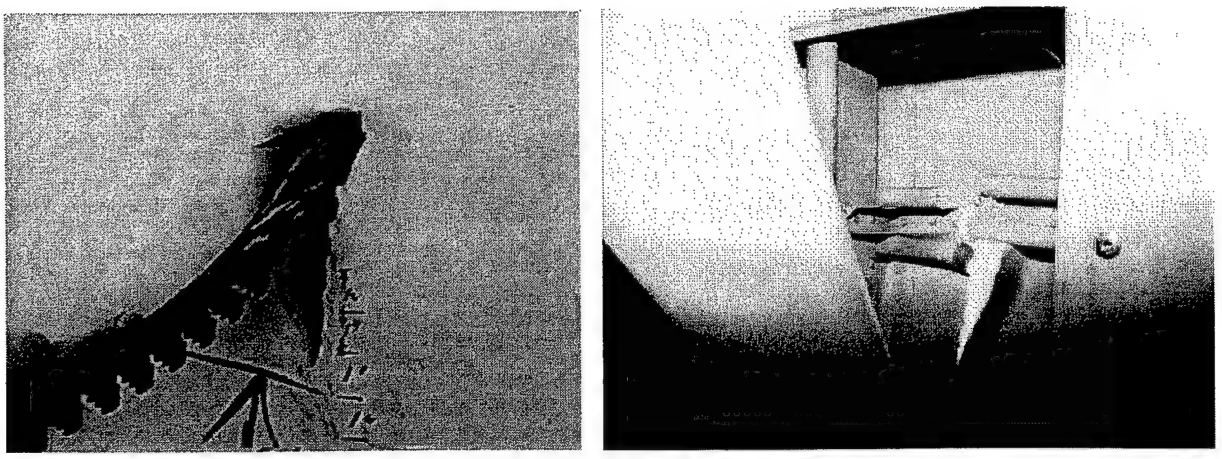

FIGURE 4-50. FUSELAGE DAMAGE FROM TURBINE RIM DEBRIS

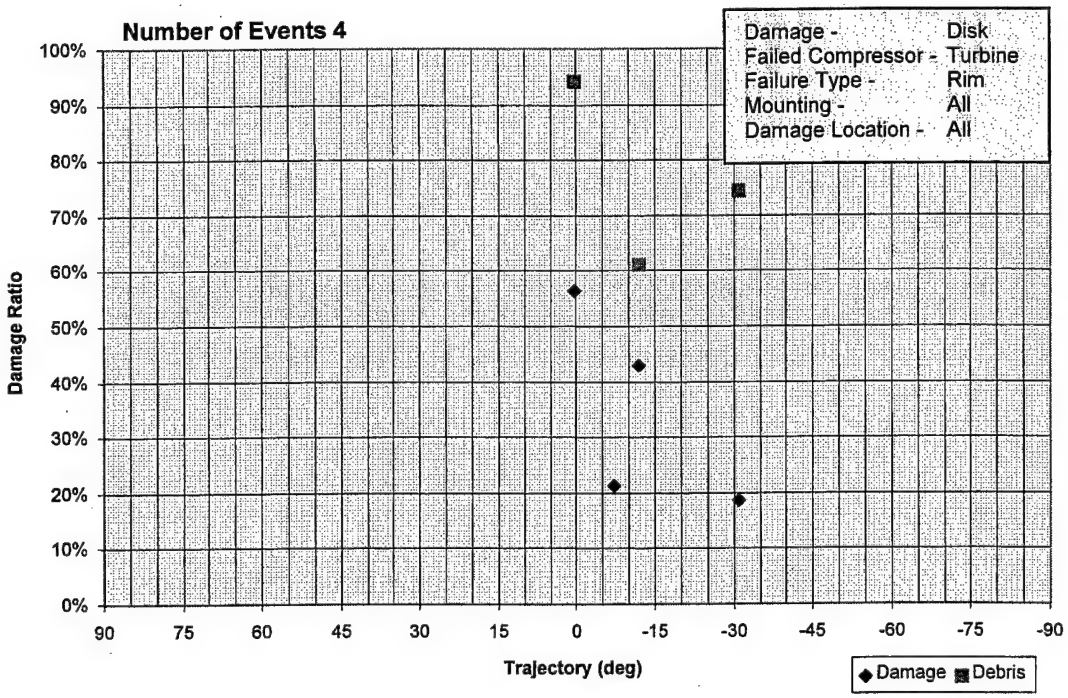

FIGURE 4-51. TURBINE DISK DAMAGE FROM A RIM EVENT

4.3.3 Turbine Blade Failure.

Figure 4-52 plots data for all blade failure events. A majority of the data are below the 50% damage ratio level with trajectory angles between 20 and -75 degrees. These trends are remarkably similar to the blade damage trends from the disk failure events.

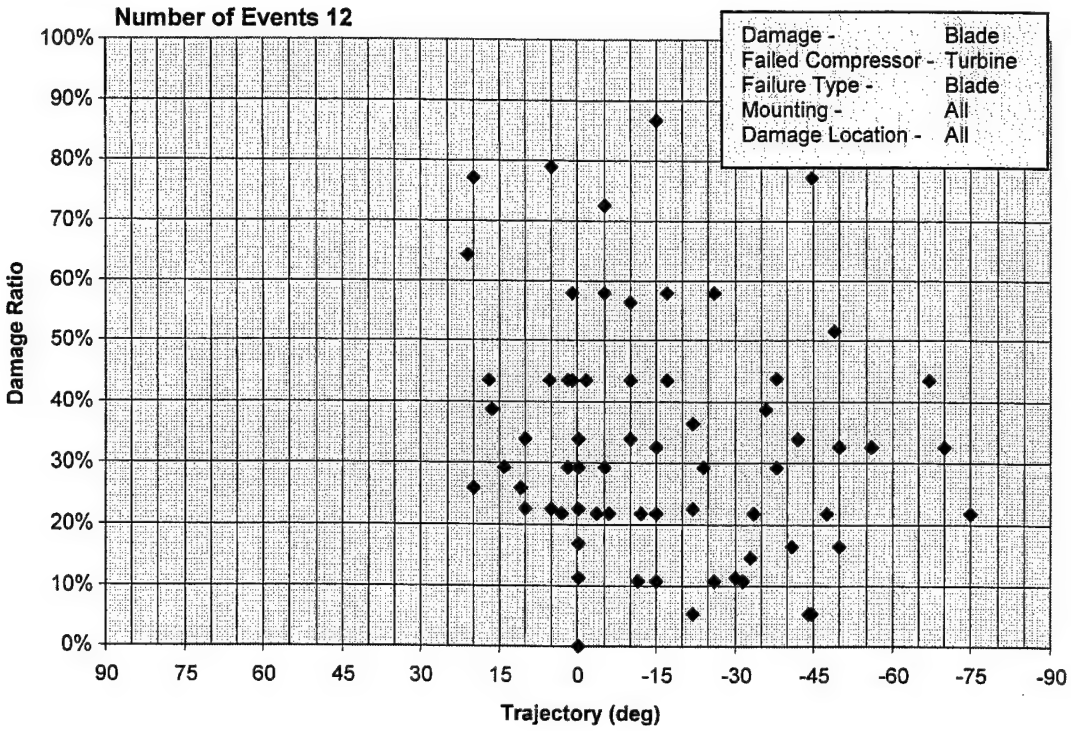

FIGURE 4-52. TURBINE BLADE DAMAGE FROM A BLADE EVENT

Figure 4-53 only plots fuselage-mounted engine data and shows the trajectory angles to range from 20 to -45 degrees. Figure 4-54 shows wing damage to range from 20 to -75 degrees. These trends are practically identical to the fan blade damage trends from disk events (figures 4-33 and 4-34, respectively). High-pressure turbine blade damage from blade events are plotted in figure 4-55. The data show a trajectory spread of 20 to -50 degrees, with fragment sizes ranging up to 90% of the blade length. Excluding the damages of unknown size at 0%, half of the damages are above 50%. Low-pressure turbine blade damage from blade events are plotted in figure 4-56. The data show trajectory spread angles of 17 to -75 degrees, with fragment sizes falling mostly within the 50% range.

There is an additional factor to address, blade failure from the last turbine stage. Seven of the twelve events shown in figure 4-53 occurred from the final stage. Three were low bypass ratio engines and are shown in figure 4-57. The trajectory angles range from 15 to -45 degrees showing no propensity for producing large aft trajectories. High bypass ratio engines do have this trend as shown in figure 4-58. Whether the large aft angles are due to the final stage failure of a high bypass ratio engine or due to inherent wing location relative to the engine cannot be resolved from the debris database. See discussion in 4.3.3.2.

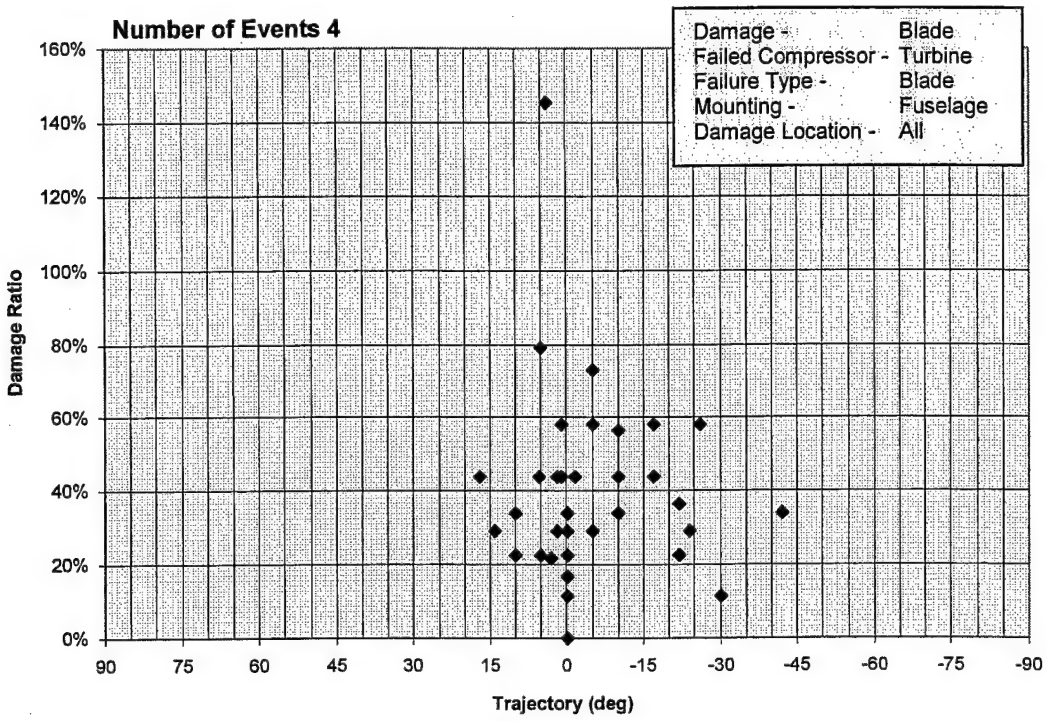

FIGURE 4-53. TURBINE BLADE DAMAGE FROM A BLADE EVENT FOR FUSELAGE-MOUNTED ENGINES

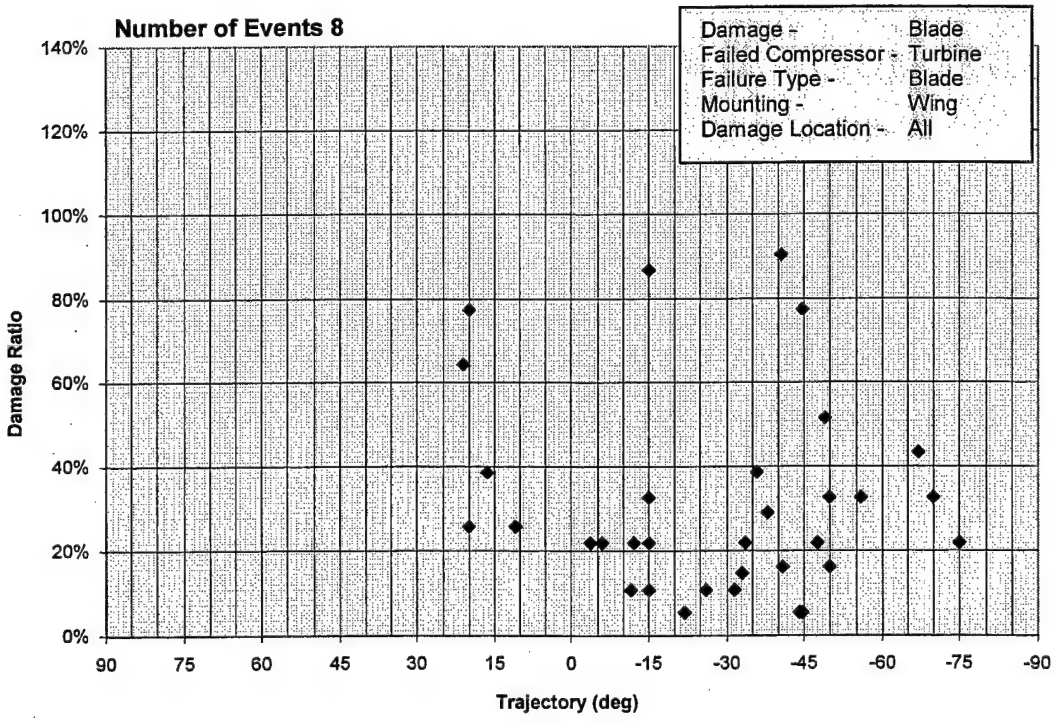

FIGURE 4-54. TURBINE BLADE DAMAGE FROM A BLADE EVENT FOR WING-MOUNTED ENGINES

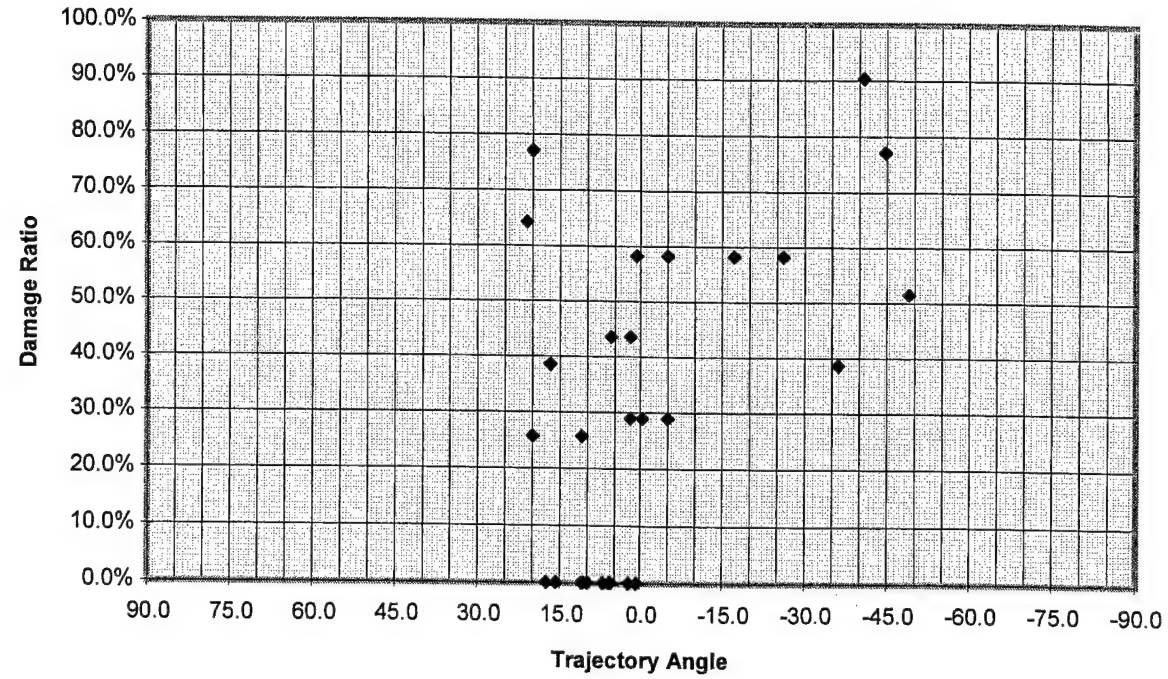

FIGURE 4-55. HP TURBINE BLADE DAMAGE FROM A BLADE EVENT

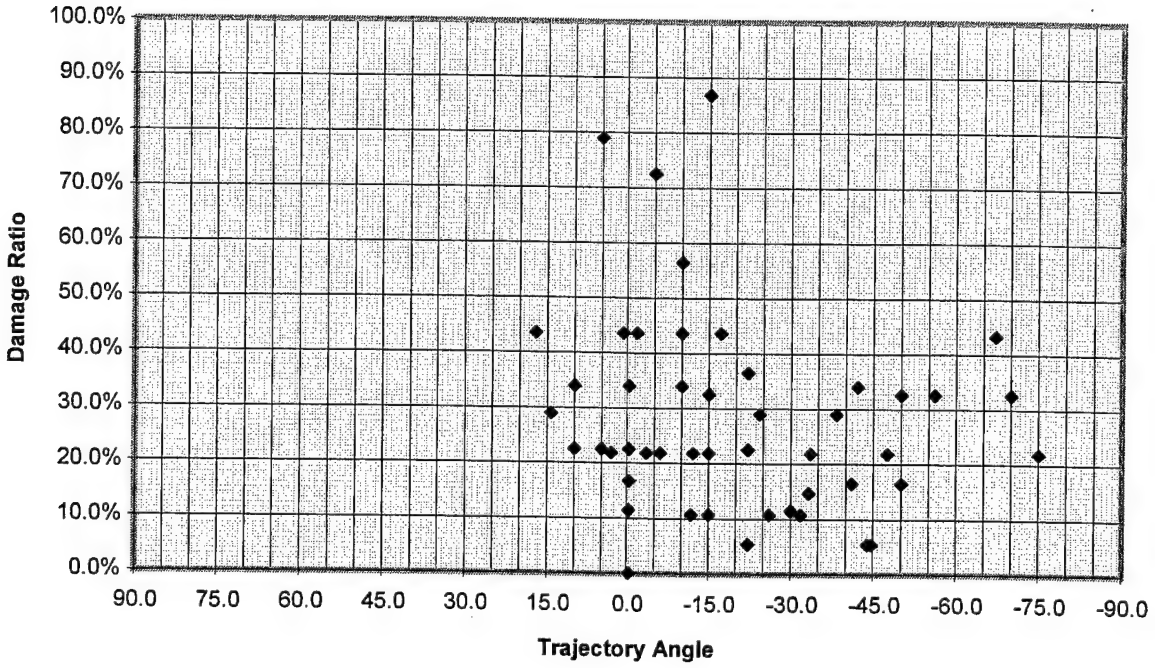

FIGURE 4-56. LP TURBINE BLADE DAMAGE FROM A BLADE EVENT

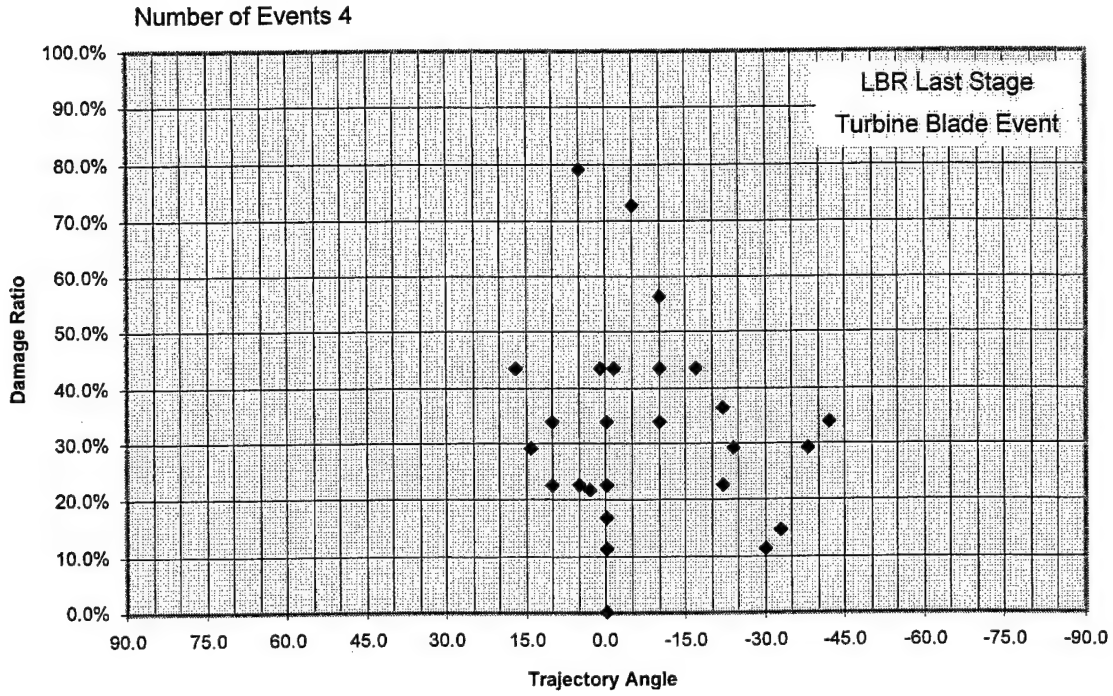

FIGURE 4-57. TURBINE BLADE DAMAGE FROM THE LAST STAGE OF LOW BYPASS RATIO ENGINES

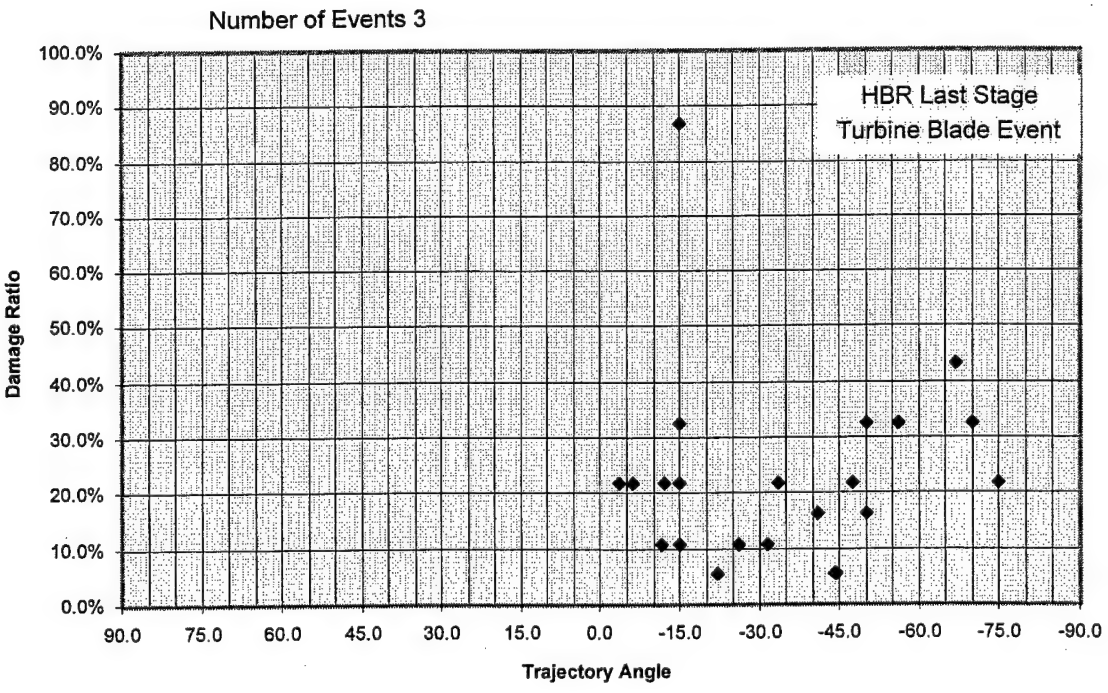

FIGURE 4-58. TURBINE BLADE DAMAGE FROM THE LAST STAGE OF HIGH BYPASS RATIO ENGINES

4.3.3.1 Engine Case Penetration Analysis.

To assess the energy levels of turbine fragments which exit the engine case from multiple blade release events, the following analysis was conducted.

For this analysis, the debris was assumed to penetrate a 0.25-inch steel turbine case, then impact a 0.04-inch aluminum cowl. This analysis was conducted at a 0 degree obliquity angle. A 100% high-pressure turbine blade fragment analysis resulted in a residual velocity of 337 ft/s, as shown in table 4-6. The residual fragment energy (436 ft-lbf) after it penetrates the engine cowl is not enough to penetrate a 0.040-inch aluminum aircraft skin. The analysis was conducted for a 50% low-pressure turbine blade fragment of an HBR engine and resulted in no engine case penetration (based on an initial velocity of 550 ft/sec, 3600 rpm). For an LBR engine, a 50% LPT blade fragment analysis resulted in a residual velocity of 378 ft/sec. Figure 4-59 shows the damage due to an uncontained LPT blade release.

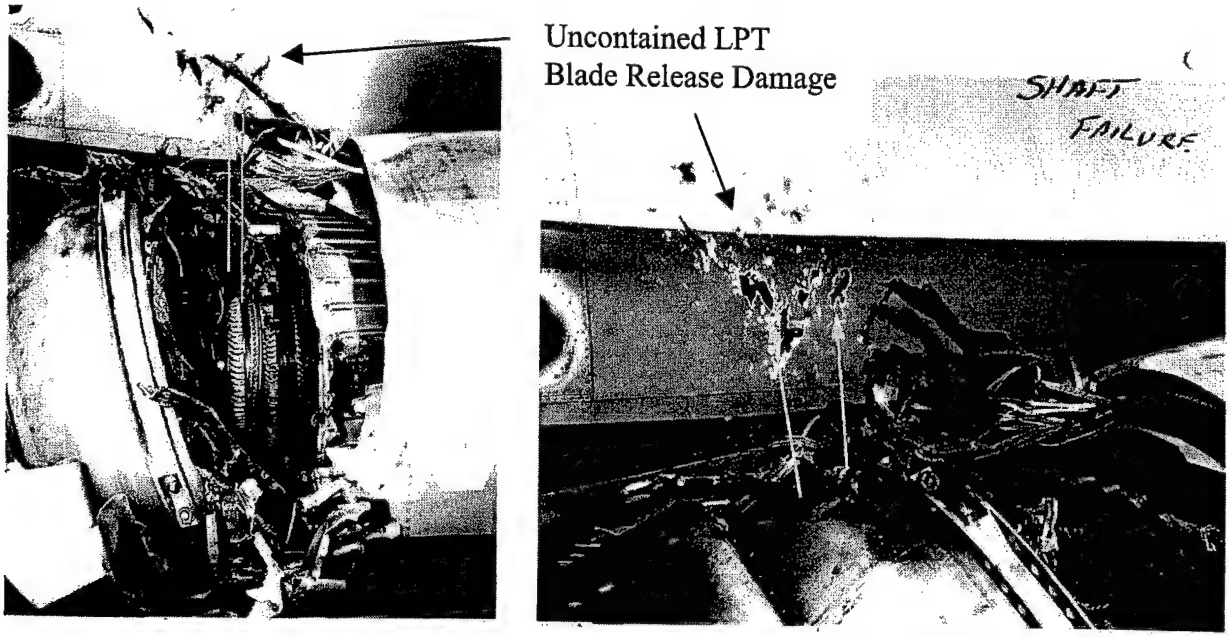

FIGURE 4-59. TURBINE OVERSPEED RESULTING IN UNCONTAINED LPT BLADE RELEASE (NEAR-FIELD FUSELAGE DAMAGE)

TABLE 4-6. TURBINE BLADE RESIDUAL VELOCITY (ENGINE CASE AND COWL)

Debris	Residual Velocity
100% HP Turbine Blade (4" x 2", 0.25 lbm)	337 ft/s
50% LP Turbine Blade HBR	No Penetration
50% LP Turbine Blade LBR (4" x 2", 0.25 lbm)	378 ft/sec

4.3.3.2 Nonengine Case Penetration—Helical Analysis.

Based on ARAC group findings, final stage turbine event blade debris has been shown to demonstrate a helical trajectory, and once the debris exits the exhaust nozzle, the debris has a significant tangential velocity resulting in large aft trajectory damages. In some engine configurations, case struts, and nozzle mixers can limit this type of trajectory. For a 50% blade traveling at 75% of its tip speed (see table 4-7), the initial debris energy is near 3200 ft-lbf. The debris does not have a soft inlet cowl to catch and induce tumbling. Instead, it is speculated that the debris would travel in a helical motion about the engine case until exiting out the rear. Then the debris would launch tangentially from the exit point.

TABLE 4-7. TURBINE BLADE RESIDUAL VELOCITY

Debris	Residual Velocity
50% HBR Turbine Blade (4" x 2", 0.25 lbm)	459 ft/s

4.3.4 Turbine Issues.

There are several issues on turbine debris analysis which need further evaluation. First, why turbine damage is limited to 20 degrees in the forward direction should be investigated. Second, why is damage with large aft trajectory angles (up to -75 degrees) only found on wings and not the fuselage. Finally, final stage blade out events should be examined for modeling purposes.

5. SUMMARY.

There are two groups of debris that have been defined: (1) multiple small blade debris that may be mitigated with shielding and (2) single large disk/rim debris that may be mitigated by geometric separation. Table 5-1 provides the most common debris size, maximum trajectory angles, and debris velocities. Also included are the trajectory angles that embrace over 90% of the data. For blade damage, the two ranges can be significantly different.

TABLE 5-1. DEBRIS CHARACTERIZATION SUMMARY

Component	Most Common Size	Maximum Trajectory Angles	Trajectory Angles for 90% of Data	Length (in)	Width (in)	Mass (lbm)	Residual Velocity (ft/s)
DISK / RIM EVENTS							
HBR Fan Blade	25%	25 to -55	25 to -35	8	8	1.80	813 figure 4-6
LBR Fan Blade	25%	25 to -55	25 to -35	4	4	0.39	897 figure 4-8
Compressor Blade	100%	40 to -45	15 to -30	4	2	0.25	642 figure 4-24
Turbine Blade, HPT	100%	15 to -75	15 to -45	4	2	0.25	871 figure 4-35
Turbine Blade, HBR LPT	50%	15 to -75	15 to -45	4	2	0.25	267 figure 4-37
Turbine Blade, LBR LPT	50%	15 to -75	15 to -45	4	2	0.25	889 figure 4-41
Fan Disk	100%	15 to -5	15 to -5	25.8	6.7	85	100,000[1]
Compressor Disk	50%	5 to -5	5 to -5	17.8	0.8	10	25,000[1]
Compressor Rim	100%	15 to 0	15 to 0	20	1	7	30,000[1]
Turbine Disk	100%	5 to -5[2]	5 to -5[2]	26	4	82	350,000[1]
Turbine Rim	100%	0 to -30	0 to -30	20	1	20	160,000[1]
BLADE EVENTS							
HBR Fan Blade							
-Blade	50%	20 to -35	20 to -35	16	8	4.5	452
-Helical Model	25%	20 to 0	20 to 0	8	8	1.8	table 4-2
-Reingestion Model	varies	20 to 0	20 to 0	varies	varies	varies	table 4-4
LBR Fan Blade							
-Blade	50%	20 to -35	20 to -35	7.5	5	1.5	697
-Helical Model	25%	20 to 0	20 to 0	4	4	0.39	table 4-3
-Reingestion Model	varies	20 to 0	20 to 0	varies	varies	varies	table 4-5
Turbine Blade							
-HBR HPT Blade	100%	21 to -50	20 to -30	4	2	0.25	337
-LBR LPT Blade	50%	20 to -75	20 to -55	4	2	0.25	378
-HBR Last Stage	50%	20 to -75	20 to -55	4	2	0.25	459

[1] Translational Energy (lb-ft)

[2] If runway rebound is included for the turbine disk, the trajectory range is 5 to -12 degrees.

Table 5-1 is divided between disk events and blade failure events. Disk events not only provide high-energy disk fragments, but they also generate high-energy multiple-blade debris. Blade fragment energy from a disk event is slightly higher compared to blade events. This is due to the assumptions used. For a disk event, the initial velocity is based on the debris centroid radius, where for the fan blade helical event the initial velocity is based on the blade tip speed.

The number of damages per event varies based on the type of event. Fan disk events generate the highest number of fragments (21.9). The average number of fragments per event is 11.6. Of the fragments that exit the engine casing, only about 10% of these have sufficient energy to cause damage to another system on the aircraft. The analysis conducted provides a definition of these higher energy fragments. The remaining 90% fragments have considerably less energy and are generally smaller or exit at a lower velocity.

6. DEBRIS PENETRATION MODEL CORRELATION.

To obtain a better understanding of validity of the debris energy analysis and penetration equations, several test cases were studied. The cases selected address several of the failure modes identified by the ARAC engine specialists and presented in this report. The test cases were also used to evaluate some of the assumptions that have gone into the analysis. Specifically, the 75% debris velocity assumption needs verification.

6.1 BLADE FAILURE HELICAL MODEL.

An analysis was conducted on two fan blade fragments that were uncontained as a result of a fan blade failure. The two fragments exited the number 1 engine and damaged the number 2 engine pylon. The number 1 inlet cowl was modeled using the same model used in the Large Engine Uncontained Debris Analysis (Plates 1, 2, and 3). Plates 4 and 5 are for the Al honeycomb number 2 pylon skin. The fan speed used in the analysis was 3300 rpm and a fragment radius of 35" for the inner blade fragment and 40" for the outer blade fragment to calculate the initial velocities. The assumption that the blade traveled at 75% of this initial velocity was used.

For the inner blade fragment, as shown in table 6-1, the analysis shows the fragment passing through one side of the pylon, with a residual velocity of 182 ft/sec. At this velocity it would take a 0.02" thick aluminum sheet to stop the fragment, as shown in table 6-2, and in fact it was stopped by the other side of the pylon skin (0.03" Al). For the outer blade fragment, the fragment has a bit more energy penetrating the number 2 pylon with a residual velocity of 632 ft/sec. At this velocity it would require a 0.2" thick aluminum plate to stop the fragment. This was accomplished by the fragment ricocheting off of the 0.3" thick diagonal brace and impacting the hydraulic reservoir.

The result of the analysis yielded a very good correlation between the model and the event data. This analysis strengthens the case for using the 75% debris initial velocity assumption. It also supports the use of the penetration equations, and the penetration assumptions (debris 45 degree impact orientation) used.

TABLE 6-1. INNER BLADE FRAGMENT

	Fan Blade Fragment								
INPUTS									
			No. of Plates	6					Material
Width	7	in	plate thickness 1	0.025	in	Frag. Ang. 1	80		1
Height	3	in	plate thickness 2	0.025	in	Frag. Ang. 2	45		1
Weight	0.608	lbm	plate thickness 3	0.04	in	Frag. Ang. 3	45		1
Release Vel.	756	ft/s	plate thickness 4	0.03	in	Frag. Ang. 4	45		1
Obliquity	15	deg	plate thickness 5	0.03	in	Frag. Ang. 5	45		1
Material Type			plate thickness 6	0.03	in	Frag. Ang. 6	45		1
1-Aluminum 2024			plate thickness 7	0	in	Frag. Ang. 7	0		1
2-Hard Steel			plate thickness 8	0	in	Frag. Ang. 8	0		1
3-Titanium			plate thickness 9	0	in	Frag. Ang. 9	0		1
			plate thickness 10	0	in	Frag. Ang. 10	0		1

Plate	*V50 (ft/s)*	*Vr (ft/s)*	*Residual Energy (ft lbf)*	*tr (in)*	*KE ratio*	*Delta Velocity (ft/s)*	*Presented Area (sq. in.)*
1	70.3	741.2	5190.8	0.34	0.96	14.8	3.65
2	250.0	656.2	4069.1	0.07	0.75	85.0	14.85
3	382.1	484.5	2217.6	0.05	0.41	171.8	14.85
4	294.7	357.4	1206.8	0.04	0.22	127.1	14.85
5	294.7	187.9	333.7	0.02	0.06	169.5	14.85
6	294.7	0.0	0.0	0.00	0.00	187.9	14.85

TABLE 6-2. OUTER BLADE FRAGMENT

	Fan Blade Fragment								
INPUTS									
			No. of Plates	5					Material
Width	7	in	plate thickness 1	0.025	in	Frag. Ang. 1	80		1
Height	3	in	plate thickness 2	0.025	in	Frag. Ang. 2	45		1
Weight	0.82	lbm	plate thickness 3	0.04	in	Frag. Ang. 3	45		1
Release Vel.	864	ft/s	plate thickness 4	0.03	in	Frag. Ang. 4	70		1
Obliquity	15.6	deg	plate thickness 5	0.03	in	Frag. Ang. 5	70		1
Material Type			plate thickness 6	0	in	Frag. Ang. 6	0		1
1-Aluminum 2024			plate thickness 7	0	in	Frag. Ang. 7	0		1
2-Hard Steel			plate thickness 8	0	in	Frag. Ang. 8	0		1
3-Titanium			plate thickness 9	0	in	Frag. Ang. 9	0		1
			plate thickness 10	0	in	Frag. Ang. 10	0		1

Plate	*V50 (ft/s)*	*Vr (ft/s)*	*Residual Energy (ft lbf)*	*tr (in)*	*KE ratio*	*Delta Velocity (ft/s)*	*Presented Area (sq. in.)*
1	53.2	852.5	9261.3	0.54	0.97	11.5	3.65
2	189.2	793.9	8031.1	0.12	0.84	58.6	14.85
3	289.3	687.5	6023.4	0.10	0.63	106.4	14.85
4	115.8	659.7	5545.4	0.21	0.58	27.8	7.18
5	115.8	632.2	5092.5	0.20	0.54	27.5	7.18

6.2. FAN DISK EVENT BLADE ANALYSIS.

A debris penetration analysis was conducted on a fan disk event to obtain a better understanding of the fragment velocities and determine if using 75% of the initial velocity is a reasonable assumption for blade fragments from a disk event. In this event, several blade fragments penetrated one side of the fuselage and impacted the other side without passing through. Both fragments were approximately 50% blade fragments, one from the root side and one from the tip side. The blade root fragment was lodged in the far side of the fuselage skin.

Figure 6-1 shows the model used in the analysis. The actual aircraft skin thickness is 0.04", but to account for frames, the thickness was increased to 0.065". The blade fragment of interest was a blade root section with the dovetail attached. This fragment was found wedged in the fuselage skin. The fragment was approximately 7 inches long and 5.5 inches wide and weighed about 1.5 lb. The initial release velocities for the blade root fragment and tip fragment were 788 and 1382 ft/sec respectively. Table 6-4 shows the analysis conducted for the blade root fragment at its initial velocity. The analysis indicates that the fragment would have penetrated both sides of the aircraft fuselage with a residual velocity of 370 ft/sec. Using 75% of the initial velocity, the fragment was unable to penetrate the far side of the fuselage, as was the case for this event (table 6-4).

For the blade tip fragment, the results are much the same. Using the initial velocity, the fragment penetrates all the way through the aircraft with a residual velocity of 420 ft/sec (table 6-5). Using 75% of the initial debris velocity (table 6-6), the fragment does not penetrate the far side of the fuselage (plate 4), again matching the event data.

Again the model correlates well with the event data. The 75% debris velocity assumption holds up well, correlating the analysis to the event data.

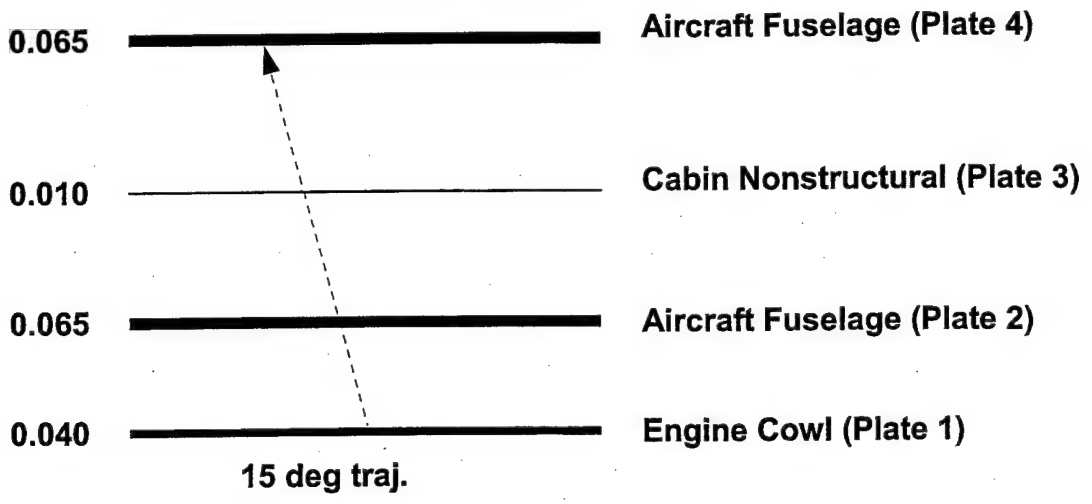

FIGURE 6-1. ENGINE COWL AND AIRCRAFT MODEL

TABLE 6-3. BLADE ROOT SECTION, 100% INITIAL DEBRIS VELOCITY

INPUTS	Blade Root Section								
			No. of Plates		4				Material
Width	7	in	plate thickness 1		0.04	in	Frag. Ang.	45	1
Height	5.5	in	plate thickness 2		0.065	in	Frag. Ang.	45	1
Weight	1.5	lbm	plate thickness 3		0.01	in	Frag. Ang.	45	1
Release Vel.	788	ft/s	plate thickness 4		0.065	in	Frag. Ang.	70	1
Obliquity	14.9	deg	plate thickness 5		0	in	Frag. Ang.	45	1
Material Type			plate thickness 6		0	in	Frag. Ang.	45	1
1-Aluminum 2024			plate thickness 7		0	in	Frag. Ang.	45	1
2-Hard Steel			plate thickness 8		0	in	Frag. Ang.	45	1
			plate thickness 9		0	in	Frag. Ang.	45	1
			plate thickness 10		0	in	Frag. Ang.	45	1

Plate	*V50* (ft/s)	*Vr* (ft/s)	*Residual Energy* (ft lbf)	*tr* (in)	*KE ratio*	*Delta Velocity* (ft/s)
1	282.2	684.2	10913.9	0.11	0.75	103.8
2	437.5	468.8	5122.5	0.07	0.35	215.5
3	80.7	453.2	4788.8	0.07	0.33	15.5
4	227.1	370.4	3197.5	0.11	0.22	82.9

TABLE 6-4. BLADE ROOT ANALYSIS, 75% INITIAL DEBRIS VELOCITY

INPUTS	Blade Root Section								
			No. of Plates		4				Material
Width	7	in	plate thickness 1		0.04	in	Frag. Ang.	45	1
Height	5.5	in	plate thickness 2		0.065	in	Frag. Ang.	45	1
Weight	1.5	lbm	plate thickness 3		0.01	in	Frag. Ang.	45	1
Release Vel.	591	ft/s	plate thickness 4		0.065	in	Frag. Ang.	70	1
Obliquity	14.9	deg	plate thickness 5		0	in	Frag. Ang.	45	1
Material Type			plate thickness 6		0	in	Frag. Ang.	45	1
1-Aluminum 2024			plate thickness 7		0	in	Frag. Ang.	45	1
2-Hard Steel			plate thickness 8		0	in	Frag. Ang.	45	1
			plate thickness 9		0	in	Frag. Ang.	45	1
			plate thickness 10		0	in	Frag. Ang.	45	1

Plate	*V50* (ft/s)	*Vr* (ft/s)	*Residual Energy* (ft lbf)	*tr* (in)	*KE ratio*	*Delta Velocity* (ft/s)
1	282.2	482.9	5436.4	0.07	0.67	108.1
2	437.5	182.1	773.3	0.02	0.09	300.8
3	80.7	160.3	598.7	0.02	0.07	21.9
4	227.1	0.0	0.0	0.00	0.00	160.3

TABLE 6-5. BLADE TIP FRAGMENT, 100% INITIAL DEBRIS VELOCITY

INPUTS	Blade Tip Fragment								
			No. of Plates		4				Material
Width	7	in	plate thickness 1		0.04	in	Frag. Ang.	45	1
Height	5.5	in	plate thickness 2		0.065	in	Frag. Ang.	45	1
Weight	1	lbm	plate thickness 3		0.01	in	Frag. Ang.	45	1
Release Vel.	1382	ft/s	plate thickness 4		0.065	in	Frag. Ang.	45	1
Obliquity	14.9	deg	plate thickness 5		0	in	Frag. Ang.	45	1
			plate thickness 6		0	in	Frag. Ang.	45	1
Material Type			plate thickness 7		0	in	Frag. Ang.	45	1
1-Aluminum 2024			plate thickness 8		0	in	Frag. Ang.	45	1
2-Hard Steel			plate thickness 9		0	in	Frag. Ang.	45	1
			plate thickness 10		0	in	Frag. Ang.	45	1

Plate	*V50 (ft/s)*	*Vr (ft/s)*	*Residual Energy (ft lbf)*	*tr (in)*	*KE ratio*	*Delta Velocity (ft/s)*
1	413.3	1185.0	21822.9	0.13	0.74	197.0
2	640.8	842.4	11027.0	0.09	0.37	342.7
3	118.2	811.1	10224.8	0.08	0.34	31.2
4	640.8	420.3	2744.9	0.04	0.09	390.9

TABLE 6-6. BLADE TIP FRAGMENT, 75% INITIAL DEBRIS VELOCITY

INPUTS	Blade Tip Fragment								
			No. of Plates		4				Material
Width	7	in	plate thickness 1		0.04	in	Frag. Ang.	45	1
Height	5.5	in	plate thickness 2		0.065	in	Frag. Ang.	45	1
Weight	1	lbm	plate thickness 3		0.01	in	Frag. Ang.	45	1
Release Vel.	1036	ft/s	plate thickness 4		0.065	in	Frag. Ang.	45	1
Obliquity	14.9	deg	plate thickness 5		0	in	Frag. Ang.	45	1
			plate thickness 6		0	in	Frag. Ang.	45	1
Material Type			plate thickness 7		0	in	Frag. Ang.	45	1
1-Aluminum 2024			plate thickness 8		0	in	Frag. Ang.	45	1
2-Hard Steel			plate thickness 9		0	in	Frag. Ang.	45	1
			plate thickness 10		0	in	Frag. Ang.	45	1

Plate	*V50 (ft/s)*	*Vr (ft/s)*	*Residual Energy (ft lbf)*	*tr (in)*	*KE ratio*	*Delta Velocity (ft/s)*
1	413.3	853.6	11324.4	0.09	0.68	182.4
2	640.8	476.6	3530.1	0.05	0.21	377.0
3	118.2	449.0	3133.6	0.04	0.19	27.6
4	640.8	0.0	0.0	0.00	0.00	449.0

7. RECOMMENDATIONS.

The most critical recommendation is to calibrate fragment penetration characteristics. The equations from BARRIER appear to do a good job of matching blade debris trajectory predictions with values seen from the debris database. These equations are empirical, however, and must be anchored with representative debris testing. This work is planned and will be used for military and civil applications.

Additional data to support each of the assumptions and analysis conducted in this debris characterization effort is needed. Many of the assumptions were made based on a very limited amount of information. Therefore data collection activities should continue.

The basic model describing disk events, figure 2-1, was initially too conservative. By using 75% of the initial debris velocity to calculate debris energy, debris velocity estimations have fallen in line (generally) with the damage data as seen in the damage trajectory plots. Using 75% of the initial velocity is a significant assumption and needs to be addressed. The obvious way to address this issue is with a full-scale engine disk burst test and analysis. Testing would also help quantify the engine case debris that may pose a threat to the aircraft. This debris may have significantly different characteristics than the blade debris presented in this report.

Predicted debris characteristics for blade and disk failure scenarios from compressors or turbines are lacking data to correlate the analysis. Of the event data collected, a good test case was not available to correlate with the model. If the test data does not exist, full-scale testing is recommended to verify the 75% velocity assumption for blade and disk fragments.

Modeling of the inlet cowl pass-through velocity for the helical moving fan blade fragment is felt by some to be too conservative. Air cannon testing against simulated inlet structures could resolve this issue.

The effect of the reverser on the escaped debris characteristics from compressor failures should be evaluated by testing if additional data is not otherwise available. Again, data as it becomes available should be used to resolve this issue.

8. REFERENCES.

1. "FAA/SAE Committee on Uncontained Turbine Engine Rotor Events Data Period 1976 Through 1983," Aerospace Information Report, Report No. AIR4003.

2. "FAA/SAE Committee on Uncontained Turbine Engine Rotor Events Data Period 1984 Through 1989," Aerospace Information Report, Report No. AIR4770, 20 July 1994.

3. "An Assessment of Technology for Turbojet Engine Rotor Failures," Mr. D. McCarthy, Massachusetts Institute of Technology, Cambridge, MA, August 1977.

4. Penetration Equations Handbook for Kinetic-Energy Penetrators, Joint Technical Coordinating Group for Munitions Effectiveness, 61 JTCG/ME-77-16, December 1986.

5. The Distribution of Fan Blade Fragments Projected Forward of the Engine Front Flange, Mr. H. J. Pinsent, GE Aircraft Engines, R93AEB346, July 1993.

6. Fluid-Dynamic Drag, Dr. Sighard Hoerner, 1965.

APPENDIX A—MODELING OF AERODYNAMIC EFFECTS ON UNCONTAINED ENGINE DEBRIS

Aerodynamic forces have two effects on liberated debris from an uncontained event. First, drag will reduce the debris kinetic energy before impacting the fuselage. Second, the airstream may bend the debris trajectory aftward. The following describes the model used to evaluate these effects and provides sample results to emphasize particular trends.

A.1. MODEL.

A.1.1 BASIC EQUATIONS.

A two dimensional model was constructed to analyze the aerodynamic effect on uncontained engine debris. The selected coordinate system in relation to the aircraft is shown in figure A-1.

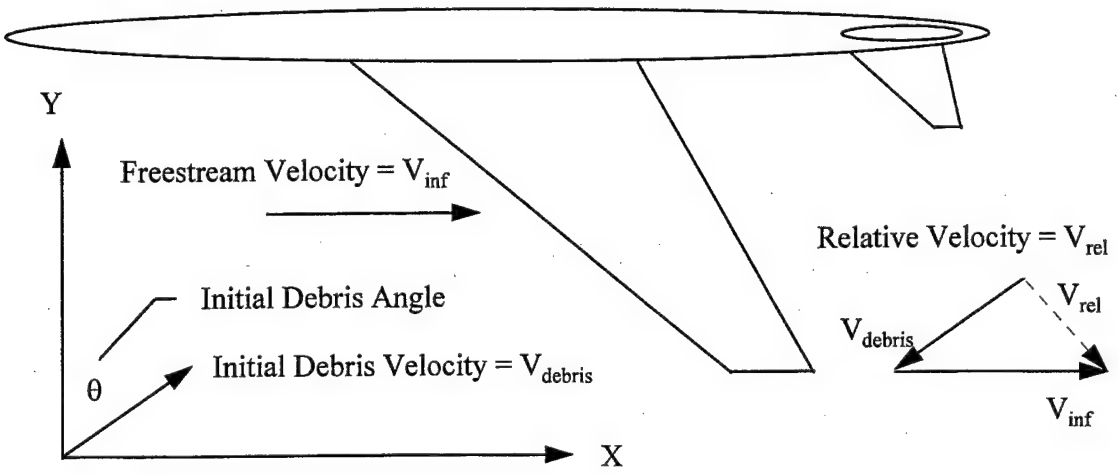

FIGURE A-1. SELECTED COORDINATE SYSTEM FOR DEBRIS TRAJECTORY MODEL

The velocity for a given piece of debris is denoted by

$$V_{debris} = V_x\, i + V_y\, j$$

where

$$V^2_{debris} = V_x^2 + V_y^2$$

Once the debris has entered the airstream, the freestream velocity component, V_{inf}, acts upon the debris (see figure A-1). Using a stationary reference for the debris, the relative wind across the debris is then represented by

$$V_{rel} = (-V_x + V_{inf})\, i - V_y\, j$$

Total drag on the debris is then calculated from

$$Drag = q\ Cd\ S = 0.5\ \rho\ V^2_{rel}\ Cd\ S$$

where

Cd = debris drag coefficient
S = debris reference area

Unit vectors are used to find the respective drag components:

$$Dx = (-V_x + V_{inf})\ Drag / V_{rel}$$
$$Dy = (-V_y)\ Drag / V_{rel}$$

To calculate the component accelerations, each drag component is divided by the debris mass. Hence

$$ax = Dx / mass$$
$$ay = Dy / mass$$

Once the accelerations are known, the equations of motion are utilized to calculate component velocity and distance. The generic equations for velocity and distance are

$$V_i = V_{i-1} + a_{i-1}\ dt$$
$$X_i = X_{i-1} + V_{i-1}\ dt + 0.5 a_{i-1}\ dt^2$$

All of the analysis was performed on blade debris, which were modeled as rectangular plates. According to reference 4, an appropriate drag coefficient for a tumbling rectangular plate is 1.17. For presented debris frontal area, an average tumbling orientation of 45 degrees was used, as show in figure A-2. This is standard practice in the vulnerability community.

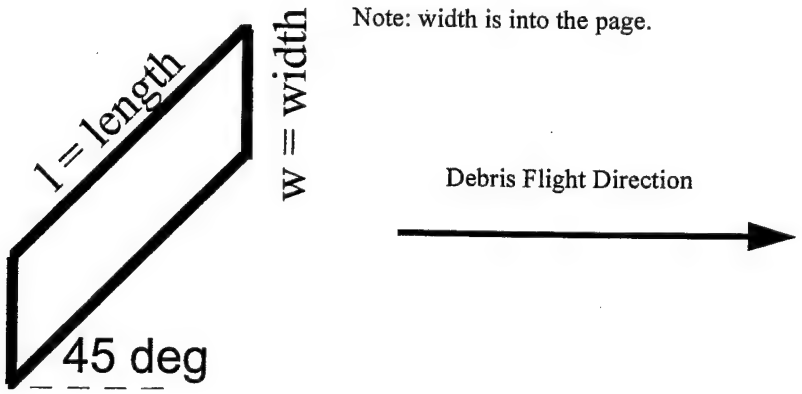

FIGURE A-2. AVERAGE DEBRIS ORIENTATION WHILE TUMBLING

A.1.2 MODEL INPUTS.

The model is used in conjunction with the debris penetration analysis. Key inputs from the penetration analysis include debris length, debris width, debris mass, initial trajectory angle, and initial velocity. Additional inputs include flight altitude, aircraft Mach number, and total distance traveled in the y-direction by the fragment.

A.2. ANALYSIS.

Regardless of the debris size analyzed, there are standard trends from aerodynamic effects. A piece of debris representing a 100% Compressor Blade has been selected to present these trends.

The debris properties for a 100% Compressor Blade are as follows:

Width	= 4 in
Height	= 2 in
Weight	= 0.25 lbm
Initial Velocity	= 1047 ft/s

Figure A-3 shows the debris velocity upon leaving the engine cowl as a function of trajectory angle. This is the initial debris velocity (V_{debris}) used in the aerodynamic analysis.

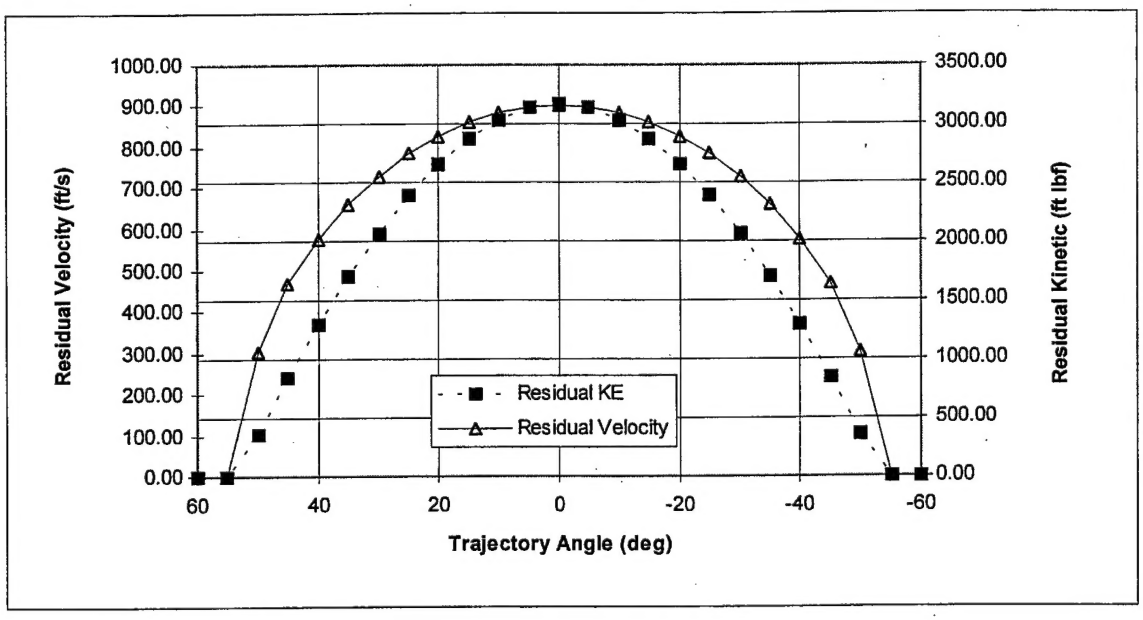

FIGURE A-3. INITIAL DEBRIS ENERGY VERSUS TRAJECTORY ANGLE

Uncontained events occur throughout the flight envelope. Hence, a cruise flight condition and a takeoff flight condition are examined to cover both spectrums. In addition, analysis for a fuselage-mounted engine and a wing-mounted engine are presented.

A.2.1 CRUISE CONDITION.

A cruise condition of Mach 0.85 at 30,000 ft was selected for analysis. For a fuselage-mounted engine the estimated distance between the fuselage and the aircraft is under 5 feet. As expected, figure A-4 shows very little aerodynamic effect on the debris.

For a wing-mounted engine assumed to be 30 feet from the fuselage, the aerodynamic effect is more pronounced as shown in figure A-5. Debris with forward trajectories experience a significant reduction in kinetic energy and up to a 15-degree shift in their trajectory angle. Since the debris is traveling into a headwind, the relative drag is much greater. Conversely, debris with moderate aft trajectories have a tailwind and experience minimal kinetic energy loss. For large aft angles the debris may actually gain energy, though the overall magnitudes are still small.

A.2.2 TAKEOFF CONDITIONS.

The takeoff condition was represented by Mach 0.2 at 500 ft. The lower altitude provides a denser atmosphere which significantly increases aerodynamic drag. The result is a greater loss in debris kinetic energy. Figures A-6 and A-7 show the results for a fuselage-mounted and a wing-mounted engine, respectively. Both show greater losses than predicted for the cruise condition (figures A-4 and A-5).

A.3. SUMMARY.

A two-dimensional model was constructed to model the aerodynamic effects on uncontained blade debris. Listed in order of importance, the two primary effects are (1) total kinetic energy lost due to aerodynamic drag and (2) the aft trajectory bend from the airstream. For fuselage-mounted engines, the aerodynamic effects can essentially be ignored. For wing-mounted engines, debris energy is significantly reduced for forward trajectories before impacting the fuselage. For aft trajectories, the total debris energy may not significantly change since the airstream is acting as a tailwind.

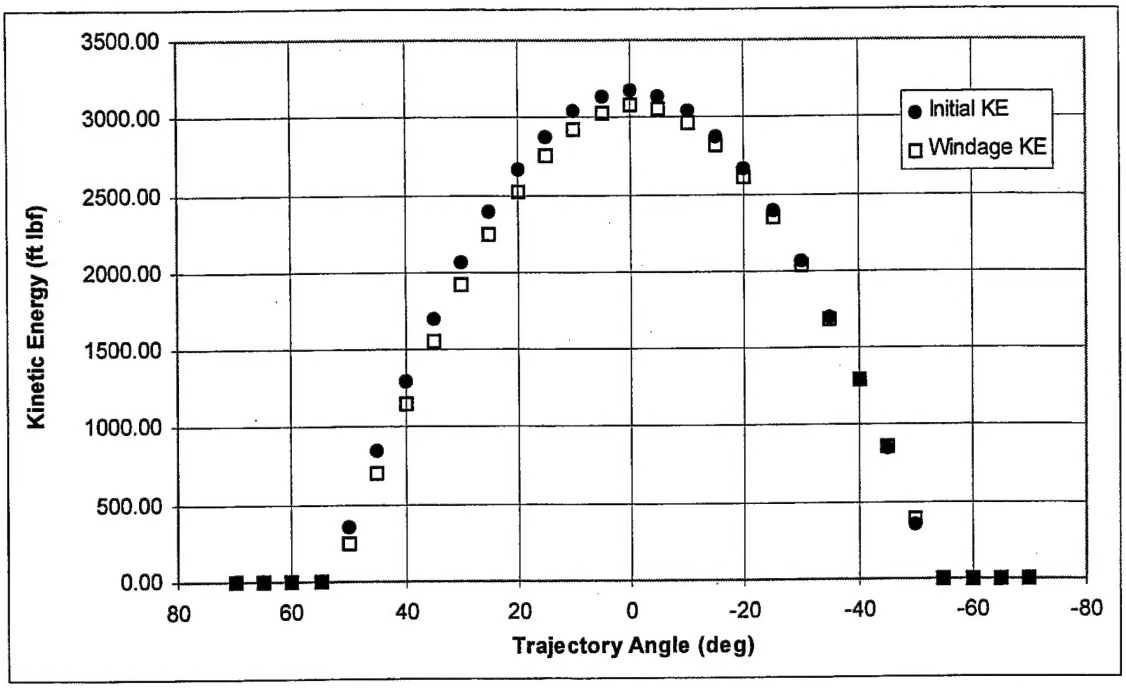

FIGURE A-4. FUSELAGE-MOUNTED ENGINE AT ALTITUDE

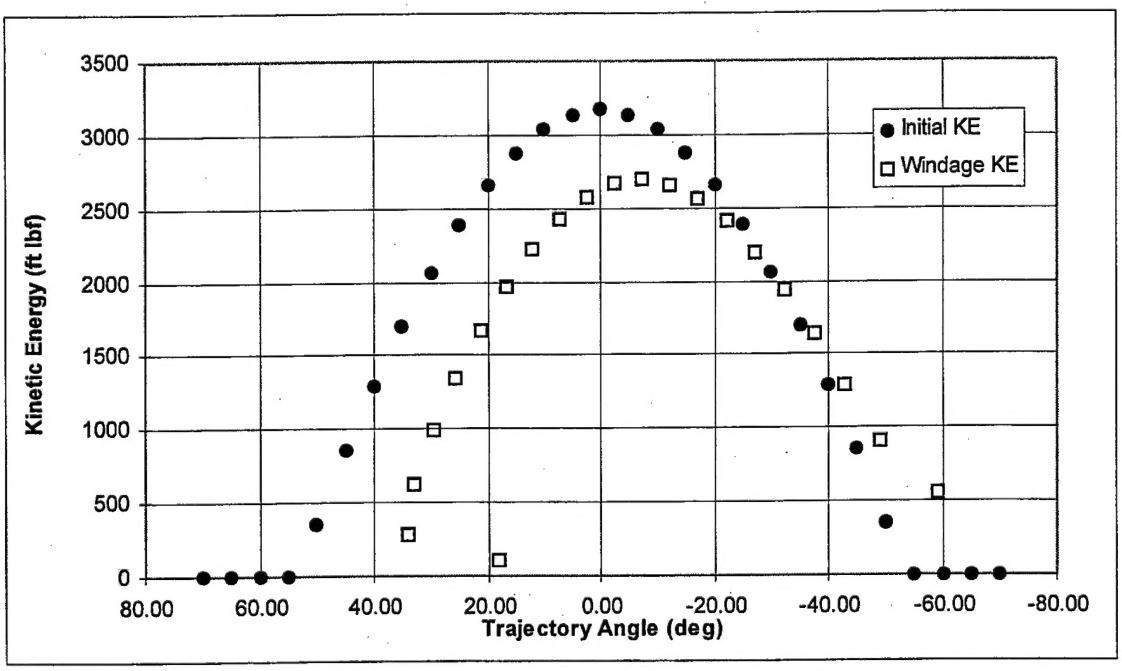

FIGURE A-5. WING-MOUNTED ENGINE AT ALTITUDE

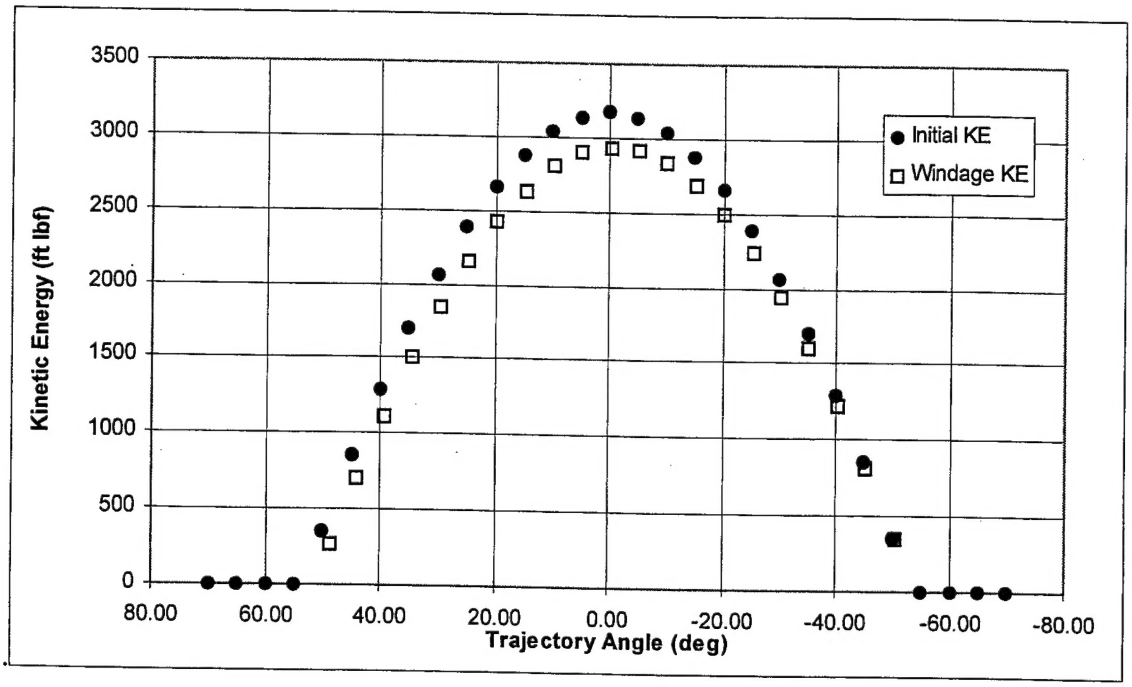

FIGURE A-6. FUSELAGE-MOUNTED ENGINE AT TAKEOFF

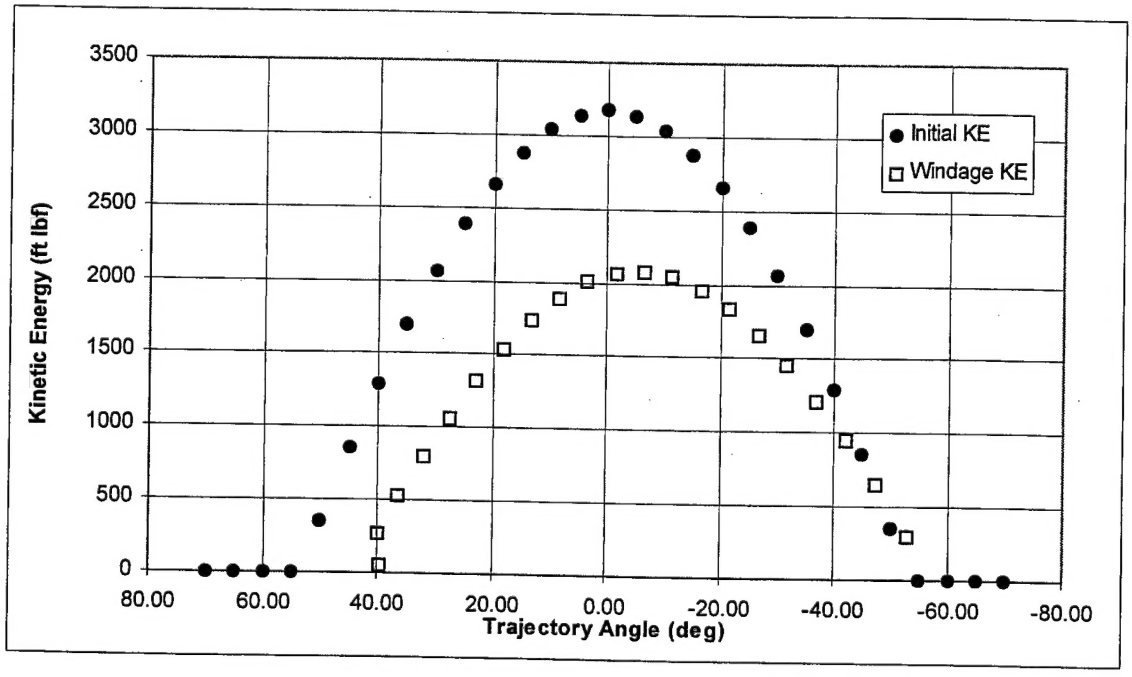

FIGURE A-7. WING-MOUNTED ENGINE AT TAKEOFF